Understanding and Engineering Azobenzene for Thermal Energy Storage

by

Eugene N. Cho

Submitted to the Department of Materials Science and Engineering
in partial fulfillment of the requirements for the degree of

Doctor of Philosophy in Materials Science and Engineering

at the

MASSACHUSETTS INSTITUTE OF TECHNOLOGY

June 2017

Signature redacted

Author . . . . .

(Department of Materials Science and Engineering
May 26, 2017

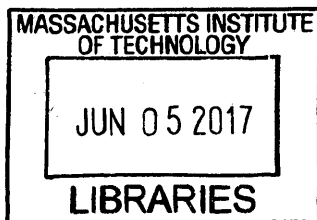**Signature redacted**

Certified by. . . .

Jeffrey C. Grossman
Professor of Materials Science and Engineering
Thesis Supervisor

Signature redacted

Accepted by . . . .

Donald R. Sadoway
Chair, Departmental Committee on Graduate Studies

Understanding and Engineering Azobenzene for Thermal Energy Storage

by

Eugene N. Cho

Submitted to the Department of Materials Science and Engineering
on May 26, 2017, in partial fulfillment of the
requirements for the degree of
Doctor of Philosophy in Materials Science and Engineering

Abstract

This thesis focuses on the understanding and engineering of a molecule known as azobenzene which holds unique properties for thermal storage applications. The azobenzene molecule undergoes structural change into a metastable state which has the ability to store energy. This thesis utilizes the energy storage and structural change properties of this molecule to develop new materials for thermal energy storage. The first is through a concept called solar thermal fuel which is storing the solar energy in rearranged bonds of the azobenzene and later releasing that energy in the form of heat. The second approach is through the structural property difference of its two states in order to moderate the phase change temperature of organic phase change materials. Essentially, the molecule azobenzene was modified and engineered to be used as a thermal battery as well as to mediate thermal energy storage in other materials. The first chapter will give a brief introduction on the concept and past examples of solar thermal fuel. Chapter 2, 3, 4 will discuss about the development of solar thermal fuel while chapter 5 discusses about a recently developed concept of using azobenzene to moderate phase change temperature.

Chapter 2 shows the first demonstration of using solar thermal fuel in the solid state through functionalizing azobenzene on a polymer template. The polymer platform allows fabrication of a thin film of this material which enabled charging, discharging, and heat release using optically chargeable molecules all within the solid-state. A demonstration of solid state application was shown by constructing a macroscopic device which resulted in heat release bringing a temperature increase of as high as 10 °C.

Next in chapter 3, azobenzene was engineered on the molecular lever with bulky aromatic groups (phenyl, biphenyl, and tert-butyl phenyl groups). The molecules were designed and synthesized for the purpose of increasing energy stored while promoting solid state solar thermal fuels. The design allowed fabrication of molecular based thin

film, which was able to be charged with light, a great improvement from the original azobenzene, which crystallized preventing switching in the solid state. Molecular engineering proved to be a powerful and effective method in improving other solar thermal fuel properties, such as energy storage in STFs, chargeability, and also the thermal stability of the molecular thin film.

In chapter 4, new diacetylene derivatives with azobenzene moieties and with varied alkyl spacers and linkers were synthesized to show photocontrolled self-assembly and disassembly of photon energy storage materials. This azobenzene decorated diacetylenes not only allowed solar energy storage but also demonstrated phase change characteristic of organic materials can be a parameter to consider in terms of designing high energy density photon energy storage materials.

Chapter 5 discusses azobenzene based dopants in organic phase change material to photomoderate the phase change temperature. Three different types, 8 in total, organic phase change materials were tested to show the possibilty of this concept in a wide variety of phase change materials. A deep understanding was developed giving parameters to achieve a large phase change temperature difference in the organic phase change materials using the structual difference of the trans and the cis state of azobenzene.

Thesis Supervisor: Jeffrey C. Grossman
Title: Professor of Materials Science and Engineering

Acknowledgments

Coming to MIT in the fall of 2012 was a beginning of a long journey with no clear direction on which paths to take. Throughout this long journery, I have gotten lost and faced many challenges and downfalls, but have also learned immensely and gained vast experience and knowledge on not only science but also about life. I have met many great people to whom I am very thankful for enhancing my experience here at MIT both scientifically and emotionally. Professor Jeremiah Johnson and Professor Robert Macfarlane both gladly accepted to be my thesis committee members and provided great feedback during our meetings. I would like to thank Dr. Nicola Ferralis with help on the raman spectroscopy and Dr. Yun Liu who gave a lot of great input from the computational side. I would also like to express my gratitude to my colleagues Dr. David Zhitomirsky for his guidance with experimental design and Dr. Grace G. D. Han for her expertise in chemistry and help with synthesis. Both were a big help with my research and experiments here at MIT.

Life of a graduate student is not complete without talking about one's advisor. Professor Jeffrey Grossman provided a welcoming atmosphere in his group full of talented and collaborative people. He was also supportive and was always optimistic and positive allowing me to see the light in times of dark. He was a great advisor not only to me but everyone in the group. Without his support and warmth, I would not have been able to finish this short yet very long run and I thank him greatly for everything.

My family had an important part during my 5 years in graduate school, who I learned more about in the recent years. My parents were always supportive throughout this entire process. My mother always provided love and care and warmth. My father was the one who suggested this path and walked down this path far long ago, helped greatly with his words of advice during times of need. He understood my situation and pushed me forward towards the end. My younger brother, currently studying in Canada, now a good friend than just a brother and my younger sister,

who is shy and not the most expressive person, always shows her affection in little ways, both are an important part of my life. I, who am not the most expressive person myself, want to say I love my family and will always do.

Club activities were also a big part of my life here at MIT. KGBA, a basketball club, was a big part of my early years bringing me great joy and excitement as well as allowed me to meet many great people. Boston 3040, a tennis club, helped me meet great people outside of MIT and allowed me to play tennis and improve my skills. Furthermore, working for KGSA, the Korean graduate student association, helped me learn the joy of working as part of an organization and organizing events for a community. And finally, finding the Korean Tennis Club was a big accomplishment I made as well as meeting and playing tennis with fellow tennis enthusiasts made the time fly.

Lastly, the friends I met during my time here at MIT made a huge impact on my graduate life. My friends Jongwon Choi, Youngsuk Jo, Hyunho Kim, and Seonghoon Woo holds many of the good memories as well as gave me great support during my greatest times of stress. My 1st year roommates Dongwook Lee and Eungkwan Lee as well as my fellow 1st year Korean DMSE friends (Hyungwon, Intak, Kyungwon, Minae, Byungjin, Dongwook, Jongwon, Jaehyun) made adjusting to MIT a more enjoyable one. I would like to thank my fellow group members for their company through my years here. Also, I would like to thank Boyoung Park for all the help and support she has given me as well as being a good friend and tennis buddy and my friend Sangwoo Kim who was always there to talk and knew the right words to say when needed. There are many more people who I have came across and the list would be endless. I would like to thank each and everyone of them for making life at MIT fruitful and full of learning.

Contents

List of Figures

Chapter 1

Introduction

Since the advancements made during the Industrial Revolution, fossil fuels have been the dominant energy source meeting for our energy demands. However, in recent years global warming and climate change due to carbon emissions from burning fossible fuels along with fossil fuel depletion have raised tremendous concens with continued use of fossil fuels as our main energy source.[1] With this, increased demand for new energy techonologies and strategies and attention has been shifted to renewable energies such as solar, wind, geothermal, hydro energy, etc. As seen in Figure 1-1, out of these renewable energies, solar energy is by far the most abundant source of energy on earth. Compared to a total of about 100TW-yr potential production, the yearly potential of solar energy which reaches earth is a much larger amount of 23,000 TW-yr. Compared to the world energy consumption of 16 TW-yr per year and 900 TW-yr of total reserves, being able to harness a small percentage of this solar energy can easily meet the world's energy demand. In fact, based on the figure, assuming we are able to harness 100% of the sun's energy that reaches earth, only 6 hour of solar energy is need to power the planet for an entire year.[1]

However, despite the vast abundance of solar radiation, efficient conversion, storage, and distribution of this resource remain a challenge and much ongoing research is taking place worldwide to solve this problem. Solar energy harvesting and con-

version into other forms of energy (i.e., electricity, chemical fuels, and heat) have been a focus of research efforts for efficient and renewable energy utilization. This is currently being done in largely three methods: Photovoltaic, the conversion of solar energy to electricity; artificial photosynthesis, the conversion of solar energy into usable chemical fuel; and solar thermal, the conversion of solar energy to heat. Out of the three, much research has been focused on photovoltaic and artificial photosynthesis, exploring new materials systems to improve efficiency. Progress has been made through exploring new materials systems where photovoltaic research explored inorganic [14], organic [15], and hybrid materials [16, 17] while artificial photosynthesis [18, 19] employ wide-band metal oxides. However, solar thermal collection and storage has depended on materials with high thermal storage capacity such as water, molten salt, or other phase-change (PC) materials [20] with little improvement or exploration of material through new research. When looking at the energy consumption distribution in the world seen in Figure 1-2, a large portion of the energy is used for heating, and thus more research on solar thermal materials is needed.

This thesis covers a unique class of chemical molecules called solar thermal fuels (STF) convert and store solar energy in rearraged chemical bonds that can be used to release heat. Our work has focused on tailoring STF molecules to enhance their potential use for converting solar energy to stored heat. First, we will discuss our work involved with templating STF molecules onto a polymer template for demonstrating the first solid-state STF. Next, we will turn to molecular engineering to increase the energy stored per molecule and show the potential of solid state STF based on molecular thin films as opposed to polymer thin films. Next, we discuss out work on increasing the stored energy by decorating the STF onto diacetylene through the use of phase change as an additional energy storage method. Finally, the STF molecule has been modified to be used as dopants in phase change materials (PCM) to control the crystallization temperature with the use of light.
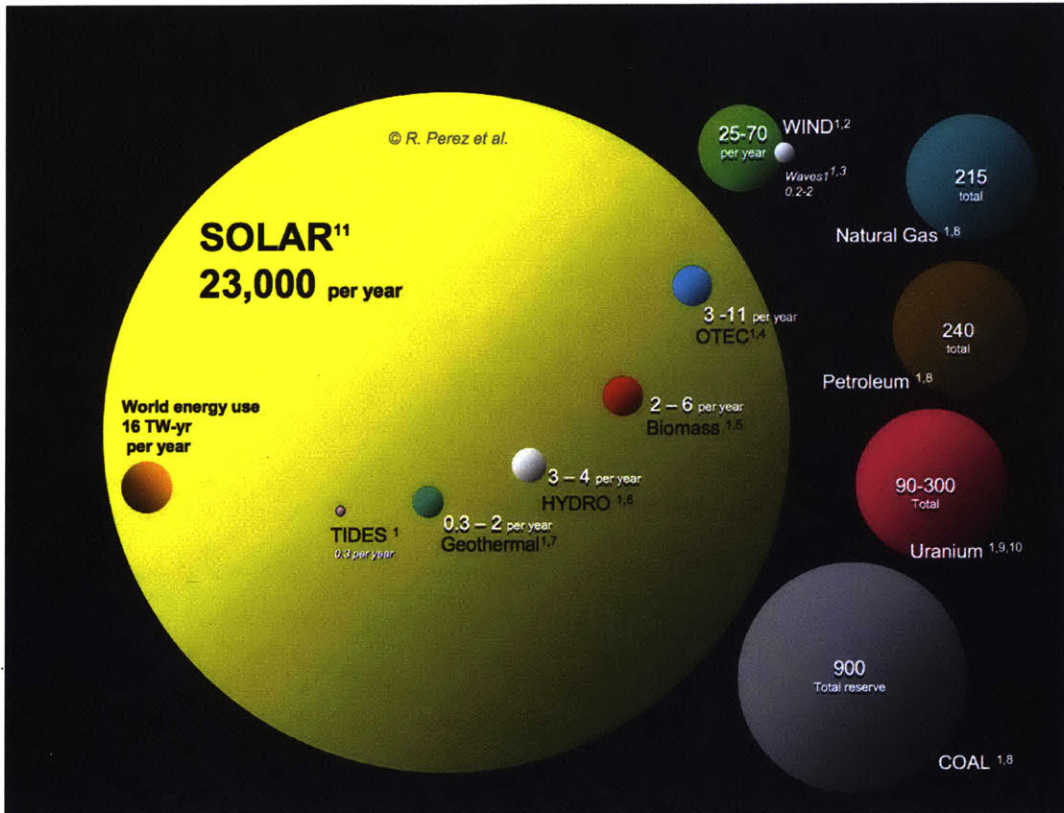
Figure 1-1: The world energy resources. Comparision between finite and renewable energy sources (Terawatt-years). The amount of renewable energy sources is represented as yearly potential while the finite energy sources are represented as the total recoverable amount. Reproduced from [1].
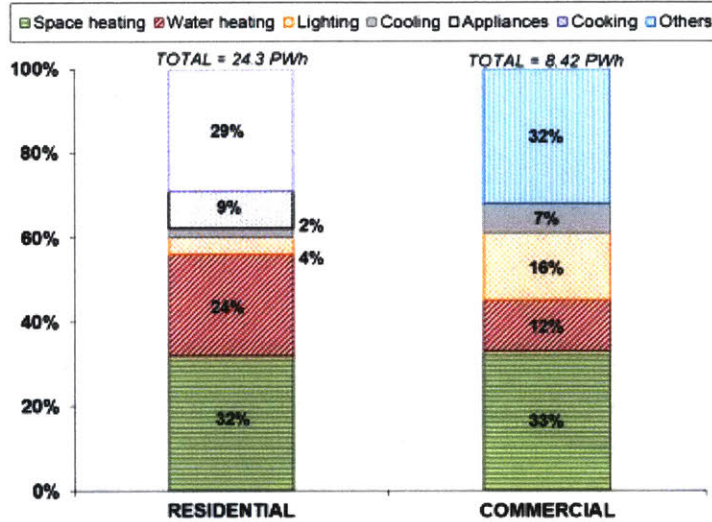
Figure 1-2: Energy consumption in the world in 2010. This shows the residential and commercial energy use distrbution. In both cases, heating holds the majority of energy comsumption. Reproduced from [2]

1.1 Solar Thermal Fuel (STF)

Currently, the most cost-effective approach to storing solar energy employs a solar thermal cycle, concentrating the solar flux to generate heat, which is then stored for some amount of time, typically via thermally-driven phase transitions. Simple versions of such energy conversion and storage are already in use [21] (water-steam, paraffin wax for low temperature, molten salts for high temperature, etc.); however, no existing solar thermal technologies provide capabilities for: i) long term, energy-neutral storage; ii) operation without additional and expensive components and massive, up-front capital costs; and iii) on-the-spot energy collection, storage, and release use[7]. Solar thermal fuels represent a class of materials that has great potential in meeting the requirements mentioned above. This type of fuel reversibly stores solar energy through structural and bond rearrangements of the material, and releases the energy in the form of heat. Thus, STFs operate in a closed cycle, converting and storing the solar energy within the same material. These features of STF allows for favorable properties such as no emissions, easy transportation, being rechargeable and renewable, and energy in the form of heat on-demand.[22] Solar thermal fuels

28

have potential in a number of application areas, including:

- Auxiliary heating in solar thermal plants. The proposed STF may be used for auxiliary heating in concentrated solar power plants; stored latent heat could be stockpiled in a portable, long-lasting, and thermal-loss resistant form that may be used on-demand or at night [23].

- Residential heating. With its simple recharging requirement (the sun) and multiple reuse cycles, the proposed STF may enable residential heating in remote, off-grid areas, as well as opportunities to decrease fossil fuel consumption used for on-grid residential and commercial heating [23].

- Water purification and cooking. Easily rechargeable and reusable modules that use STFs to provide heat for water purification and cooking would be extremely useful in areas that lack clean water supplies and power sources, as well as in various military and humanitarian aid settings [22].

- De-icing applications. With the recharging and storage mechanisms, the STF shows great potential in de-icing without the use of electricity. An important area for this is in electric cars where the use of electricity is critical and de-icing without electricity can greatly benefit the battery lifetime of electric cars.

1.2 Fundamental Background

Solar thermal fuels store solar energy through a photochemical conversion process known as photochromism. The idea of a STF was first proposed in 1909 by Weigert after observing the fuel capability of anthracene photodimerization.[24] This process, by definition, is a reversible chemical conversion between two states, say A and B, induced in either one or both directions through the absorption of electromagnetic radiation [3, 25]. The two states possess different absorption or emission spectra, due to their different physical and chemical properties. A representation of the absorption
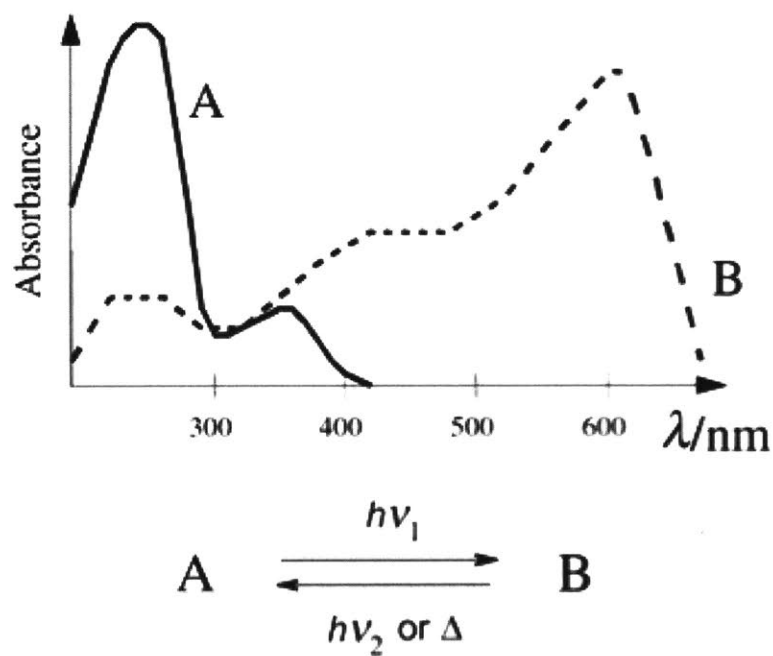
Figure 1-3: Photochromism between A and B. A and B possess different absorption spectra, indicating the difference in their physical and chemical properties. A undergoes a photoinduced transition to B through irradiation energy hv_1. The reverse reaction can occur due to an external trigger such as light energy hv_2 or thermal energy Δ. Reproduced from [3].

spectra for a molecule undergoing photochromism can be seen in Figure 1-3. Form "A" represents the thermodynamically stable form while form"B" is the metastable form transformed from "A" through irradiation. This structural change is reversible and the reverse reaction can occur using external triggers including heat or light. Ideally for practical applications, the photochromic cycle could be repeated indefinitely, although side reactions can occur that lead to subsequent degradation of the process.

As can be seen from the energy diagram shown in Figure 1-4, the photochromic process occurs in the following manner. First, the ground state precursor molecule absorbs photon energy hv and in promoted into an excited state. In the photoexcited state, the molecule undergoes a conformational change. In the new state, referred to as the metastable state, an energy ΔH is stored in the chemical bonds. In order to access this stored energy, an external trigger is applied to the molecule. The stored solar energy is released in the form of heat with the amount being ΔH. While releasing heat, the molecule reverts back to its original form. In Figure 1-4, E_a is the energy barrier for the reverse reaction from metastable state to ground state. The exmaple shown in Figure 1-4 is for the azobenzene molecule, although many different molecules can undergo photochromism, some of which will be discussed in the next section.

For a unimolecular system, photochromism can occur through several possible chemical processes and undergo transformation. Some of these chemical processes are bond cleavage, oxidation-reduction, and isomerization [25, 26] . Of these three, isomerization, or more specifically photoisomerization, is the most favorable photochromism for STF. Photoisomerization is divided largely into two types: E/Z (cis/trans) isomerization and valence isomerization. In the case of E/Z isomerization, a noticeable structural change is observed, while for valence isomerization, no significant steric position difference is seen, rather electronic structures are rearranged. Because E/Z isomerizaration shows a simple mechanism, characteristic differences between the two states, and sizeable quantum yield, this chemical process is well suited for use as STF.
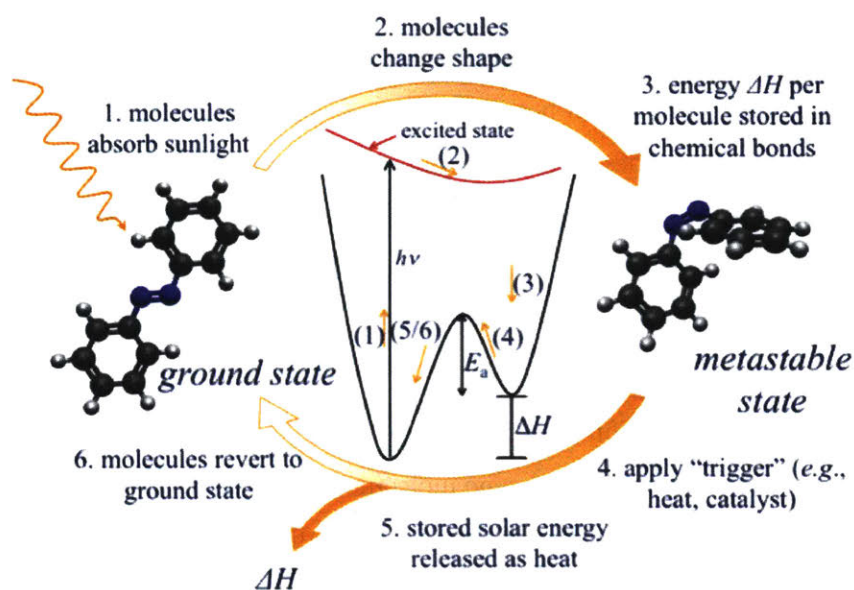
Figure 1-4: Energy diagram for a STF cycle. 1) the molecule absorbs sunlight and becomes excited. 2) in this excited state the molecule undergoes conformatinal changes and 3) the molecule is now in the metastable state with energy ΔH stored in the chemical bonds. 4) the external trigger is applied and 5) energy ΔH is released in the form of heat while 6) the molecule reverts back to the ground state. The STF cycle shown is that of azobenzene.

1.3 Previous Solar Thermal Fuels

Since the idea of STF was first proposed in 1909, many candidates for STFs have been explored. Among the most promising have been the norbornadiene-quadricyclane reaction, the (fulvalene) tetra carbonyl diruthenium molecule, and azobenzene. The case of norbornadiene-quadricylane has perhaps shown the greatest potential as a STF Figure 1-5A due to: (1) a high energy density of 0.97MJ/kg; (2) a high quantum efficiency with long life time; (3) design flexibility due to the fact that both the ground and excited states are in liquid form at room temperature; (4) a simple back-reaction trigger using a transition metal complex catalyst, and (5) easy, low-cost synthesis. [25, 27, 28, 4] Yet, despite all of these advantages, this "champion" STF has several major drawbacks which some of which only recently has been improved: namely, the poor absorption profile of norbornadiene, and critically, the degradation of the system with time, limiting drastically the number of possible cycles and preventing any practical use of this system. Through molecular modification of norbornedine using aryl substituents the norbornadiene-quadricyclane system has shown great improvement of cyclability.[29, 30] However, attempts to improve the absorption profile with sensitizers caused chemical reactions with the photochrome leading to accelerated degradation of the material. [31]

More recently, the photochromic (fulvalene)tetracarbonyl-diruthenium system, Figure 1-5B, showed promising advantages as this organometallic molecule can cycle through the energy storage/release process numerous times without degradation and it circomvents the need for sensitizers.[32] Though highly appealing for this reason, this photochrome still falls short of the requirements for an economically viable technology for two reasons. First, the volumetric energy density of this compound is extremely low (<0.1 Wh/L) [5], making it impractical for both small and large-scale applications. Second and more importantly, Ru, which plays a crucial role in this photochrome, is a rare earth metal and at $3000/kg is far too expensive for a practical solar energy technology.
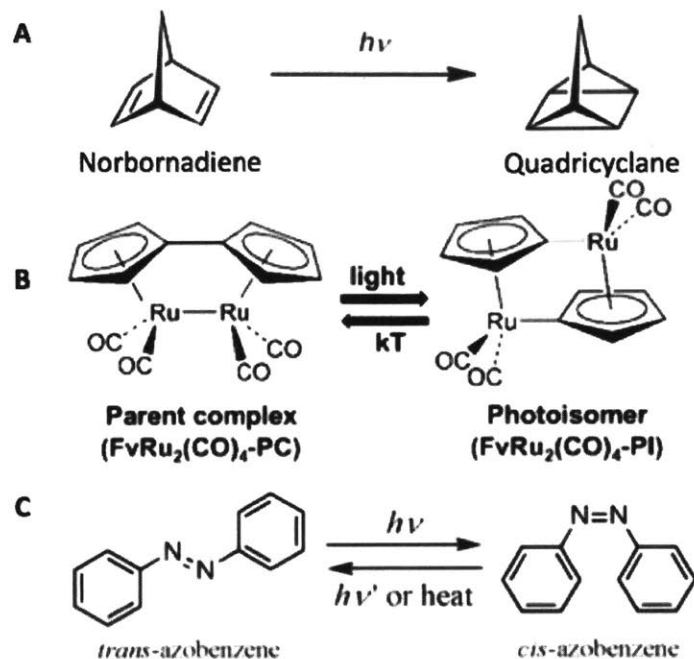
Figure 1-5: The schematic diagram of photoisomerization of A) Norbornadiene-Quadricyclane B) (fulvalene) tetracarbonyldiruthenium9 and C)Azobenzene. Reproduced from [4, 5, 6]

Last, azobenzene (Figure 1-4C) has also been in the spotlight as a potential STF with its promising absorption profile of the photostable state giving a solar conversion efficiency of 10%, high cyclability, and a reasonable thermal reversion lifetime with a half-life of a couple of days. However, pure azobenzene by itself has not been able to meet the requirements for practical applications because of its low energy storage capacity due to the low ΔH of 0.51eV released from the metastable state. Other challenges with azobenzene include a low quantum yield due to the photoinduced back reaction as well as the difficulty in controllably triggering the back reaction [7, 25, 6] Efforts to solve these problems, e.g. by adding substituents, have consistently resulted in the deterioration of other favorable traits such as the thermal reversion lifetime or optical absorption efficiency.[33]

Despite decades of research and promising features as STF, all previous chemistries continue to face challenges. Attempts to improve these materials through engineering of the STFs led to trade-offs of advantageous properties leading to other, often worse

problems to solve. Thus, a new approach to optimize and engineer the STFs properties was greatly needed. Out of the three candidates described above, in this work we focus on azobenzene was to implement new designs for STF applications. Azobenzene holds a large window of opportunities for rich chemical functionalization of the molecule. Azobenzene derivatives also has low cost, facile synthesis, and remarkable chemical stability over repeated operation of photoisomerization and reverse thermal isomerization between trans and cis forms, all of which makes it well suited for STF applications.

1.4 Nanotemplated Solar Thermal Fuels

A novel class of STFs comprising nanoscale templates functionalized with photo-switchable azobenzene derivatives was proposed and both theoretically and experimentally proven.[7, 9] The study was initially carried out through computation for hybrid nanostructures composed of carbon nanotube substrates covalently bonded to azobenzene derivatives. In this design, the photomolecule was imposed on the carbon nanotube in a close-packed and highly ordered array, as shown in Figure 1-6a. This crystalline-like structure provides two key improvements. One is the increase in volume density due to the packing of the photomolecule per volume compared to the solution of free molecules. Second and more importantly, the ordered arrangement in close proximity and steric interactions enables new ways to design the inter- and intramolecular bonding, leading to a predicted increased storage capacity, ΔH, to 1.55eV per azobenzene (compared to the calculated ΔH=0.6 eV for the isolated molecule) (Figure 1-6b). The volumetric energy density of this type of STF was predicted to be comparable to that of state-of-the-art Li-ion batteries and 10,000 times greater than that of the current Ru-fulvalene STF.[21, 7]

As a result of these improvements, the proposed calculation was applied to a wider selection of templates and azobenzene moieties (Figure1-7). This "platform chemistry" showed promising storage energy density, showing that this design principle is
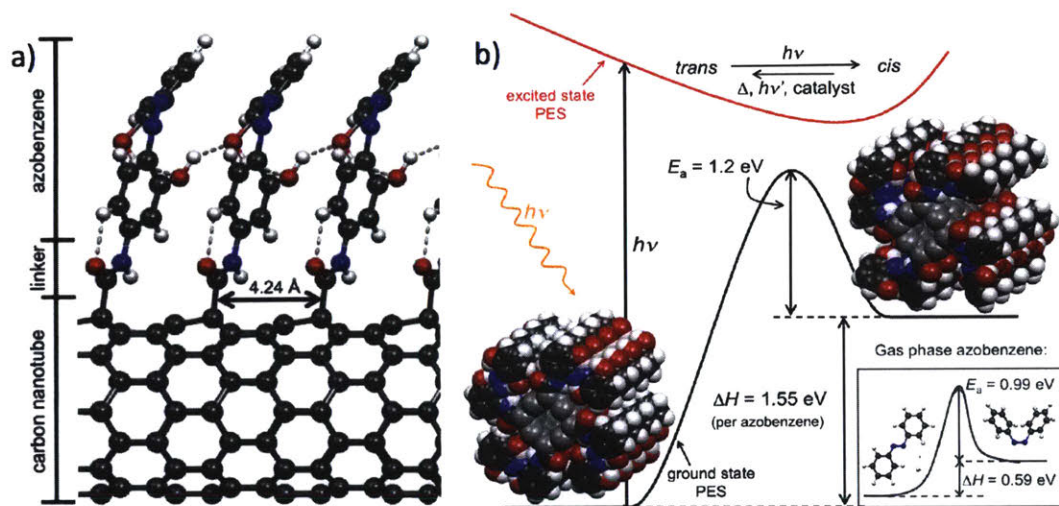
Figure 1-6: Solar thermal energy storage, 2',2',5'- trihydroxydiazobenzene molecules covalently attached to a carbon nanotube. a) Side view of the hybrid nanostructure. The azobenzene derivative aligned along the nanotube axis in a close packed manner resulting in optimal energy density properties. White, gray, blue, and red spheres represent H, C, N, and O atoms, respectively; nanotube carbons are a lighter gray for clarity. b) Energy diagram of the charging cycle of the azobenzene functionalized onto carbon nanotube. The azobenzene/CNT hybrid undergoes a photoinduced trans-to-cis isomerization, storing $\Delta H = 1.55$ eV per azobenzene. A thermal barrier, E_a, prevents the back reaction from occurring under storage conditions; an external trigger controls the release of the stored energy. The inset shows the corresponding parameters for untethered azobenzene molecules. Reproduced from [7]

36
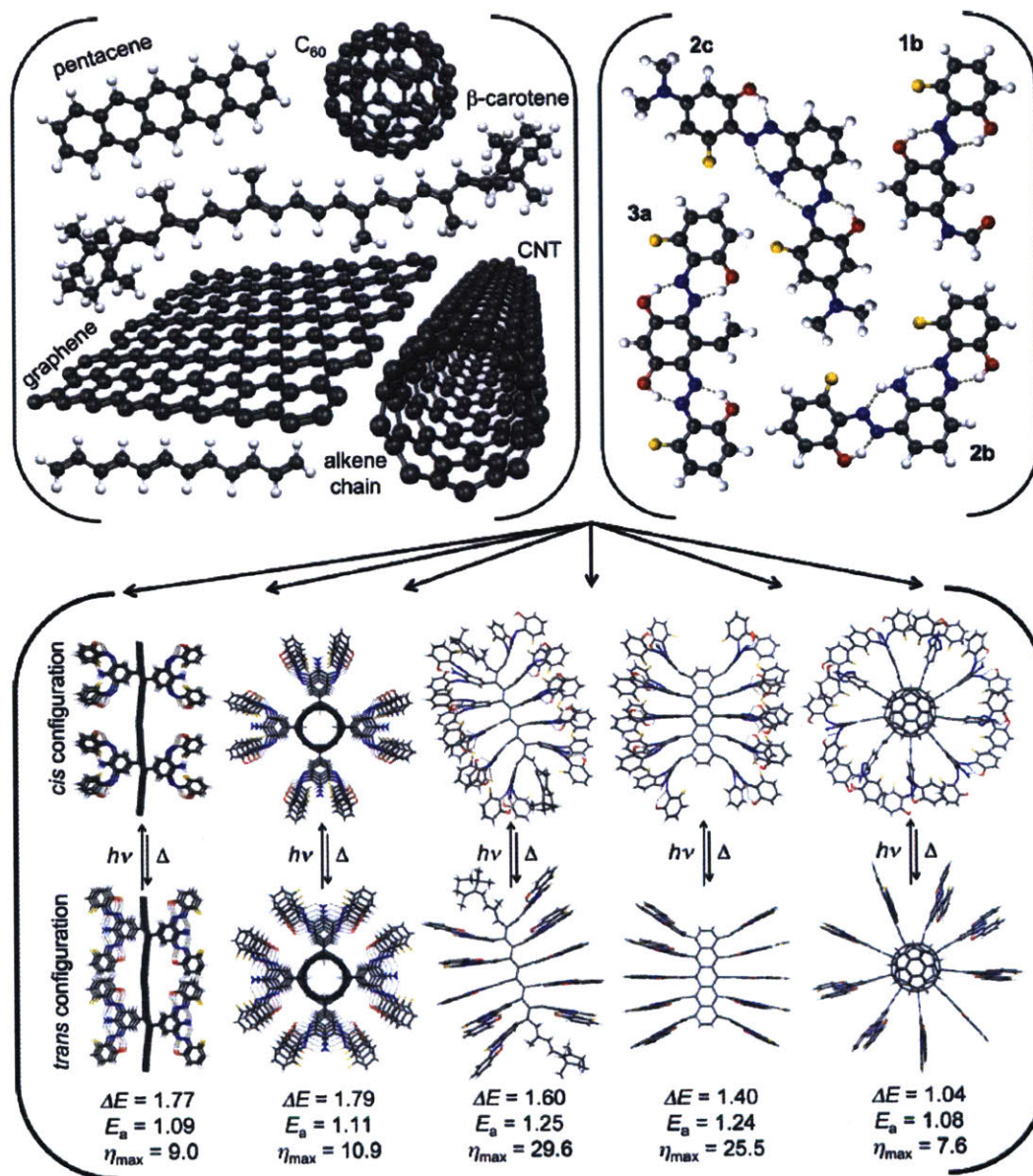
Figure 1-7: The top shows the nanotemplates and azobenzene derivatives. The bottom is the nanohybrid structures with ΔE, the energy stored per molecule, E_a, the energy barrier for the back reaction, and η_{max}, the maximum external energy. Reproduced from [8].

not limited to only carbon nanotube templates and the idea was general giving this novel class hybrid nanostructures great potential as STFs.[8]

Recently, our group experimentally demonstrated that this nanohybrid design improves the properties of azobenzene as a STF, as predicted computationally. The azobenzene functionalized onto a single wall carbon nanotube(Azo-SWCNT) showed photo-switching and thermal isomerization properties. No apparent degradation was seen after thousands of cycles demonstrating the stability of the hybrid system Figure1-8. Furthermore, through an iteration of a radical-initiated functionalization process, record high functionalization of 1 azobenzene per 18 carbon atoms on SWCNT (1/18 functionalization density) has been achieved. In the theoretical studies, the ideal packing density for maximum performance was determined as 1/8 functionalization density. However despite this difference in functionalization density, differential scanning calorimetry on the solid state azobenzene/carbon nanotube hybrid showed an increase in energy density from 56 kJ/mol for the free azobenzene to 124 kJ/mol for templated azobenzene. While the doubling of energy density observed experimentally was encouraging, the discrepancy from the computational prediction (which was a factor of 3 rather than 2 as measured for this case) required further understanding. Subsequent computational studies showed that the difference was not due to the functionalization density, but rather the fact that in experiments the energy storage increase was due to steric hindrance from neighboring carbon nanotubes. For example, azobenzene functionalized in an ordered array at 1/16 functionalization density can interdigitate in terms of the spatial positioning of azobenzenes between neighboring nanotubes Figure1-9. In this structure, the simulations agree well with the doubling observed experimentally.[9]

Both computational and experimental results proved that templating is an effective method in tuning azobenzene properties, bringing a new design space for such types of STFs. Although, the azobenzene/SWCNT increased energy stored per molecule, many trade-off was see,n which will be explained in further details in the next chapter. Carbon nanotube was one of the many templates proposed through computational
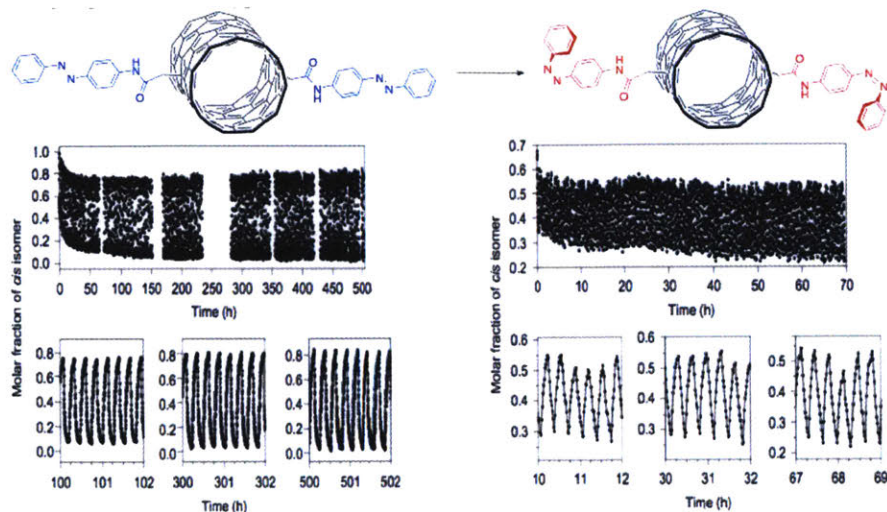
Figure 1-8: Top: Schematic of Trans and Cis Azobenzene functionalized carbon nanotube Botton: Photochemical(left) and photochemical/thermal(right) cycling of azobenzene/SWCNT nanohybrid. Photochemical switching was done through exposure to wavelength of 350nm/450nm light. Thermal cycling was done at temperature of 75°C. Reproduced from [9].
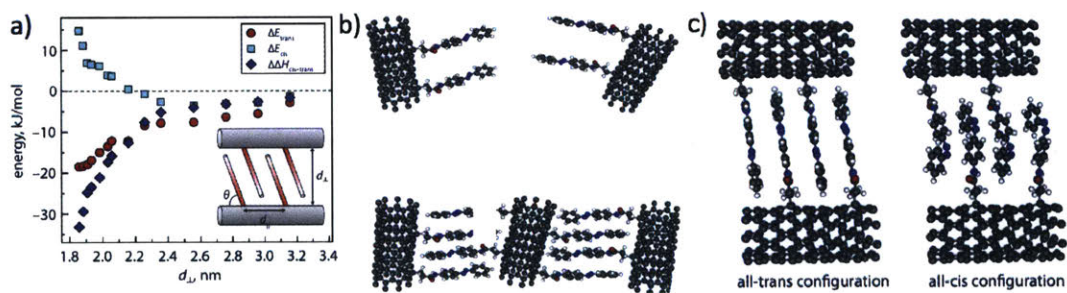
Figure 1-9: a) Enthalphy difference for the intercalated Azo-SWCNTs and the total energy of the trans and cis state as a function of SWCNT separation. Computational study using 1/16 packing density. b) In solution, little change in the stored energy density, Enthalpy ΔH, is seen in the Azo-SWCNT nanohybrids. However, when solid-state differential scanning calorimetry is measured, increase in ΔH is seen showing that a decrease in the distance between azobenzene occurred. c) The computed atomic structures at the minimum-energy separation distance. Reproduced from [9].

39

studies, thus the templating approach needs to be expanded to other materials systems to test the potential of it. Out of the many templates proposed, the polymer template was selected due to the rich chemistry and engineering possibilties of polymers. The next chapter talks about translating this approach to a polymer system, and through synthesis and careful characterization of the new material, new favorable properties were seen.

Chapter 2

Polymer Templated Azobenzene

2.1 Introduction

Most previous approaches for STF focused on use in the liquid or solution state. [34, 9] However, recent templating methods of azobenzene functionalized onto carbon nanotube showed improvements in STF properties in the solid state.[9] Solid state has remained largely unexplored and transitioning fully to the solid-state offers the possibility of integrating STF materials into a multitude of existing solid-state devices such as coatings for deicing, or novel applications such as solar blankets and other consumer oriented heating equipment. The only recent study on such was done on a semi-solid photoliquefiable ionic crystals reaching energy densities of 35 Wh kg^{-1}.[35]

If properly engineered, STF materials could be controllably tailored within the solid-state, although until now, there has not been an efficient method to accomplish this. The most recent STF reports have relied on carbon scaffolds[9, 36] that while successful in some repects (i.e. stored energy density), remain challenging in others including increased synthesis complexity, cannot be deposited into uniform films, the carbon scaffold contributed to the optical density without resulting in photocharging, and introduced uncontrollable morphological effects that may limit charging and

reversible switching in the solid-state.[37] Similarly, single-molecule thin films do not make homogenous layers, can often result in crystallization, and melt at low temperatures ($\approx$70 °C for azobenzene) thus limiting their utility in the solid-state. Fortunately, a wealth of literature exists on azobenzene-based materials in solid-state applications for microswitches, microactuators, and sensors.[38, 39, 40, 41, 42, 43] We postulated that the ideal material class to form solid-state STF coatings would need to (1) form smooth films with controllable thickness, (2) be resilient at high temperatures, (3) preserve the heat release properties of the molecular STF counterparts and maximize the energy density, (4) enable charging, storage, and discharging on device-relevant timescales, and (5) exhibit feasibility for large area heat release applications. In this regard, a polymer solid-state platform was developed, and if engineered correctly, would be sufficiently tunable and scalable to satisfy these requirements. Importantly, the rich chemistry available on both the monomer and polymer backbone enables the application of the same computational design principles previously employed for single molecule STFs,[10] while also revealing a newly accessible engineering space given polymer-polymer chain interactions, cross-linking degree, and conjugation within the polymer backbone.

2.2   Experimental Methods

Density Functional Theory. We carried out standard ab initio calculations within the DFT framework, using the Vienna Ab Initio Simulation Package (VASP, v5.3). Plane wave and projector-augmented wave (PAW) type pseudopotentials with kinetic-energy cutoffs of up to 400 eV were employed, along with the Perdew-Burke-Ernzerhof exchange-correlation functional.

Monomer Synthesis. The monomer was synthesized based on a published recipe.[44] Briefly, phenylazophenol (2 g) was dissolved in tetrahydrofuran (THF, 25 mL) and triethylamine (1.4 mL) in anhydrous and oxygen free conditions. Methacryloyl (3 mL) chloride was added dropwise under inert conditions, while cooling reaction

in an ice bath (resulting in gas evolution, dark color change, and salt precipitate). The reaction was left stirring at room temperature for 48 h. Extraction was done by diluting four times with a 3:1 mix of dichloromethane (DCM) (or chloroform) and water. The organic phase was dried with sodium sulfate and dried under vacuum (<0.1 mbar) overnight. The resultant material was purified in a silica column using 1:1 DCM:hexanes. The overall reaction yield was between 70% and 80%.

Polymer Synthesis. In a typical homopolymerization, the monomer (0.1 g) was dissolved in anhydrous THF (1 mL) and azobisisobutyronitrile (AIBN, 3 mg) was added. The solution was subjected to three freeze/pump/thaw cycles. The reaction was run under inert conditions at 65 °C for 3 h. The polymer was isolated in a solution of stirred methanol and then filtered and rinsed with additional methanol. The reaction is easily scaled to 1 g. Maximum yields obtained were 80%.

Size Exclusion Chromatography. SEC measurements were performed on 0.5 mg mL^{-1} samples in stabilized, High Performance Liquid Chromatography (HPLC)-grade tetrahydrofuran using an Agilent 1260 Infinity system with variable-wavelength diode array (254, 450, and 530 nm) and refractive index detectors, guard column (Agilent PLgel; 5 μm; 50 mm x 7.5 mm), and three analytical columns (Agilent PLgel; 5 μm; 300 mm x 7.5 mm; 105, 104, and 103 Å pore sizes). The instrument was calibrated with narrow-dispersity polystyrene standards between 1.7 and 3150 kg mol^{-1}. All runs were performed at 1.0 mL min^{-1} flow rate and 35 °C. Molecular weight values were calculated using Chemstation Gel Permeation Chromatography Data Analysis Software (Rev. B.01.01) based on the refractive index signal.

UV-Vis Measurements. Absorption was carried out using a Cary 5000, with 100 μm concentrations in a 10 cm path length quartz cuvette. Solid-state measurements were carried out on 1 in. circular quartz substrates. Charging in situ was done using a high-power UV lamp, while cycling was done by optical charging and discharging using an arc lamp and filters to excite the $\pi > \pi^*$ and n $> \pi^*$ transitions of the trans and cis isomers, respectively.

Image Acquisition. Film photographs were obtained using a conventional optical microscope. High magnification images and cross-sections were obtained using a Zeiss Merlin scanning electron microscope by depositing materials on a single crystal silicon substrate.

Solid-State Film Preparation. Spin coating was carried out at 1000 rpm on 1 in. quartz substrates. Films were dried overnight in air ambient conditions. Cross-linked films were made by dissolving the polymer in poly(ethylene glycol) diacrylate (n = 250) under inert conditions and using a 2,2-dimethoxy-2-phenylacetophenone photoinitiator. A UV lamp (3 W) was used to cross-link the film. Thickness measurements were obtained using a DekTak 6.

Charging and Differential Scanning Calorimetry. Solution samples in toluene were charged using a 365 nm 100 W UV lamp while cooled at 25 °C while stirring. Solid-state samples were kept at 30 °C using a cooling stage while charged using the 100 W lamp at a distance of 10 cm. Films were subsequently redissolved in DCM or toluene (solvent had no impact on DSC energy density values). The solutions were dried in DSC pans in the dark and sealed, giving a final mass of 1 mg of material. DSC was carried out using a TA Instruments DSC Q20.

Macroscopic Heat Release.The polymer (100 mg) was charged in a large flask while being cooled to 10 °C first in toluene for 16 h and then transferred to acetone and charged overnight. The charged material was dried using vacuum to a volume of 1 mL and then drop cast in several steps with a 30 min vacuuming step in between. A final vacuum (1 mbar) was applied for 6 h before discharge. Discharging was done relative to an uncharged control on a hot plate while monitoring with an infrared camera (FLIR Ax5).

2.3 Results and Discussion

While several reports have employed azobenzenes as part of the polymer backbone,[45, 46] we instead opted for an approach with more conformational freedom where azobenzene moieties comprised the polymer side chains while simultaneously maximizing the azobenzene density in the form of homopolymers.[47, 48, 49] Figure 2-1a depicts such a polymer, where the backbone is comprised of an alkyl chain while the side chains are made up of azobenzenes. When illuminated with photons of an appropriate energy, the low energy trans-azobenzene molecules would ideally change their conformation to the cis-state, despite any steric effects resulting from neighboring side-chain interactions.

Our chosen monomer along with a synthetic route is shown in Figure 2-1b, where an acrylate group is attached to an azobenzene derivative to enable polymerization with common radical initiators. Given that adding new functional groups can drastically change the energetic[10] and optical[50] properties of azobenzenes, we first verified our intended monomer via density functional theory (DFT). DFT simulations revealed a modest potential energy density of 68 Wh kg^{-1} for the monomer species, indicating the additional substituent had not caused a major change in the expected energy density compared to azobenzene (76 Wh kg^{-1} from DFT).

Size exclusion chromatography (SEC) on the synthesized polymer (Figure2-1c) enabled us to estimate an average of 45 monomer units per polymer chain (referenced to polystyrene), and reproducibly scale to the gram scale with an overall reaction yield of $\approx$60%. Despite a high probability for steric hindrance during synthesis, these polymers grow to sufficiently large sizes and are capable of being dissolved in organic solvents compatible with spin coating in order to make solid-state thin films. Additionally, generating these materials in a facile two-step chemical process presents an attractive avenue toward scalability and inexpensive production.[51]

The key aspect of effective materials design relies in leveraging the excellent prop-
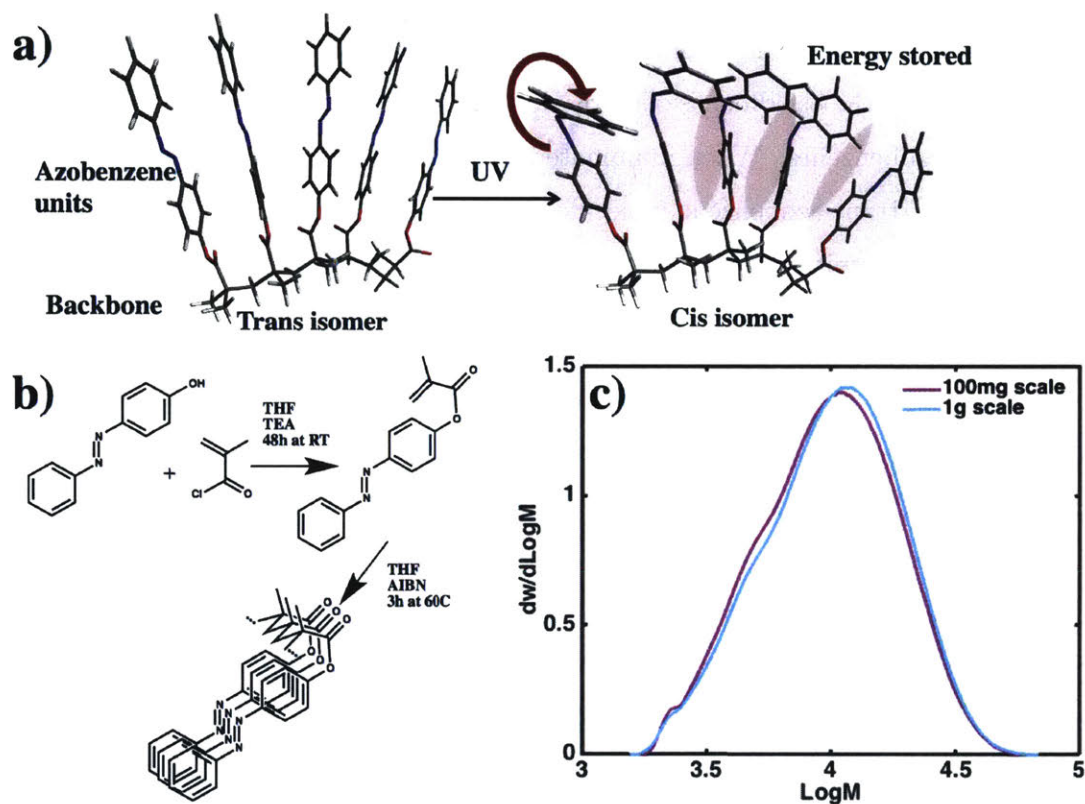
Figure 2-1: Solid-state solar thermal fuel polymer concept. a) A schematic of an azobenzene polymer consisting of four monomers in the trans-state being converted to the cis-state upon UV illumination. The result is the apparent rotation of that azobenzenes about the N=N double bond. b) Chemical synthesis scheme for generating the homopolymer by employing a radical polymerization of an azobenzene monomer. c) Size exclusion chromatography performed to analyze polymer samples and deduce the distribution, as well as reproducibility with a scaled-up synthesis.

erties of certain small molecule STFs and transitioning them into the solid-state in the form of polymers. In this respect, it is important to compare the monomer and polymer moieties to ensure retention of STF properties. Absorption spectra (Figure 2-2a) revealed consistent optical properties between the two materials, with a slight reduction in absorption in the polymer. Similar to azobenzene, the trans-dominant peak exists in the UV at 325 nm, while the cis-state develops an optically accessible peak at 450 nm. As has been extensively reported for azobenzene,[52] exciting these materials via the $\pi > \pi^*$ transition results in the reduction of the high-energy peak and emergence of the low-energy peak. The magnitudes of these peaks play a crucial role in the extent to which solid-state films of the polymer may be charged. In Figure 2-2b, an Eyring-Polanyi plot enables to extract the reverse isomerization energy barrier often denoted as Ea, for the monomer (95 ± 2 kJ mol^{-1}) and polymer (86 ± 2 kJ mol^{-1}). Azobenzene derivatives may be engineered to have a cis-state lifetime spanning several microseconds to days by tailoring the functional groups attached to the phenyl rings.[53, 54] Our materials exhibit room temperature (25 °C) half-lives (time taken for 50% of the cis isomer to decay back to trans) of 92 ± 1 h and 55 ± 1 h for the monomer and polymer species suitable for energy storage in applications requiring daily cycles. Finally, in order to be suitable for long-term use, the cyclability of these materials was tested in Figure 2-2c, where photon sources were used to cycle the materials between the trans- and cis-states; retention of the optical and thus material properties was maintained for over 100 cycles.

In order to transition the materials to the solid-state, several facile strategies are available, such as tape-casting, drop-casting, and spin-coating. The former two techniques generally result in morphologically poor films, however enable high thicknesses, while the latter results in good morphology but at the cost of low thickness or incomplete coverage at low spin speeds. Figure 2-3a depicts the development of our solid-state STF platform by constructing a simple solar thermal energy capacitor (STEC) using a transparent fixed-size 1 in. quartz substrate and depositing the STF materials on top using toluene via spin-coating. Such a device ensures that it is pos-
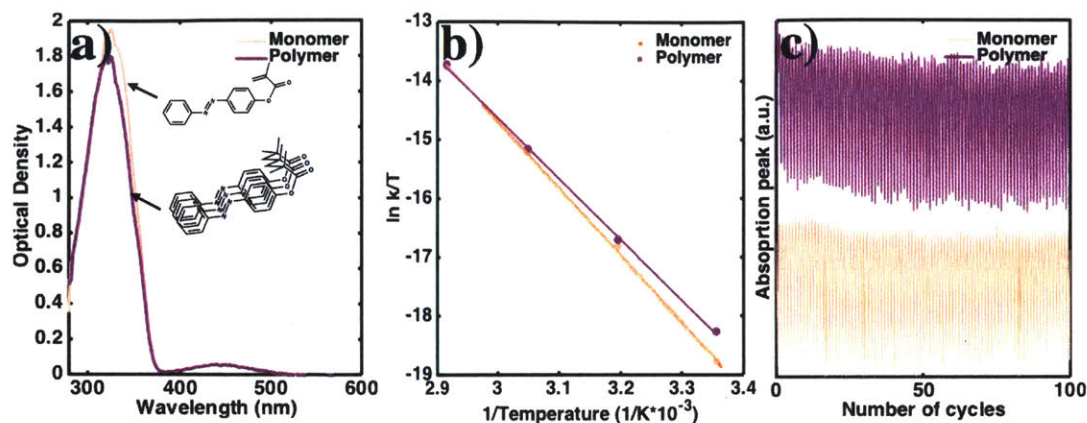
Figure 2-2: Monomer and polymer properties. a) Solution absorption spectra of the monomer and polymer exhibiting two prominent peaks, where the high-energy peak at 325 nm corresponds to the $\pi > \pi^*$ transition enabling trans to cis isomerization. b) Eyring-Polanyi plots used to extract the reverse thermal isomerization barrier energy associated with the discharge process. c) Cycling plots demonstrating the long-term cyclability of the two species to ascertain the feasibility for long-term material use.

sible to monitor the optical properties during charging and discharging cycles, and allows for highly reproducible samples. Upon inspection of optical microscope images comparing the monomer and polymer STECs in Figure 2-3b,c, it is immediately evident that the polymer approach is ideal for the development of smooth and crack-free films. Cross-sectional analysis (Figure 2-3d) revealed that the polymer films are highly uniform in thickness.

In order to see the scalability of the spin-coating process, we experiment with solution concentrations spanning 25-100 mg mL^{-1}, where the latter regime approaches the solubility limit of the material in toluene. Figure 2-3e shows that using the 50 mg mL^{-1} process, more than 99% of the light is absorbed, while the 100 mg mL^{-1} process saturates the detector. In Figure 2-3f,g, the mass and thickness of the STF film is plotted for each type of STEC process (in this case, concentration variation). Importantly, a film of 1 μm has a mass in the range of several milligrams and can already absorb all of the light in the UV region. This result, along with the energy density of the material, is crucial in determining the thickness and charging requirements for the material because while at greater thicknesses and masses the
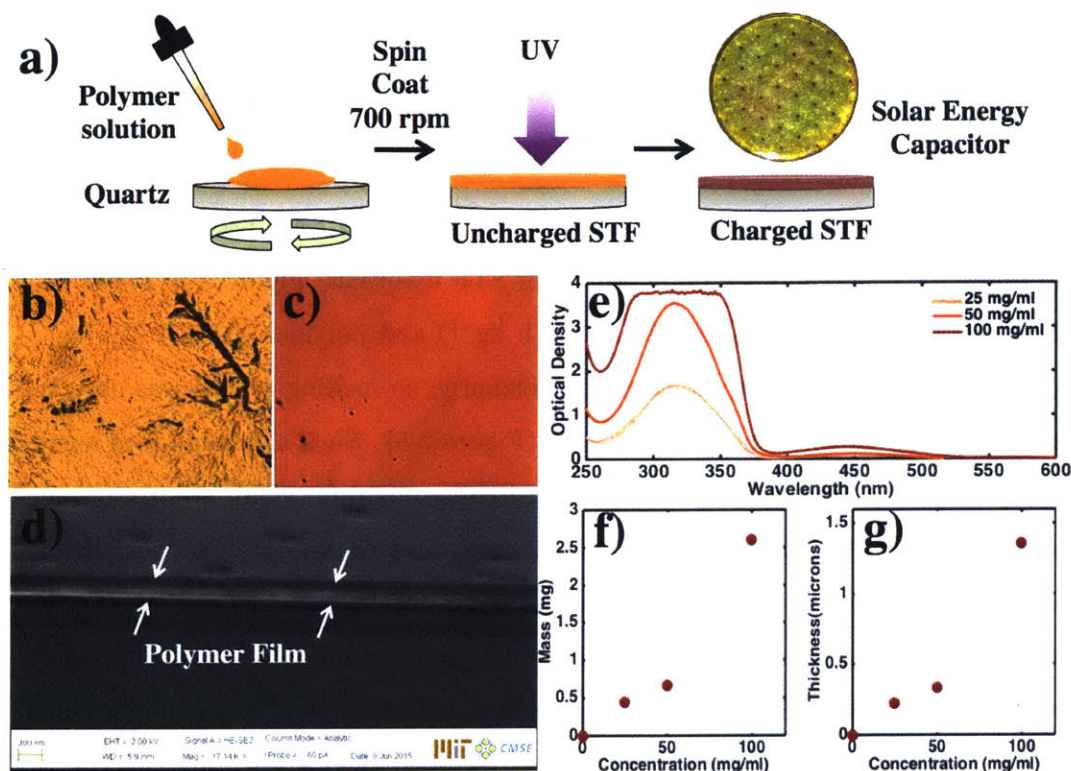
Figure 2-3: Solid-state polymer solar thermal fuel films. a) Schematic of the spin-coating process employing the polymer solution in toluene with a transparent quartz substrate. Charging is accomplished with UV illumination using a lamp centered at 365 nm. Inset shows a 1 in. diameter semi-transparent solar thermal energy capacitor atop a clean room matt. b,c) Color-adjusted optical microscope images of the monomer and polymer spin-coated films, respectively (2 mm y-axis). The polymer films are smooth compared to the highly rough monomer films. d) Cross-sectional SEM image of the polymer film atop silicon exhibiting uniform thickness. e) Solid-state absorption spectra obtained on several samples with variable processing conditions based on polymer STF concentration in solution. f,g) Polymer film mass and thickness, respectively, for the processing conditions in (e).

Table 2.1: Heat storage and release properties of the azobenzene-based monomer and polymer

Property	Monomer	Polymer
Energy density [Wh kg^{-1}]	42±2	29±2
Half-life [h]	92±1	55±1
Cycling stability [no. of cycles]	>100	>100

total energy is increased, the photon penetration depth and thus charging is highly stagnated given some nonunity photostationary cis-state.[55]

Differential scanning calorimetry (DSC) measurements were used to accurately determine the energy storage potential of our STF materials. Figure 2-4a shows heat release curves for the monomer (42 ± 2 Wh kg^{-1}) and polymer (29 ± 2 Wh kg^{-1}) moieties charged in solution (toluene); importantly, no melting regime was observed for the polymer in this temperature range (Figure 2-5). Such a difference in energy density may arise from variation in photoswitching quantum yield, absorption, and thermal reversion barriers, influencing the photostationary state.[55] Steric hindrance may prevent photoswitching in the solid-state due to the presence of both rotation (steric-sensitive) and inversion mechanisms for isomerization,[56, 57] thus limiting the performance of the STECs. In order to test this, we illuminated our polymer STEC with UV (365 nm center mercury lamp) and recorded their absorption spectra. As shown in Figure 2-4, the initial uncharged STEC transitions to a charged state upon irradiation, evident through a reduction in the 325 nm peak corresponding to the $\pi > \pi^*$ transition and emergence of the 450 nm peak (corresponding to the cis n > π^* transition). Upon mild heating (80 °C), the initial spectrum is fully recovered, with more rigorous heat resilience tested at temperatures approaching 180 °C (Figure 2-6). Despite optical evidence of photoswitching, the exact energy density of the STEC must be measured once it is charged in solid-state. In order to achieve this, an STEC (25 mg mL^{-1} process) was charged and redissolved and dried within a DSC pan. As shown in Figure 2-4a, a similar energy density was measured as in the solution-state, with an average energy density of 26 ± 1 Wh kg^{-1} based on five identical trials. Compared to conventional electrochemical storage methods, the

energy density stored within our solid-state STF materials approaches the lead acid battery (30-50 Wh kg^{-1}) and is superior to supercapacitors (0.05-5 Wh kg^{-1}).[58] A summary of the heat release and storage properties of these materials is presented in Table 2.1.

To achieve a large heat release per unit area, the total energy stored within the material is most easily increased with thickness, but at the cost of light penetration. As the material is charged, it consists of an advancing front of newly converted cis isomer (weakly absorbing UV) followed by the uncharged trans portion; however, due to a nonunity photostationary state in these systems, and nonzero absorption by the cis isomer in the spectral region of our UV lamp, the UV penetration will be stagnated thus greatly increasing the charging time. Figure 2-4c shows STECs that have been charged and measured to within 90% of their fully charged state for two different processing conditions. The rise of the energy density as a function of time is very rapid at first but then stagnates. For the 100 mg mL^{-1} process ($\approx$1-2 μm, 2-3 mg), the charging time is more than a day; however, charging still takes place despite over 99.9% of the light being absorbed within the first 400-500 nm in the uncharged film (Figure 2-3e,g). Similar to the charging properties of the STEC, it is important to verify the discharging expectation when transitioning between solution and film. Figure 2-4d plots the relative fraction of remaining cis isomer after charging in both solution and solid-state. Fitting with an exponential decay, the solid-state material can achieve 20%-40% (best, plotted) improvement in the decay constant, extending the lifetime of the charged stage. This is consistent with crystalline-phase azobenzene small molecules having greatly increased thermal activation barriers for the cis isomer in the solid-state. [59] Importantly, such length-scales are sufficiently adequate for daily solid-state applications where energy may be stored effectively for later use.

In order to meet the requirements of a tunable solid-state STF platform, the STEC must have thickness (and thus mass) control well into the micrometer and millimeter scales. Ideally, the spin-coating process could be extended to make multiple layers by repeated deposition cycles; however, we found that repeated exposure to more STF
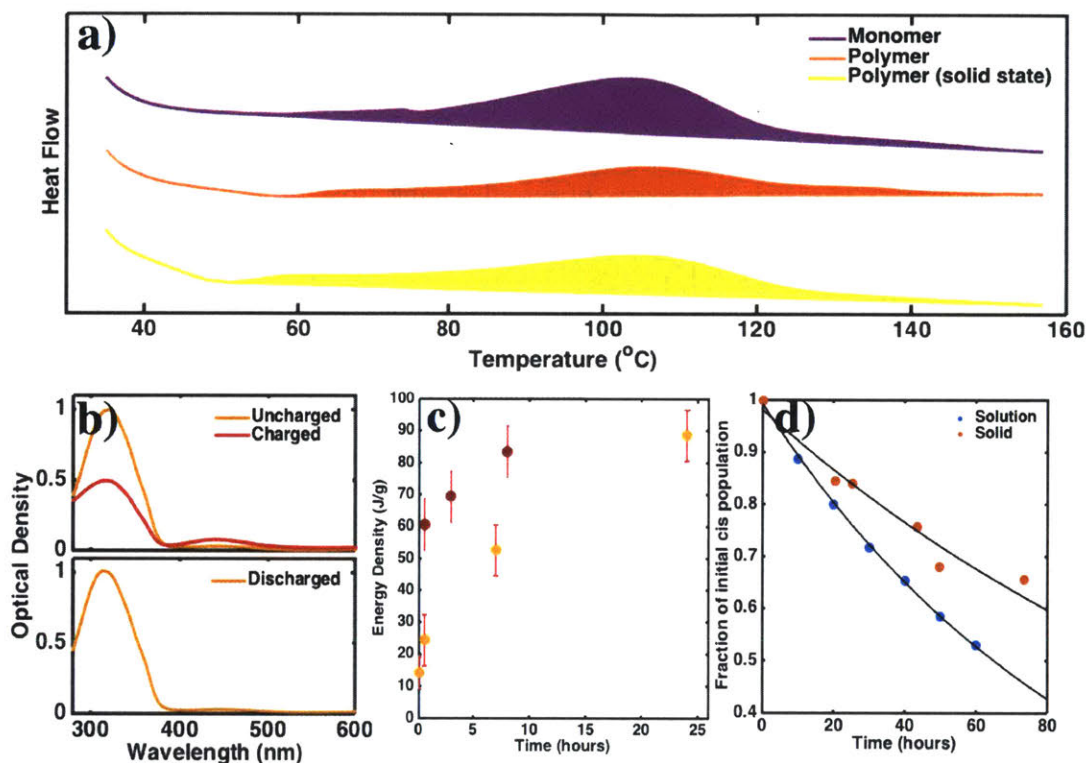
Figure 2-4: Charging, discharging, and thermal properties of solid-state polymer solar thermal fuels. a) Differential scanning calorimetry traces for monomer and polymer charged under various conditions. +y direction represents heat release and the Gaussian regions colored overtop a flat baseline represent the integrated energy release. b) Photocharging of the polymer STF film visualized through absorption. Reduction of the high-energy 325 nm peak and increase in the 450 nm peak is indicative of the trans to cis transition. A single film is first charged (top) and then discharged (bottom) returning to its original state. c) Energy density measured on solar thermal energy capacitors charged in the solid-state as a function of time. With greater thickness the charging time is dramatically increased. d) Comparison of discharging the polymer STF samples in the dark between the solution and solid-state. The solid-state STF polymer has enhanced lifetime for the cis-state.
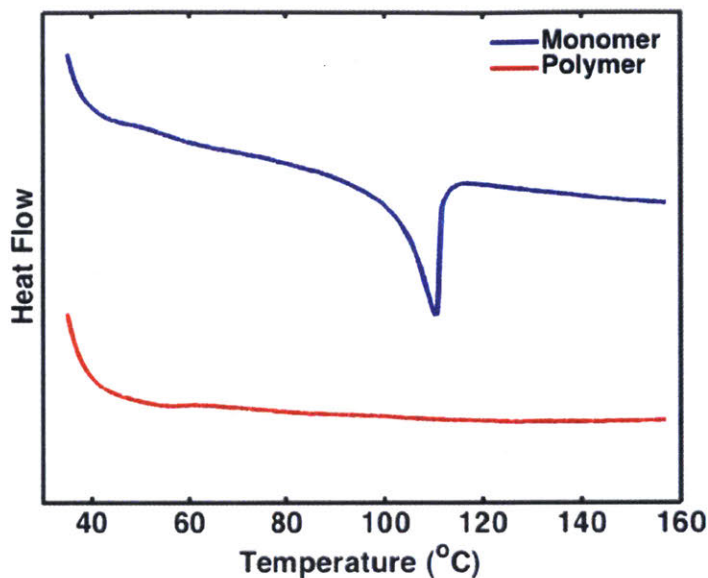
Figure 2-5: Differential scanning calorimetry on discharged materials. The monomer shows melting at approximately 110 °C while the polymer exhibits a flat curve without any peaks. In solid state applications, the melting at these temperatures may not be desireable.
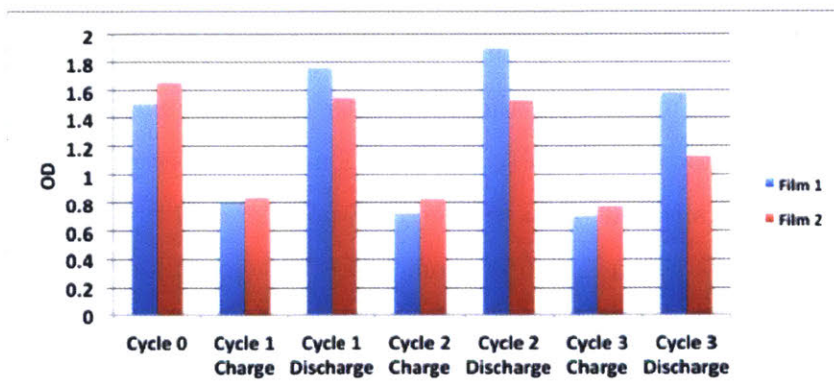
Figure 2-6: Cycling behavior in the solid state. Cycling of solid-state films prepared with the 25 mg/ml process, tracking the 325 nm peak on two films. Discharging was done using a hotplate at a temperature of 150 °C. Variation arises due to having to repeated re-alignment for absorption measurements and slightly different spots on the film being measured after each discharge cycle. Stress testing the film showed a degradation onset at approximately 180 °C observable by eye and from UV-vis spectra.

in a solvent simply redissolved the underlying film. To remedy this, we developed a hybrid scheme where a liquid cross-linking polymer (poly(ethylene glycol) diacrylate PGda, n = 250) was used to readily dissolve our STF polymer. The resultant solution is then spin coated and UV cured (Figure 2-5a) thereby generating an insoluble layer. The film thickness may be controllably increased in such a way, however, with the drawback of a reduction in the gravimetric energy density.

As an initial test of this approach, we were able to generate a thick (>1 mm), flexible, and freestanding polymer STF film (Figure 2-5b) by UV-crosslinking the liquid STF hybrid. This large-scale film was insoluble and showed incorporation of the STF given its orange color. Upon cross-linking, the PGda forms a rigid network that traps the STF polymer inside (Figure 2-5c). Given that the number of PGda units is tunable, such an approach can generate films with different steric properties that could in principle be designed to increase the energy density of the STF themselves.[8] Additionally, the cross-linker may be tailored to have absorption that overlaps strongly with the cis isomer, thus limiting the rate of back reaction and leading to a higher photostationary state. Absorption spectra on single layer films with and without cross-linker (Figure 2-5d) revealed that the cross-linking does not interfere with charging of the STF films, as evident by the reduction of the 325 nm peak after charging. Furthermore, the cross-linker does not limit absorption, given minimal absorption for a comparable thickness film in the spectral region required for the $\pi > \pi^*$ STF transition. However, the STF polymer may prevent cross-linking of PGda itself due to its strong absorption, hence UV crosslinking requires careful balancing of both species.

In order to demonstrate the formation of a layer-by-layer film, the polymer STF was mixed into the UV-crosslinker at a 1:10 STF to cross-linker unit ratio. Tailoring the spin speed enabled to form thin viscous layers atop a silicon substrate that were then readily cross-linked into insoluble solid-state films by UV irradiation. As a proof of concept, three such layers were constructed atop one another and imaged with scanning electron microscopy (SEM). The cross section in Figure 2-5e depicts
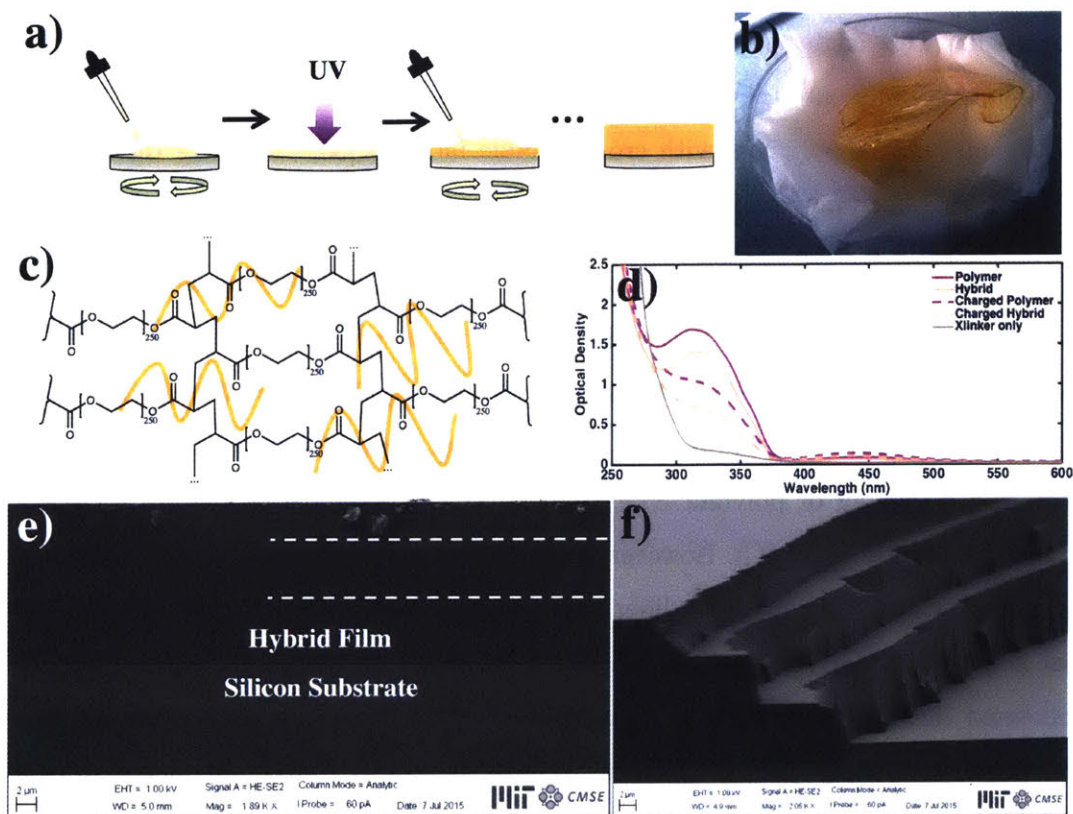
Figure 2-7: Cross-linking approach for layer-by-layer solid-state STFs. a) Cross-linking concept of the STF polymer film employing a hybrid solution of STF and cross-linker. UV curing results in an insoluble layer allowing new layers to be deposited on top. b) Photograph of a freestanding, large area polymer STF film generated using the cross-linking approach. c) Molecular concept for the incorporation of the polymer STF into a cross-linked poly(ethylene glycol) diacrylate matrix. d) Charging properties of the polymer and hybrid films, as well as optical properties of cross-linked poly(ethylene glycol) diacrylate. e) Cross-sectional SEM image of three layer-by-layer hybrid films where individual layers may be resolved (dashed lines), exhibiting exceptional uniformity and adhesion between layers. f) Sheared hybrid film from (e) where three layers may be clearly resolved atop one another.

a thick hybrid film where individual layers may be resolved. To better resolve the three layers, the film was intentionally sheared to reveal the profile shown in Figure 2-5f. Importantly, these films are very uniform, adherent to one another, and present a scalable way to make variable thickness STECs not limited by the spin-coating approach. This engineering concept presents further opportunities to incorporate cross-linking units onto the azobenzenes themselves in order to increase STF loading or to construct co-polymers with cross-linkable moieties,[60, 61] where the ratio of STF to cross-links may be precisely controlled.

Though the charging, discharging, and appreciable energy release have been demonstrated for our STF polymer materials, it still remains to determine their efficacy as macroscale heat-release STECs for realistic solid-state applications. Within the STEC platform, the substrate mass is ≈1.8 g, with a heat capacity of 0.8 J g^{-1}, effectively requiring ≈100 mg of polymer STF to show any appreciable temperature change upon heat release (5-10 °C). However, given the mass required and thickness scaling from Figure 3f,g (approximately linear with mass), a thickness on the order of 50-100 μm is desirable. Given the considerations in Figure 2-4c, such a film would require increased charging requirements. Hence, in order to ensure complete charging and demonstrate macroscopic heat release, we instead rapidly charge our materials at a low concentration (≈1 mg mL^{-1}) in the solution state, where charging and deposition solvents need to be chosen judiciously to maximize the energy density (Experimental Section). Then, we develop a multistage drop casting method in order to build up a thick film, though with greater morphological variation than our spin-coated STECs. In order to measure the heat release, we design an experimental setup that triggers the reverse thermal isomerization using a heating stage (Figure 2-8a), while simultaneously measuring the spatial temperature profile with an infrared camera. The response shown in Figure 2-8b from the uncharged and charged films is vastly different, where after initial stabilization such that the temperature difference between the two films is constant, the charged film temperature sharply overtakes the control film at ≈100-110 °C, consistent with independent DSC measurements. Given the scale

of the experiment, thermal coupling within the system, and some inhomogeneity be-
tween the STECs, the temperature variation was as high as 2-3 °C for control trials
on several uncharged films (Figure 2-9), indicating that the measured result was well
above this temperature variation. To gain a better appreciation for the temperature
release, in Figure 2-6c we normalize the curve at the point where they have both
reached a constant temperature difference ($\approx$160 s, 40 °C in Figure 2-6b) and plot
the temperature difference. A dramatic temperature spike at 220 s results in a $\approx$10
°C average temperature difference between the charged and uncharged STECs. Im-
portantly, this heat release results in a temperature difference on the order of several
tens of seconds, which is important for certain rapid heat-release applications, and
serves as the first demonstration of macroscopic, solid-state application-oriented heat
release from an STF material.

2.4 Conclusion

The development of the solar thermal fuel capacitor platform using polymer films
has enabled the charging, discharging, and heat release using optically chargeable
molecules within the solid-state. Polymer STF materials enable uniform morpholo-
gies that can span thicknesses of 100 nm to several tens of micrometers with added
tunability by employing UV-activated cross-links. By studying the charging and dis-
charging properties, and the heat energy stored within the STECs, it was possible
to construct a macroscopic device resulting in temperature differences as high as 10
°C, demonstrating the feasibility of these devices for solid-state applications. Given
the rich chemistry available on the monomer and the polymer backbone, future ap-
proaches can leverage these additional degrees of freedom to enhance the energy den-
sity, improve the optical chargeability and photostationary state, and collect photons
across a greater portion of the solar spectrum. With such unprecedented materials
flexibility and demonstrated feasibility for solid-state applications, STF materials em-
ployed in the solid-state present a tremendously attractive avenue for both fundamen-
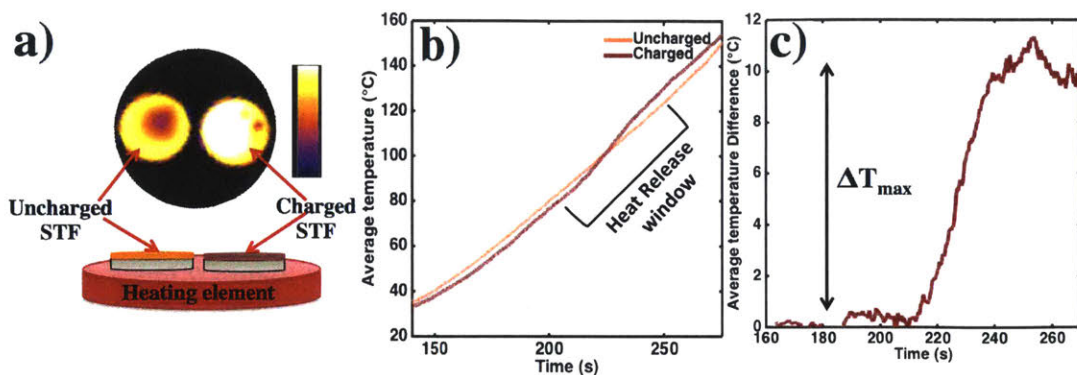
Figure 2-8: Macroscopic STF polymer heat release. a) Top-view IR heat map of uncharged and charged solar thermal energy capacitors (STECs) placed on a heating element, with side-view illustration below. Heat map depicted for maximal temperature difference between samples with color bar indicating relative heat magnitude. b) Average temperature recorded on the surface of each STEC plotted as a function of experiment time. c) Average temperature differences between the two STECs after normalization at the stabilization temperature ≈160 s into the experiment, at least a 10 °C total change (ΔT_{max}) in temperature is observed between the samples due to heat release by the charged STF polymer.
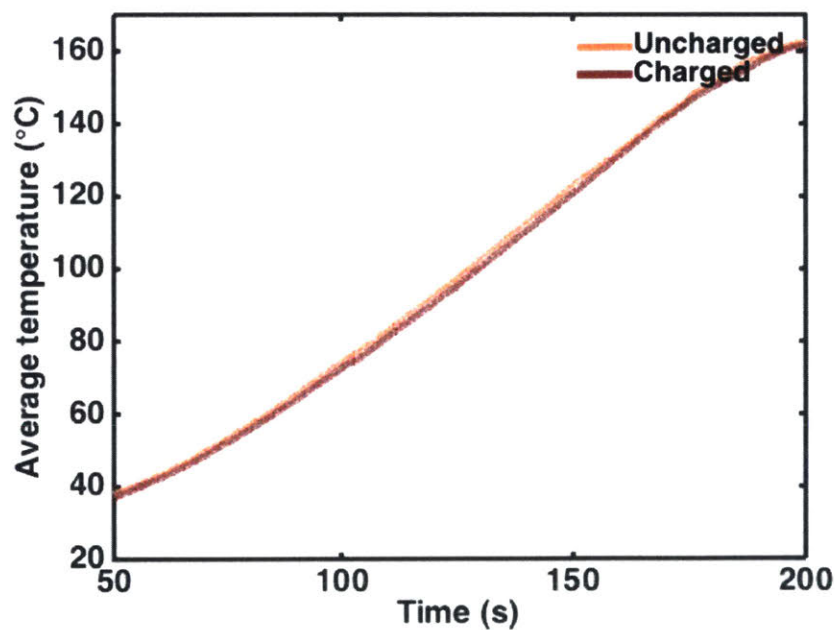
Figure 2-9: Macroscopic heat release control run. Control runs do not show any appreciable temperature difference between two identical uncharged drop cast films.

tal light-matter interaction science and novel solid-state applications for renewable energy storage and heat release.

Chapter 3

Molecular Engineered Azobenzene

3.1 Introduction

The polymer approach from the previous chapter proved successful allowing robust solid-state STF with macroscopic heat release.[62] However, templating the solar thermal fuel molecule onto a polymer presents limitations in chargeability in the solid state, presumably due to the packed azobenzene hindering photoswitching,[63] and shows a substantial reduction in energy storage compared to the monomer. In this chapter, we overcome these limitations by revisiting the design of purely molecular azobenzene-based derivatives targeted for solid-state solar thermal fuels. As mentioned in chapter 2, previous work showed that pristine azobenzene results in poor film morphology due to crystallization, which prevents photoisomerization of the molecule.[64] Solid-state forms of azobenzene have been achieved via functionalization onto gold surfaces,[65, 66] polymer backbones,[67, 68, 69] Langmuir-Blodgett films, [70, 71, 72] and in the form of liquid crystals.[73, 74, 75] Here, we opt for a molecular design of solid-state azobenzene films towards the goal of high efficiency STF applications, where film morphology must be optimized concomitant with energy density, cyclability, and thermal stability. Past efforts to modify azobenzene to increase its energy density, e.g. by adding substituents, have resulted in the dete-

rioration of other favorable traits such as the thermal reversion lifetime or absorption spectrum.[33] Recent computational work on solar thermal fuels revealed that decorating photo-switches with functional groups could result in property enhancement due to both intermolecular[7] and intramolecular[10] interactions. With the aim of probing these sometimes competing properties and using computational work as guidance, here we synthesize and characterize three molecules based on tailored modification of azobenzene. In this work, we choose functional groups that could promote improved solar thermal properties while simultaneously resulting in switchable amorphous thin-films. Suitable chemical modification of azobenzene would ideally maintain photoswitchability while increasing the energy stored per molecule, improve thermal robustness, and stabilize a uniform film morphology in both the charged and ground states.

3.2 Experimental Methods

Synthesis of compound 2. A solution of 2, 2'-dimethyl-5, 5'-dicarbomethoxyazobenzene (200 mg, 0.614 mmol) in THF (8.0 ml) was added to 0.5 M THF solution of 4-biphenyl MgBr (5.5 ml, 2.75 mmol) dropwise in a glovebox under nitrogen. The mixture was allowed to warm to 30 °C and stirred for 24 h. The reaction was quenched by adding sat. NH_4Cl (aq) until the solution turned from brown to orange. The resulting mixture was extracted with dichloromethane and was dried with $MgSO_4$. The solvent was removed under reduced pressure. The crude product was purified by silica gel column chromatography (dichloromethane as an eluent) to give compound 2 (489 mg, 0.556 mmol, 90.5 %). The synthesis scheme, and NMR can be seen in the following Figures 3-1, 3-2, 3-3.

^{1}H-NMR (400 MHz, THF) δ (ppm): 2.58 (6H, s), 5.72(2H, s), 7.27-7.72 (42H, m) ^{13}C-NMR (400 MHz, THF) δ (ppm): 16.23, 80.53, 115.36, 125.92, 126.70, 126.94, 128.46, 128.52, 130.32, 130.55, 139.38, 139.54, 140.83, 146.54, 147.00, 150.11 HRMS (ESI Pos) Calcd for $C_{64}H_{50}N_2O_2$ [M+H]$^+$: 879.3945, Found 879.3965
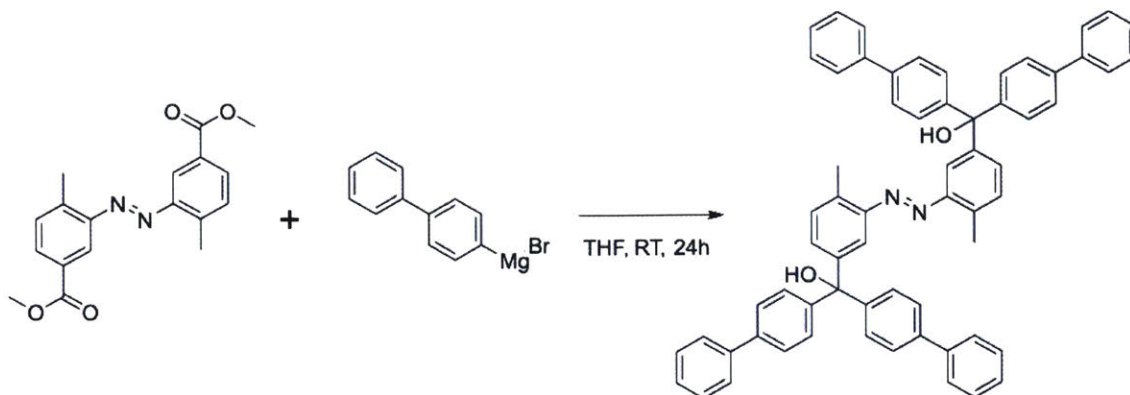
Figure 3-1: Synthesis scheme of compound 2
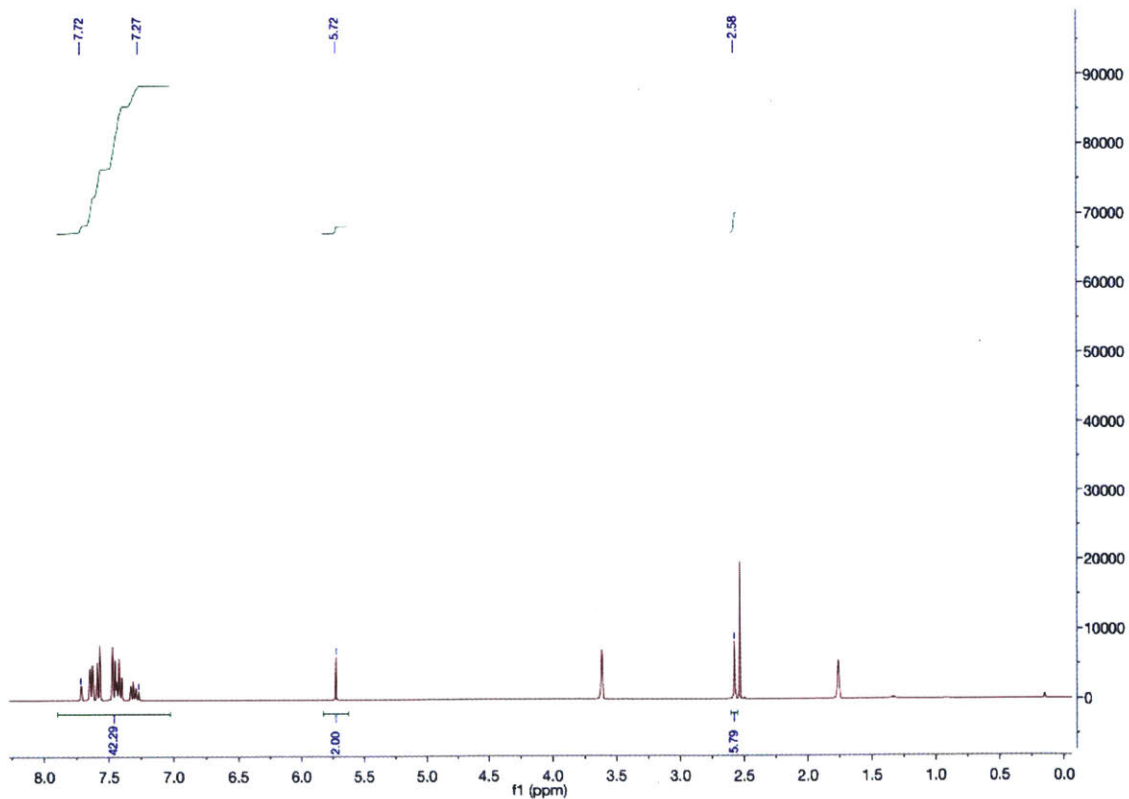
Figure 3-2: ^{1}H NMR of compound 2
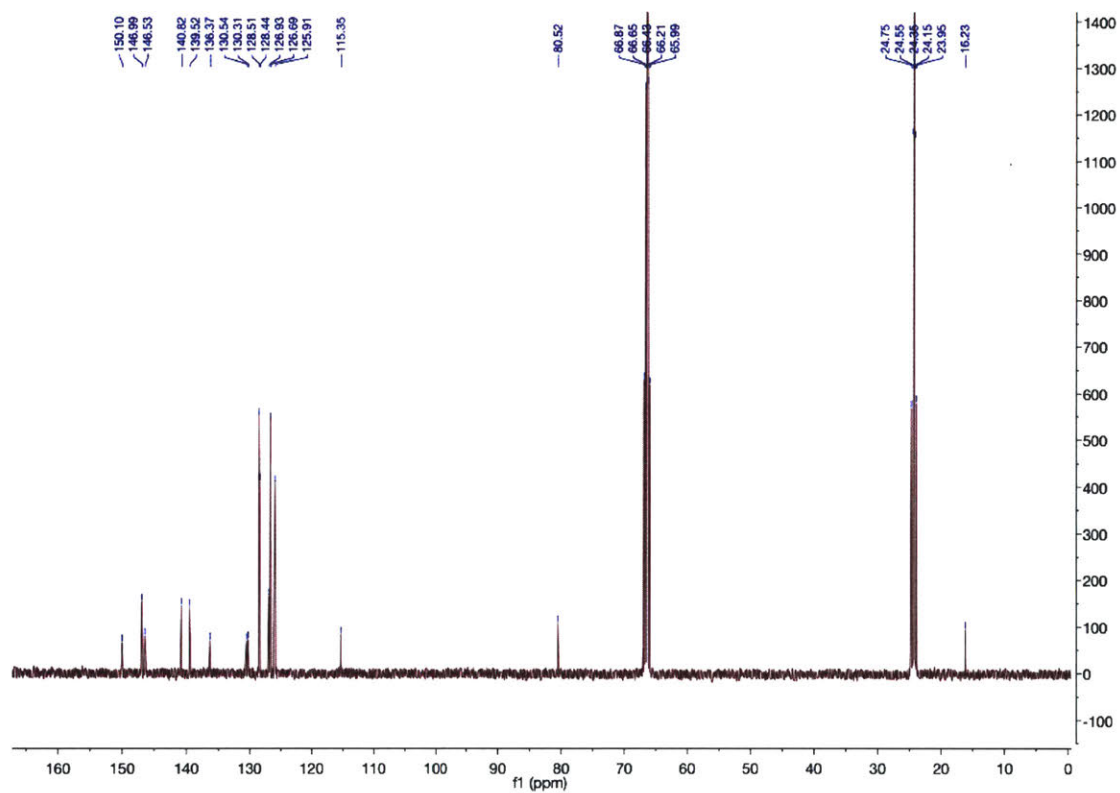
Figure 3-3: ^{13}C NMR of compound 2

Synthesis of compound 3. A solution of 2, 2'-dimethyl-5, 5'-dicarbomethoxyazobenzene (210 mg, 0.643 mmol)) in THF (8.0 ml) was added to 0.5 M THF solution of 4-tert-butyl phenyl MgBr (5.5 ml, 2.75 mmol) dropwise in a glovebox under nitrogen. The mixture was allowed to warm to 30 °C and stirred for 24 h. The reaction was quenched by adding sat. NH_4Cl (aq) until the solution turned from brown to orange. The resulting mixture was extracted with dichloromethane and was dried with $MgSO_4$. The solvent was removed under reduced pressure. The crude product was purified by silica gel column chromatography (dichloromethane as an eluent) to give compound 3 (450 mg, 0.564 mmol, 91.9%). The synthesis scheme, and NMR can be seen in the following Figures 3-4, 3-5, 3-6. ^{1}H-NMR (400 MHz, CDCl3) δ(ppm): 1.34 (18H, br s), 2.55(6H, br s), 2.81(2H, br s), 7.21-7.38 (20H, m), 7.50 (2H, d) ^{13}C-NMR (400 MHz, CDCl3) δ(ppm): 17.07, 31.33, 34.45, 81.56, 115.20, 124.77, 127.53, 130.22, 130.80, 137.03, 143.81, 145.53, 150.03 HRMS (ESI Pos) Calcd for $C_{56}H_{66}N_2O_2$ $[M+H]^+$: 799.5291, Found 799.5306

UV-Vis Measurement. Solution state absorption was carried out using a Cary60 equipped with a Quantum Northwest TLF 50 temperature controller. 39 μM concentration of compound 1 and azobenzene in chloroform were measured in a 10 mm path length quartz cuvette at 25 °C. Solid-state UV-Vis measurements were performed using Cary5000 on a 1in quartz disks. Charging was done by 365 nm wavelength 100 W lamp while discharging was done by heat at 100 °C or visible light in air.

HPLC Measurement. Agilent 1290 UPLC system equipped with a 6150 single quadrupole mass spectrometer was used for the measurement separated using column (Zorbax Eclipse Plus C18 Rapid Resolution HD 2.1 x 50 mm column with 1.8 μm particles) maintained at 25 °C. Single direct injections were introduced via a bypass loop in a Syrris AFRICA Sampler and Diluter, which diluted samples by a factor of $5^{-1}0$ before transferring them into the high-pressure flow path of the UPLC. Image Acquisition. Images of the thin films were obtained using a conventional optical microscope. High magnification images of the thin films were obtained using Zeiss Merlin Scanning Electron Microscope on a single crystal silicon substrate.
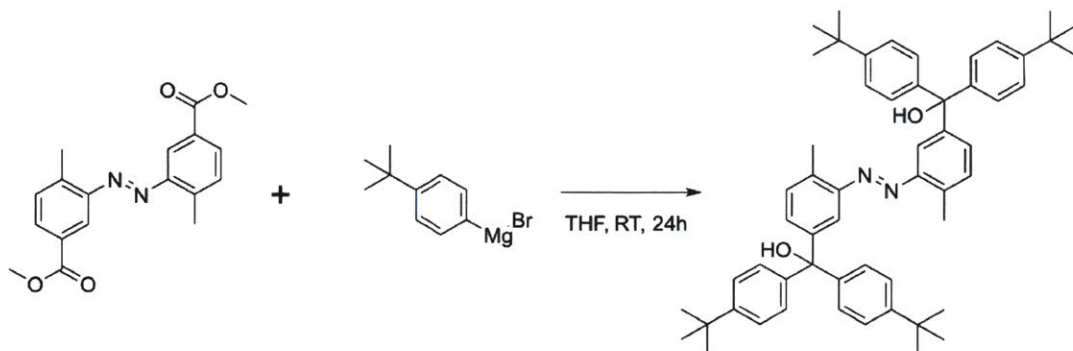
Figure 3-4: Synthesis scheme of compound 3
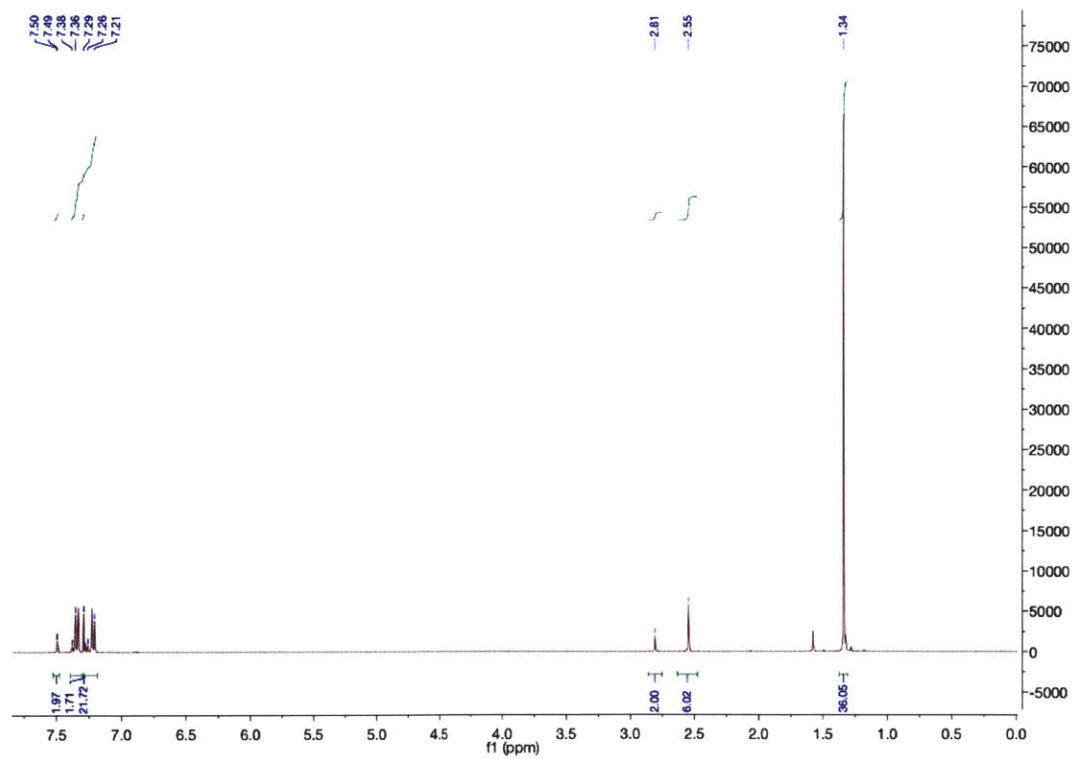
Figure 3-5: ^{1}H NMR of compound 3
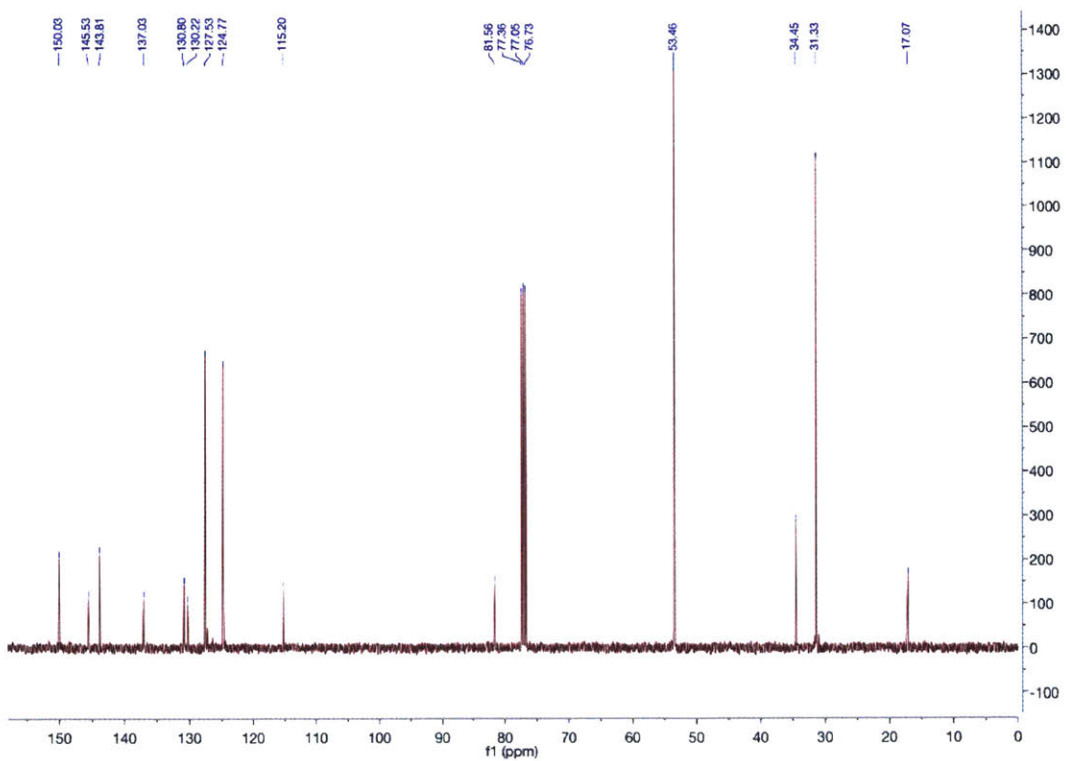
Figure 3-6: ^{13}C NMR of compound 3

Differential Scanning Calorimetry (DSC) measurements. Samples were charged in a stirring solution using 365 nm 100W UV lamp while cooled at 20 °C until photostationary state was achieved. The solution was then concentrated by drying the solvent and was transferred to the DSC pan which was then fully dried under vacuum. The measurement was taken at a rate of 5 °C/min. The ratio between the cis and trans was obtained using HPLC. The measurement was taken using TA instrument DSC Q20.

Solid-State Sample Preparation. The solid-state STF samples were prepared in THF based solution of azobenzene and compound 1 with 30 mg/mL and 25 mg/mL respectively. The THF based solution was then dropcasted onto a 1 in quartz disk and spincoated at 1000 rpm. Compound 2 and compound 3 solid-state samples were produced similarly using 45 mg/mL and 50 mg/mL solution of THF, respectively. The film thickness of the sample varied between 400 and 600 nm.

Raman Spectroscopy and Fluorescence Spectra. Raman spectroscopy and fluorescence spectra were done on a Horiba Labram HR800 Raman Spectrometer using a He-Ne laser (633nm wavelength) through a 100X objective. The solid-state samples were dropcasted from chloroform for all three of the compounds. The measurements were done on a temperature control module. The temperature resolved fluorescence spectra was taken on the cis state film of compound 1, temperature being ramped up at 5 °C/min. The trans state film was done similarly but stopped every 25 °C and held for 5 min for compound 1, compound 2, and compound 3. Optical image of the film was taken during each stop.

X-ray diffraction. XRD was done on Bruker D8 Discover GADDS with a stationary area detector with the center at 30deg 2θ. The sample to detector distance was 16.25cm. The sample was prepared by dropcasting methods with solution of compound 1, 2, and 3 in THF with concentration 20mg/mL, 40mg/mL, and 46mg/mL. The solution was dropcasted onto 100 orientation silicon substrate with the substrate heated to 45 °C. The variation of temperature was done *ex-situ* by heating the sample

on a hotplate for 5min at temperature starting at 25 °C with increment of 25 °C to 150 °C. XRD measurements were taken at each step.

Solid-State Chargeability Measurements. The chargeability measurement was done by charging the sample *ex situ* with UV light and characterized with solid-state UV-Vis measurements. Compound 1, compound 2, and compound 3 samples were prepared by spincoating on 1 in quartz disc with the solution concentration of 0.06 M in THF for each compound. The sample was then heated to 50 °C for two hours to get rid of any residual solvent while allowing the film to change to the trans state. The sample was exposed to the 365 nm light for 20 seconds at a time in the beginning. After each exposure, solid-state UV-vis measurements were taken. As the change in the absorption decreased, the exposure time was gradually increased, up to 60 seconds.

Reversible solid-state charging and discharging of 2 and 3 films. Charging was done using 365nm wavelength 100 W lamp and discharging was done thermally at 110 °C. The sample was prepared using dropcast method of saturated solution of compound 2 and 3. Variation arises due to repeated realignment for absorption measurements and offset in spot area on the film for each measurement.

3.3 Results and Discussion

3.3.1 Design of Solid-State Solar Themal Fuel Molecules

When trans azobenzene (Figure3-7(a)) is exposed to UV light (300-365 nm), the molecule photoisomerizes to the higher energy cis state. A modified molecule was selected base on criteria from computational work[7, 10] that is expected to increase the cis/trans energy difference, shown on the right side of Figure3-1(a) (referred to henceforth as compound 1). The addition of a bulky phenyl group causes the cis form to achieve a higher energy state due to the repulsion and steric hindrance, increasing
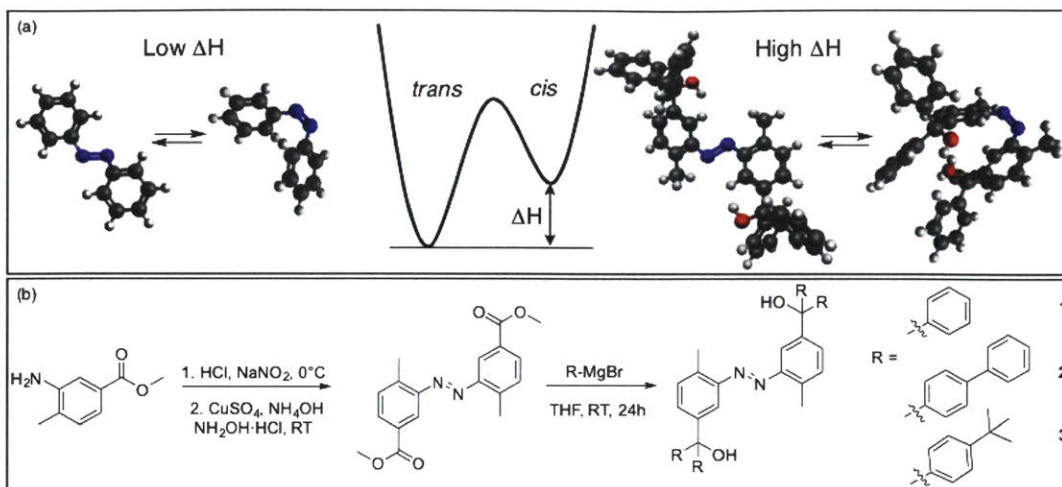
Figure 3-7: (a) Comparison of trans and cis forms of pristine azobenzene and the trans and cis forms of functionalized azobenzene predicted computationally (referred to as compound 1).[10] The energy diagram and the difference in energy stored ΔH is shown. (b) Schematic of synthesis of compound 1-3 via the diazotization of an aniline precursor followed by the addition of different aryl groups using Grignard reagents.

the energy difference ΔH between the trans and cis states. Beyond increased energy density, the addition of bulky phenyl groups to the azobenzene base molecule is expected to improve solid-state film formation, by promoting amorphous thin films, although the interplay between energy density, photoswitchability, crystallization, and temperature robustness is unknown. In order to understand and explore these properties further, we synthesize two additional variations, one with the addition of a biphenyl group (compound 2) and one with a tert-butyl phenyl group (compound 3). The synthesis of these three molecules is shown schematically in Figure3-1(b), where starting from the precursor material, a two-step prroess was adapted from previous work on the synthesis of compound 1 for catalyst applications.[11]

3.3.2   Optical and Thermal Properties of Compound 1

The azobenzene molecule possesses two main absorption features resulting from the $\pi \rightarrow \pi^*$ and $n \rightarrow \pi^*$ transitions (Figure 3-8(a), top). In the trans state, the dominant $\pi \rightarrow \pi^*$ transition absorption peak lies at 325 nm and the much weaker $n \rightarrow \pi^*$ ab-
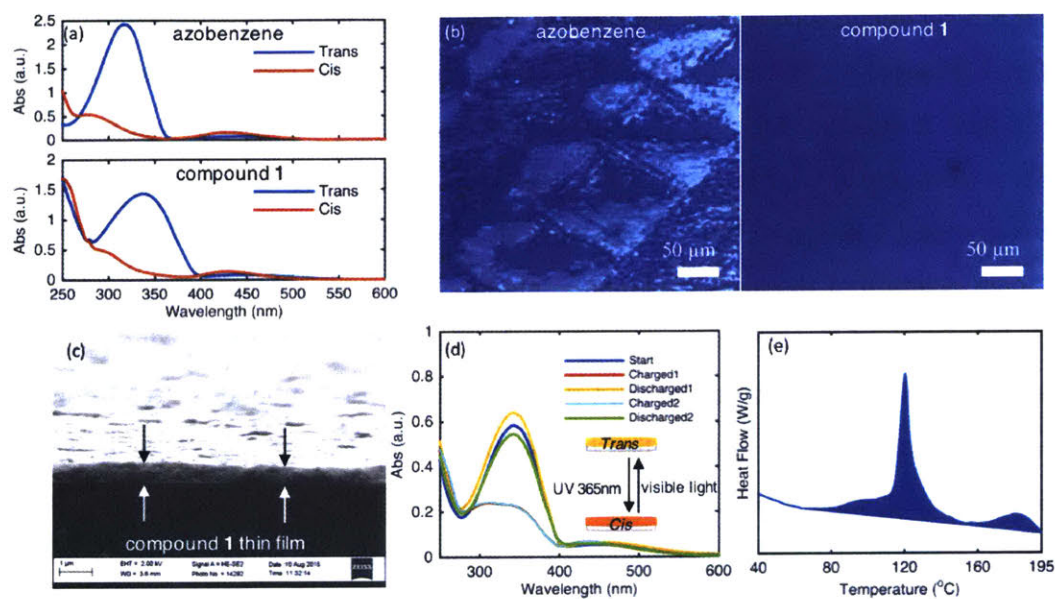
Figure 3-8: (a) UV-Vis absorption spectra of azobenzene (top) and compound 1 (bottom) for comparison, showing a red shift in the trans $\pi\to\pi^*$ transition from azobenzene to compound 1. (b) Optical image of spin coated azobenzene (left) and compound 1 (right) on quartz disks. (c) Cross-sectional SEM of compound 1 film; (d) UV-Vis spectra of compound 1 film upon cycling via UV and visible light. The red line (Charged1) is behind the cyan line (Charged2) (e) DSC trace of 95% cis compound 1 at 5 °C/min scan rate.

sorption peak is at 450 nm. When the molecule is photo-isomerized to the cis state, the $\pi \rightarrow \pi^*$ transition peak disappears while the n$\rightarrow \pi^*$ peak shifts to 430 nm. For compound 1, the $\pi \rightarrow \pi^*$ transition red shifts to 347nm in the trans state, with little change for the n$\rightarrow \pi^*$ absorption upon photo-excitation to the cis state (Figure3-8(a), bottom). Exposure to a 365 nm wavelength UV light source at the photostationary state (over 12 hour exposure) gives a trans: cis ratio of 5:95 as confirmed by liquid chromatography-mass spectrometry (LC-MS). Comparison of spin-coated thin-films under optical microscope reveals non-uniform morphology for the pristine azobenzene material (Figure3-8(b) left) and smooth crack-free coverage for compound 1 (Figure3-8(b) right). A cross-sectional SEM image (Figure3-8(c)) of compound 1 confirmed the uniform thickness of the film. The difference in film morphology between azobenzene and compound 1 is due to the bulky phenyl groups on the tertiary carbon center on the meta position of the azobenzene molecule in compound 1, which causes a break in the planarity of the structure preventing the molecules from crystallizing.[76, 77] This allows photoisomerization of solid-state thin films of compound 1. Retention of absorption characteristics was verified by comparing solution and solid-state spectra, which indicated minimal change in the spectra (Figure 3-9). Optical cycling experiments in solution and NMR of compound 1 in solution after extended period in room light can be seen in Figure ?? and ??. Photo-induced isomerization was used to test the charging and discharging properties of the films, with UV light at 365 nm at room temperature to charge the film (12h) and visible light (3h) to discharge the film. The state of the film was measured using UV-Vis absorption with two cycles taken for compound 1 as shown in Figure3-2d), and no visible morphology change was observed over such optical cycles. This switchability in the solid-state for the compound 1 film is in contrast to that of azobenzene, for which the crystal structure prevents isomerization under illumination due to the lack of free volume.[78]

The enthalpy difference between cis and trans isomers was determined using differential scanning calorimetry (DSC) in the solid-state (Figure3-8(e)), which showed a heat release (4 measurements) of 134 $\pm$ 6 J/g or 77 $\pm$ 3 kJ/mol for compound
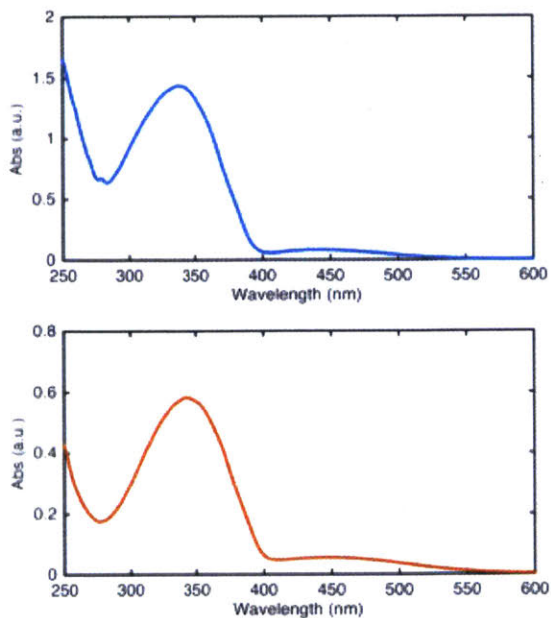
Figure 3-9: Solution-state and solid-state absorption spectra of compound 1. top: UV-vis spectra of compound 1 in chloroform. bottom: UV-vis spectra of compound 1 thin film
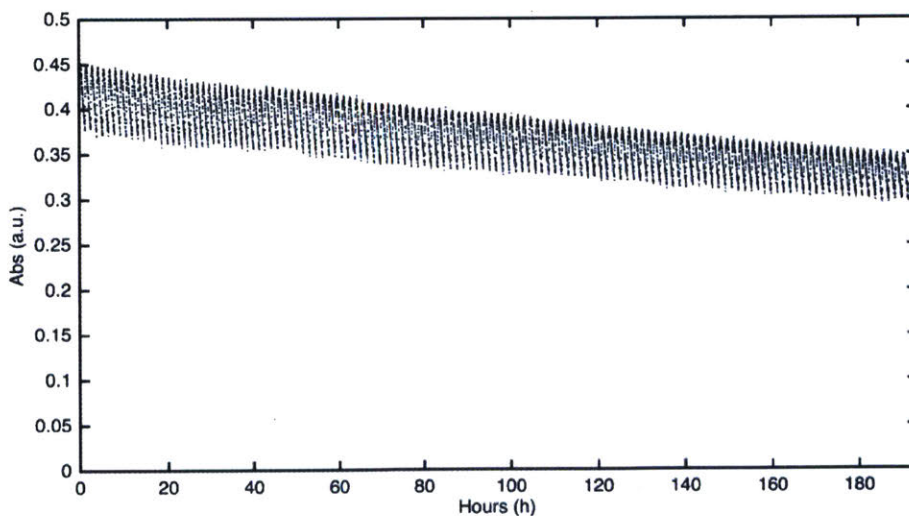
Figure 3-10: Optical Cycling of compound 1 measured using UV-Vis spectroscopy. The cycling was done in $CHCl_3$ by irradiating at 340nm and $\geq$450nm. The solution was irradiated at 340 nm for 60 min while irradiated at $\geq$450 nm for 20 min. The optical cycling was done over a span of 100 cycles.

73
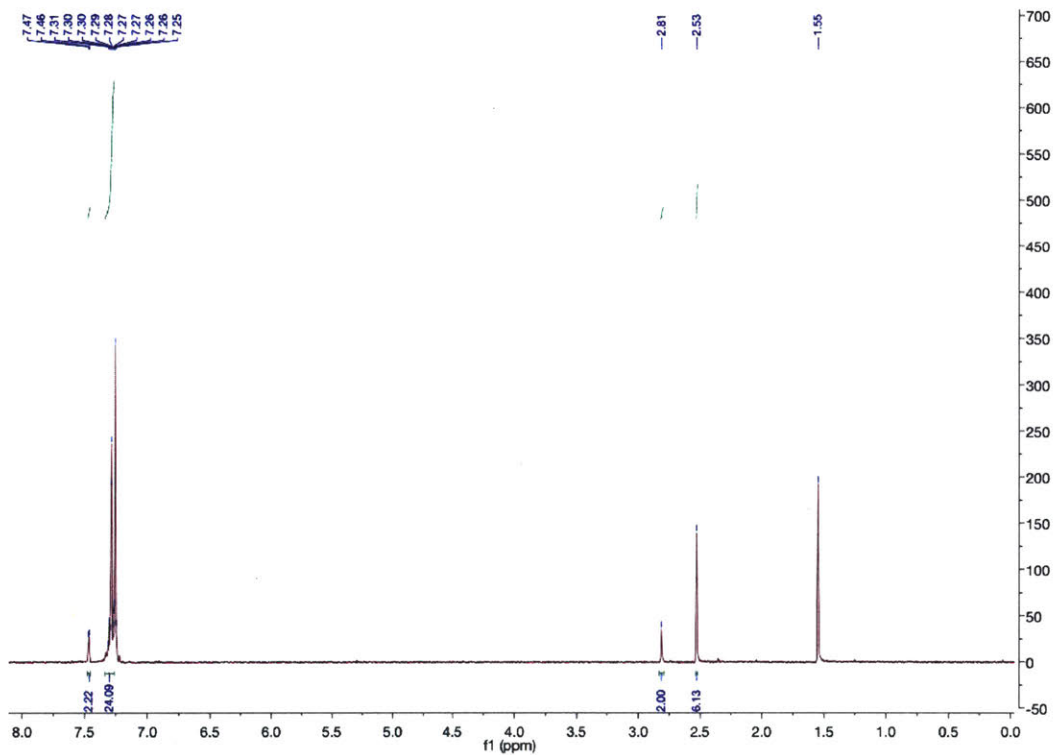
Figure 3-11: NMR of compound 1 in CDCl$_3$. Compound 1 was exposed in room light for extended period of time. Below is the NMR signal reported in literature. [11] ^{1}H-NMR (400 MHz, CDCl$_3$) δ(ppm): 2.53 (6H, br s), 2.83(2H, br s), 7.28 (24H, br s), 7.47 (2H, br s)

1, significantly larger than that of azobenzene (49kJ/mol) and over a 30% increase from the polymer azobenzene.6,10 In contrast to azobenzene and azobenzene template structures that typically yield one exothermic peak for the cis to trans release of stored heat,[9, 62, 79, 36] compound 1 showed two peaks, which reveals an important aspect of proccessing small-molecule films as STF materials, as will be discussed below.

3.3.3 Analysis of Thermal Properties of Compound 1

Thermal isomerization properties can change depending on the environment in which the azobenzene molecule is placed.[80, 81] To further understand the DSC results, the morphology change of the compound 1 film under varying temperatures was analyzed using an optical microscope and Raman spectroscopy. A cis compound 1 film was made by dropcasting a solution of compound 1 in chloroform that has reached the photostationary state (95% cis) through illumination. The dropcasted film showed relatively uniform morphology. At around 107 °C, the cis compound 1 molecular film was observed under the optical microscope to form the droplets (Figure3-3(a)) as well as a drastic increase in fluorescence. The sudden drop in the fluorescence to zero at 107 °C is due to the formation of the droplet and the laser losing the compound 1 target. The laser was immediately refocused on the droplet for the measurement shown by the recovery of the fluorescence signal. Increased fluorescence occurs in azobenzene when the conformational freedom is restricted and isomerization is inhibited by the surrounding environment.[82, 83] Fluorescence starts to decrease once enough thermal energy is present for the switching.[9] After peaking at 117 °C, the fluorescence decreased and then started to increase again at 125 °C showing that the conformational freedom is restricted once more.

In order to test the effects of morphological changes, DSC was carried out on an 82% cis sample, ramped once to 150 °C, cooled down to 25 °C, then ramped to 200 °C (Figure3-3(b)). This showed a single peak during each of the ramps, indicating that
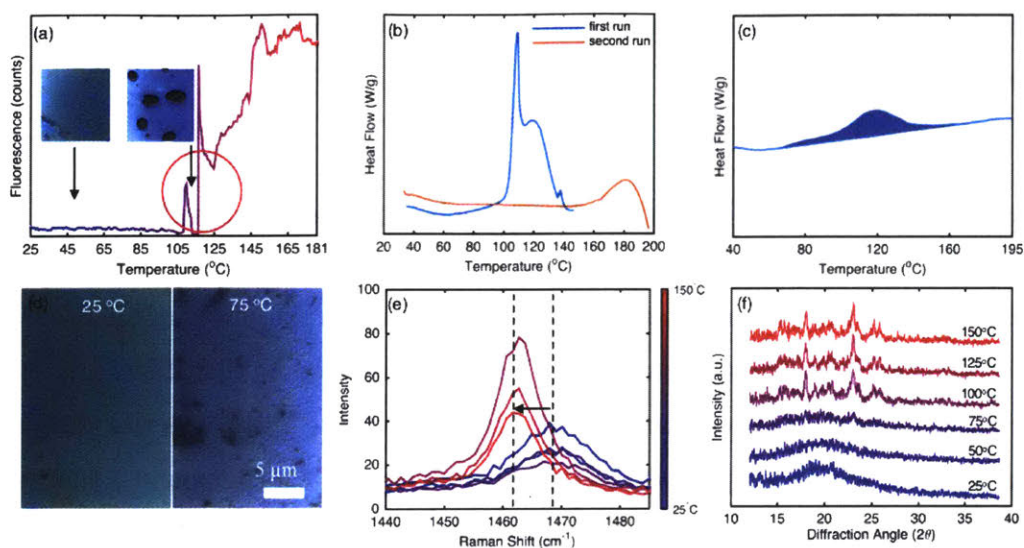
Figure 3-12: (a) Temperature resolved fluorescence spectra of cis compound 1 in the film state.) Temperature vs. Fluorescence spectra was averaged over a range from 1250 cm^{-1} to 1350 cm^{-1}. The temperature of the stage was ramped at a rate of 5 °C/min. The drop in the signal is due to the film undergoing morphological change into a droplet and the laser losing the target. At around 107 °C, the fluorescence count increases as compound 1 aggregates and forms droplets. This phenomenon is seen in only cis compound 1 dominant films and not in trans compound 1 dominant films. (b) DSC of 82% cis compound 1 sample. The sample was ramped to 150 °C the first run (blue) and then to 200 °C in the second run (orange). (c) DSC of 35 % cis compound 1 sample. (d) Left: optical image of trans dominant compound 1 film on silicon at 25 °C. Right: optical image of trans dominant compound 1 molecular film on silicon at 75 °C. (e) Temperature resolved Raman mapping of trans compound 1 in film state. The temperature of the stage was ramped at a rate of 5 °C /min. The shift from the 1469 cm^{-1} to 1462 cm^{-1} and the increase in the sharpness of the peak indicates that the molecular thin film system is in a more crystalline state. (f) *ex situ* temperature XRD on compound 1 film (scan time 60 seconds)

the two peaks arise from separate populations of molecules. Steric hindrance and local environment affects the thermal isomerization process, effecting the thermal isomerization kinetics.[80, 81] Thus, the cause of the two peaks is related to the inherent morphological changes experienced by the cis-film as temperature increases, resulting in different sub-populations of azobenzene that release heat at different rates due to their local steric environments.

DSC for samples (5 measurements) of a trans dominant film with 35% cis (Figure3-3(c)) showed a single peak heat release. Considering the percentage of charged (cis) molecules and calculating the energy stored per molecule, this translates to $\Delta H = 81 \pm 3$ kJ/mol, which is similar to that of the 95% cis sample with two release peaks. No droplet formation was observed in a trans dominant compound 1 molecular film. A pristine film appears clear while after heating turns opaque at 75 °C (Figure3-3(d)). To understand the thermal properties of the trans dominant film, temperature re-solved Raman mapping was performed, Figure3-3(e). The peak between 1450 cm^{-1} and 1500 cm^{-1} was measured as its position and shape are associated with the stretch-ing of the N=N azo bond. [84, 85, 86, 87] At 25 °C, the Raman peak is broad, centered at 1469 cm^{-1} while at 75 °C the peak shifts to 1462 cm^{-1} with a narrower width, signifying that the material has become more crystalline. This was further confirmed using *ex situ* temperature-dependent XRD shown in Figure 3(f). The film at 25 °C showed a single broad XRD peak, which suggests that the film was in an amorphous state. When heated to 75 °C, sharp XRD peaks started to appear that translate to the formation of crystalline regions.

Compared to azobenzene, the added bulky phenyl to the carbon on the metapo-sition of azobenzene in compound 1 proved to be effective in improving azobenzene molecule for purely molecular solid-state solar thermal fuel in three ways: 1) By red shifting the $\pi \rightarrow \pi^*$ transition absorption peak allowing 95% charging of the material under 365 nm light source 2) by preventing crystallization of the molecule at ambient conditions allowing solid-state switching of the film, and 3) by increasing the energy stored per molecule. The increase in percent charged and increase in energy stored

per molecule is important because although the molecular weight of compound 1 is 3 times that of azobenzene, the gravimetric energy density is measured to be 134 J/g (37 Wh/kg), which is comparable to the azobenzene molecule and higher than that of the polymer template azobenzene by 30%.[62, 33] The prevention of crystallization of compound 1 allows for the fabrication of stable, amorphous thin films. Crystallization (as in the case of pure azobenzene) presents a challenge for solid-state applications because the steric hindrance between the molecules in the crystal prevents the molecule from switching between the trans and the cis state. The fact that compound 1 films remains amorphous leads to much improved chargeability in the solid-state. This allows the individual molecule in the amorphous film to have the necessary free volume to achieve photoisomerization. However, the molecular film was not able to retain its original amorphous state when heated. When thermally triggered, the film needs to be able to withstand temperatures up to the reversion temperature. The trans rich film crystallized at around 75 °C while the cis rich film formed droplets at 105 °C. In both cases, the change in film morphology brought on by crystallization prevented the compound 1 film to charge from trans to cis after this thermally induced transformation. This crystallization hinders optical charging of the film because the crystal structure prevents isomerization through illumination due to the lack of free volume.[88] Thus, another strategy was needed for the film to retain its original amorphous state while allowing thermal switching of the material.

3.3.4 Bulkier Functionalization on Azobenzene Scaffold

Compound 1 was modified further by adding non-planarity to the molecule, which has been suggested previously as a means to maintain the amorphous state at higher temperatures.[76]. Compound 2 and compound 3 molecules (Figure3-7(b)) were synthesized to understand the effect of non-planarity on the thermal stability, charging rate, and switchabilty of the molecule in the solid-state. Compound 2 extends the existing planarity break with an additional phenyl group while compound 3 breaks the planarity further and reduces stacking of the azobenzene derivatives due to π-π

interactions with the addition of a tert-butyl group. When the two compounds were spincoated to a thin film, SEM showed that compound 2 and 3 had improved film morphology compared to compound 1 (Figure3-8(a), (b)). Compounds 2 and 3 resulted in smoother and less grainy films than compound 1, indicating better propensity to make uniform and well-controlled thin-films.

One important aspect of solid-state STF is the chargeability of the STF molecule in the solid-state. The chargeability of the solid-state film of compound 1, compound 2, and compound 3 was characterized using *ex-situ* photocharging and solid-state UV-vis spectroscopy. Figure3-13(c) shows the cis fraction of the solid-state STF films based on photocharging time. The samples were prepared to give similar optical densities. The three compounds in the solid-state showed nearly identical $\pi{\rightarrow}\pi^*$ transitions centered at around 350 nm. The change in UV-vis spectrum of each of the compounds with exposure time can be seen in the Figure 3-14,3-15, and 3-16.The fraction of cis was approximated by taking the ratio of the absorption of $\pi{\rightarrow}\pi^*$ and the initial trans dominant film absorption ratio and subtracting it from 1.

$$Fraction_{cis} = 1 - \frac{\pi \rightarrow \pi*_{final}}{\pi \rightarrow \pi*_{initial}}$$

The $\pi{\rightarrow}\pi^*{}_{final}$ was taken from when the film was exposed to elongated time and the peak no longer shifted, which we assumed that the film has reached photostationary state.

It is important to note two key properties that have improved from compound 1. One is the charging rate and the second is the photostationary state or the charged amount. First, to determine the charging rate at which the film changes from trans to cis, the first 140 seconds was linearly fitted from the time vs fraction of cis graph (Figure 3-17). Compound 2 and 3 showed over 65 % increase in charging rate from that of compound 1. Further, the addition of the bulky groups improved the photostationary state of the solid-state films. Compounds 1, 2, and 3 showed cis fractions
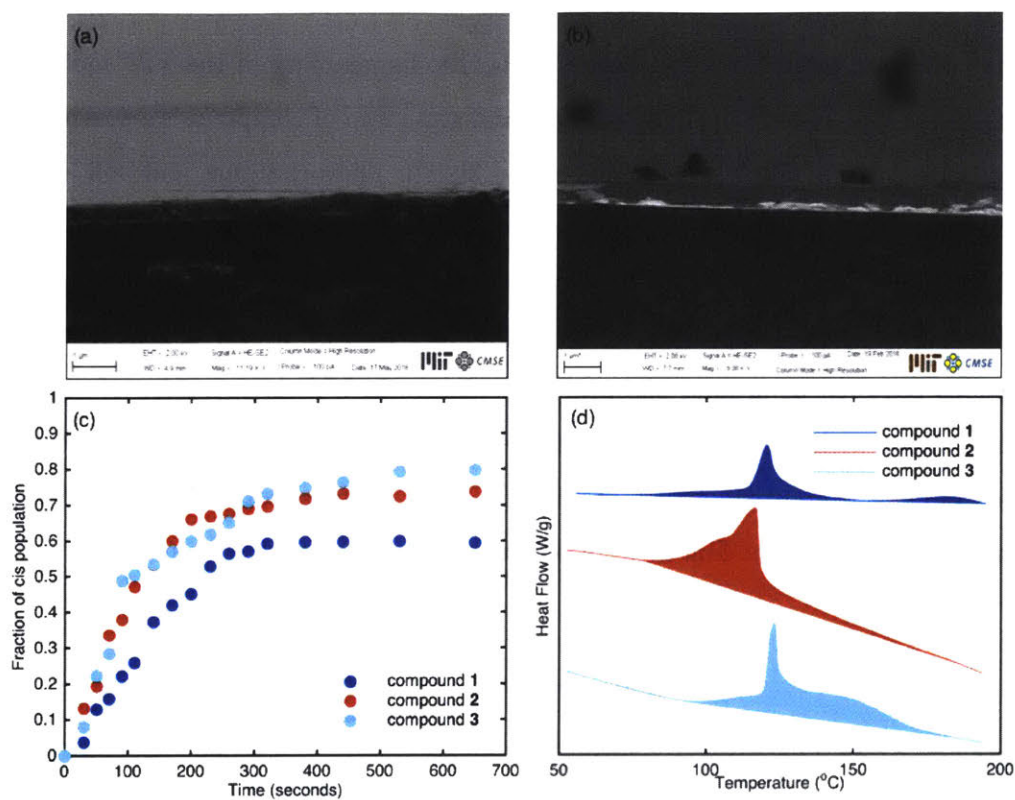
Figure 3-13: (a) Cross-sectional SEM of compound 2 film (b) Cross-sectional SEM of compound 3 film (c) Chargeability of compound 1, compound 2, and compound 3. Process was done *ex situ* where the sample was charged under 365 nm UV light for a set time then solid-state UV-vis spectra was taken. (d) Differential Scanning Calorimetry traces for compound 1, compound 2, and compound 3 from top to bottom. The y direction represents heat release and the region enclosed with the flat baseline represents the area integrated to obtain energy release.
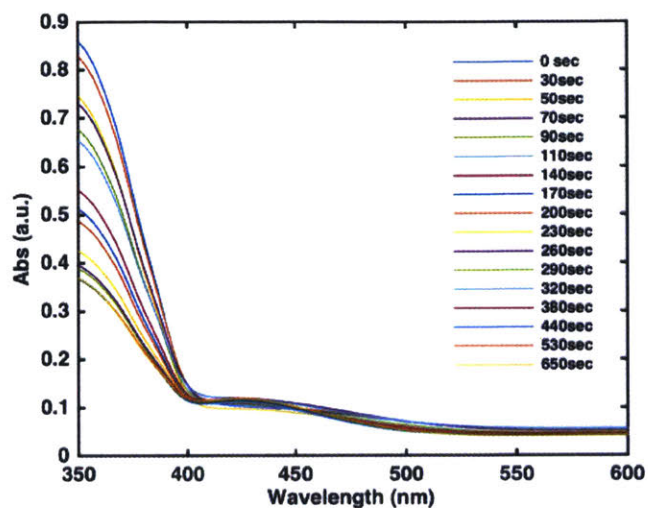
Figure 3-14: UV-Vis spectrum of solid-state film of compound 1 with exposure time to UV light.
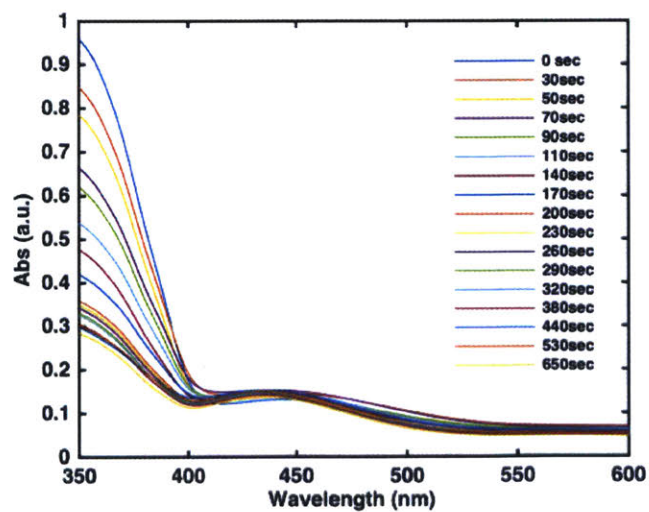
Figure 3-15: UV-Vis spectrum of solid-state film of compound 2 with exposure time to UV light.
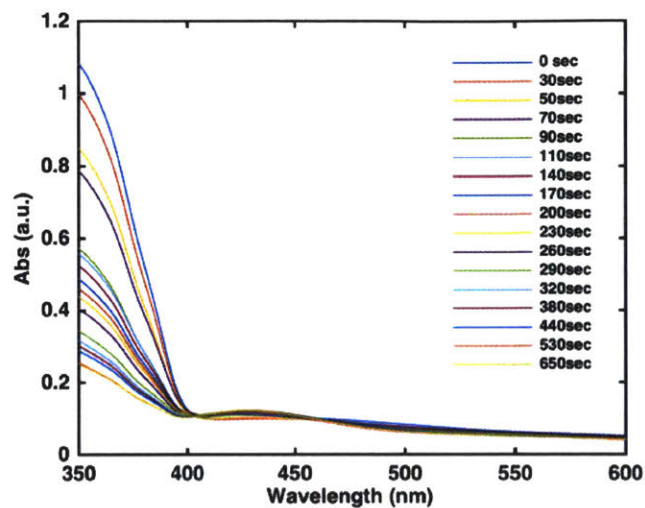
Figure 3-16: UV-Vis spectrum of solid-state film of compound 3 with exposure time to UV light.
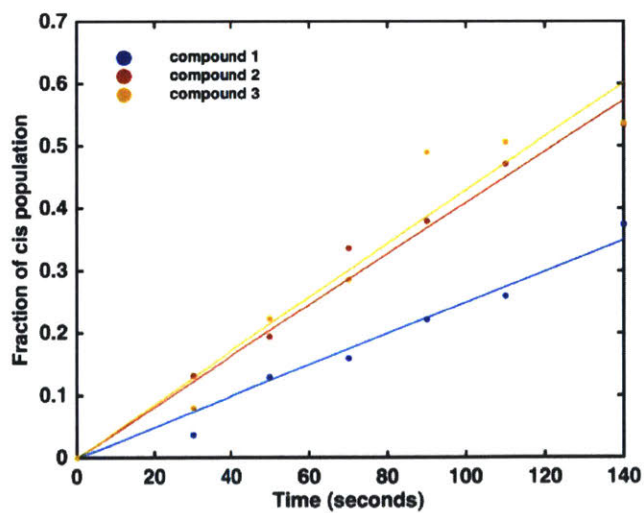
Figure 3-17: Fraction of cis linear fit. The slope of the fit was 0.0025, 0.0041, and 0.0043 in the order of compound 1, 2, and 3.

of 0.60, 0.74, and 0.80, respectively, indicating that compounds 2 and 3 allow more complete charging of the solar thermal fuel. The bulky structures functionalized for compounds 2 and 3 act as spacers, which create additional free volume in the amorphous matrix and allow the molecules to undergo photoisomerization from trans to cis at a faster rate.

Figure3-18(d) shows our DSC measurements for charged compound 2 and 3. Unlike compound 1, both showed heat release a single region with compound 2 (3 measurements) giving 100 ± 4 J/g or 88 ± 4 kJ/mol and compound 3 (3 measurements) giving 108 ± 2 J/g or 87 ± 2 kJ/mol. In both cases, the energy per molecule increased compared to that of compound 1. The majority of the heat was released in the range of 90 °C to 125 °C for compound 2 and 90 °C to 175 °C for compound 3. We note that the heat release trace is not a smooth peak, and can propose to attribute this to differences in activations energies for different sub-populations of molecules due to differences in local environment. Though the films are amorphous in either cis or trans state, slight spatial differences may arise due to a presence of a small fraction of trans isomer, as was seen with compound 1 that had 2 release peaks. In certain applications the ideal case would be for the heat release to proceed simultaneously; however, this also presents a potential avenue to control the rate of heat release once the precise inter-molecular mechanisms for controlling the activation energy are better understood.

Importantly, both thin films of the synthesized materials showed thermal stability within these ranges of heat release. As can be seen in the optical images, the compound 2 film started dewetting at 150 °C while the compound 3 film remained intact up to 175 °C (Figure 3-20, 3-21). Temperature resolved Raman spectroscopy on the N=N azo bond stretch showed that in both cases the peak remained in the same position indicating that compound 2 and 3 films remained in their amorphous states (Figure3-19(a), (b)). *ex situ* temperature-dependent XRD showed that in both cases the film showed amorphous peaks and maintained its amorphous state throughout heating of the film (Figure3-19(c), (d)). The higher thermal stability of the com-
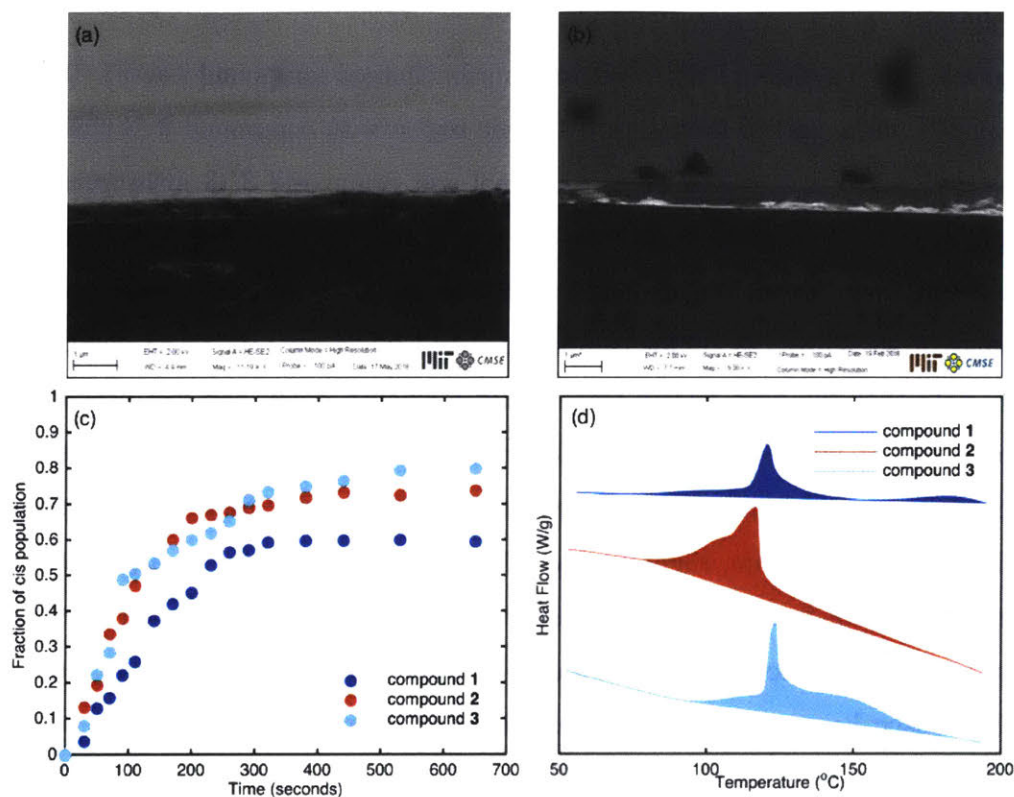
Figure 3-18: (a) Cross-sectional SEM of compound 2 film (b) Cross-sectional SEM of compound 3 film (c) Chargeability of compound 1, compound 2, and compound 3. Process was done *ex situ* where the sample was charged under 365 nm UV light for a set time then solid-state UV-vis spectra was taken. (d) Differential Scanning Calorimetry traces for compound 1, compound 2, and compound 3 from top to bottom. The y direction represents heat release and the region enclosed with the flat baseline represents the area integrated to obtain energy release.
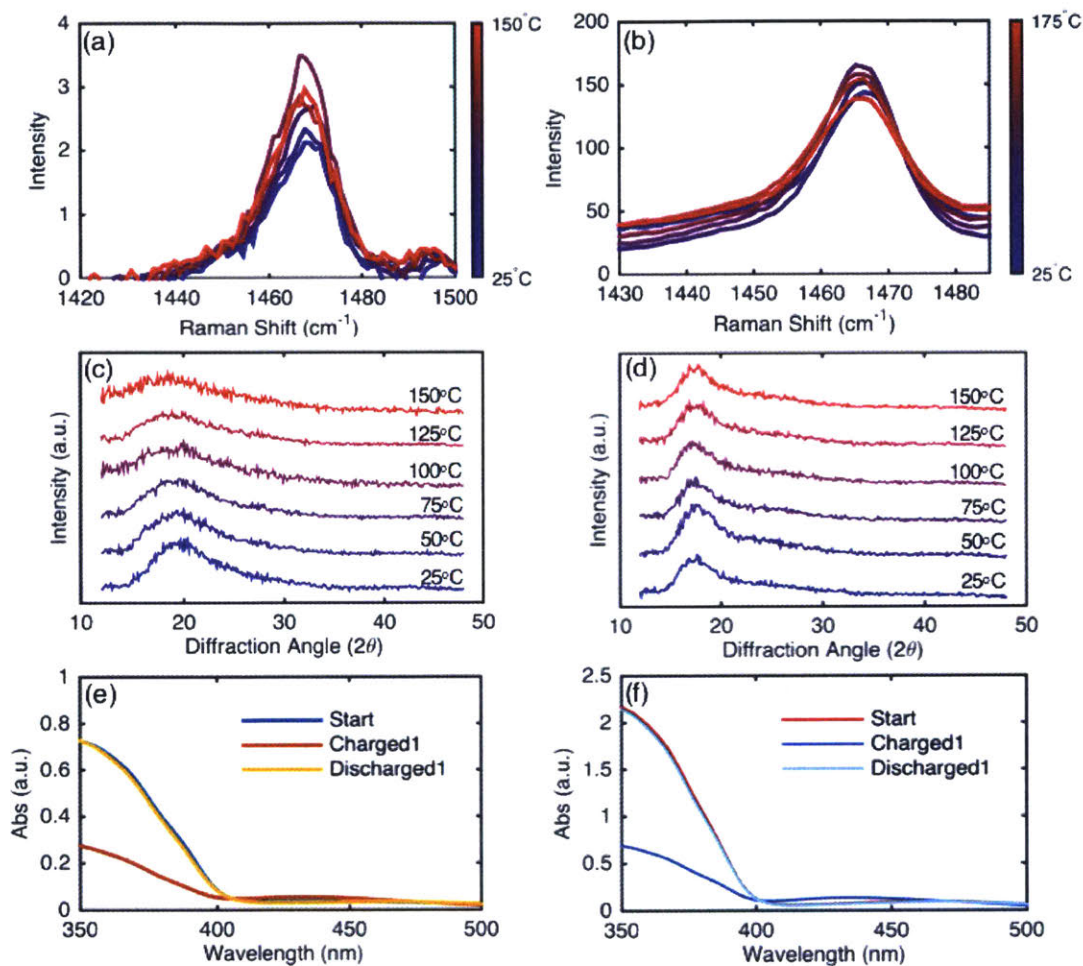
Figure 3-19: (a) Temperature resolved Raman mapping of compound 2 in film. No shift in the Raman peak and sharpness indicates that the state of the film is preserved throughout the heating process. (b) Temperature resolved Raman mapping of compound 3 film. (c) *ex situ* temperature XRD on compound 2 film (scan time 60 seconds) (d) *ex situ* temperature XRD on compound 3 film (scan time 60 second). UV-vis spectrum of light charging and heat discharging of (e) compound 2 and (f) compound 3 film.

Table 3.1: Comparison of heat storage properties, chargeability, and switching in the solid state. Complied from [6, 9, 62, 30]

	Energy Density (J/g)	Energy Density (kJ/mol)	Solid State Chargeability	Solid State Thermal Switching
Azobenzene	161	49	X	X
Azopolymer	104	28	O	O
Norbornadiene Derivative	629	124	X	X
compound 1	134	77	O	X
compound 2	100	88	O	O
compound 3	108	87	O	O

pound 3 films confirmed that the addition of tert-butyl groups effectively prevents the π-π stacking of the azobenzene derivative under thermal annealing conditions at higher temperatures. The switching of the solid-state film between the trans and cis states was confirmed using UV-vis spectroscopy (Figure3-19(e), (f)). The two films were charged using 365nm UV light confirmed by the decrease in the $\pi{\rightarrow}\pi^*$ transition. However, this time the discharge of the material was performed using thermal triggering. After charging, the film was placed in the dark at 100 °C for two hours. Unlike the compound 1 film, the two films recovered the $\pi{\rightarrow}\pi^*$ transition peak fully with no observed morphological change and was able to charge once more. Additional switching of this can be seen in Figure 3-22 and 3-23. In effect, compounds 2 and 3 prevent the films from undergoing irreversible morphology changes, thus allowing them to cycle many times. In contrast, compound 1 crystallizes after 1 charging/discharging cycle making it impossible to charge again.

Table 3.1 shows the summary of heat storage properties and chargeability of azobenzene based solid-state solar thermal fuels. Although a decrease in gravimetric energy density is observed, the addition of the phenyl and tert-butyl group proved to be an effective strategy in improving the energy stored per molecule, chargeability, and thermal stability of the molecule. The energy stored per molecule for compound 2 and 3 increased by more than 12% compared to compound 1. The rate of charging for compound 2 and 3 increased by 60% compared to compound 1 while photostationary
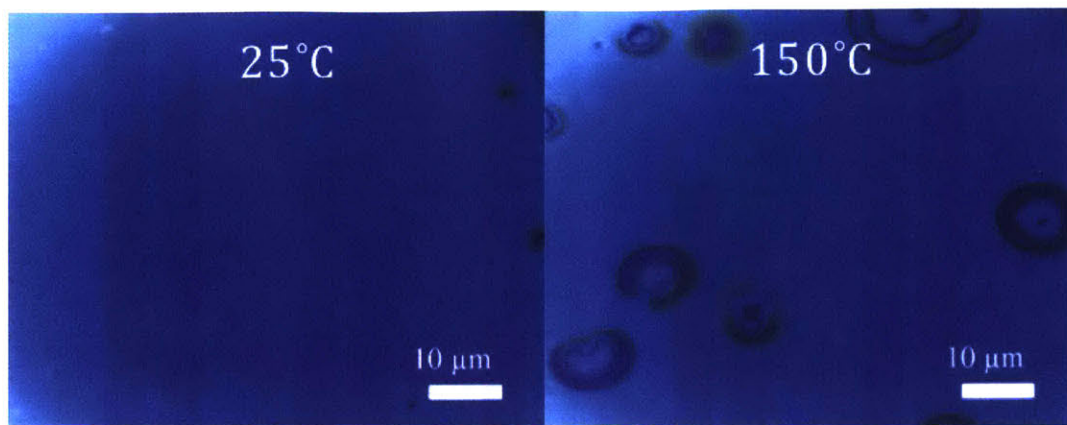
Figure 3-20: Optical image of trans dominant compound 2 film. Left: at 25 °C. Right: at 150 °C.
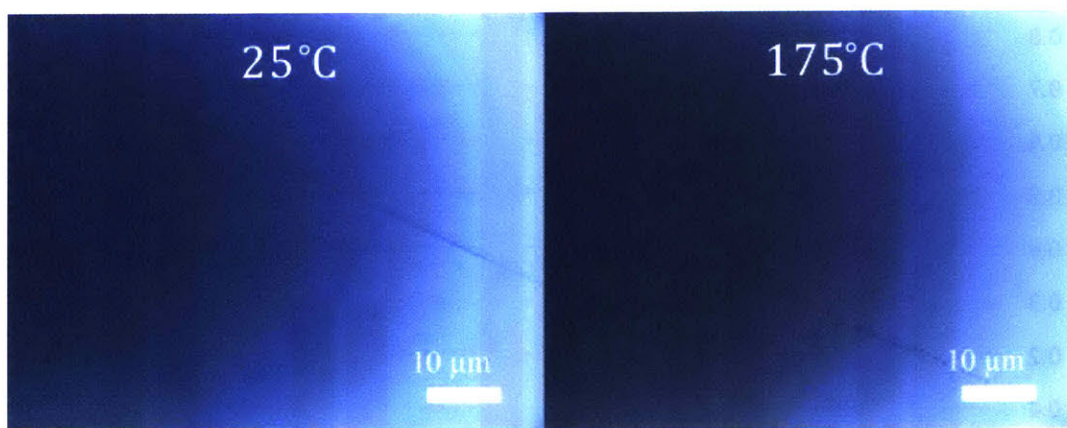
Figure 3-21: Optical image of trans dominant compound 2 film. Left: at 25 °C. Right: at 175 °C.
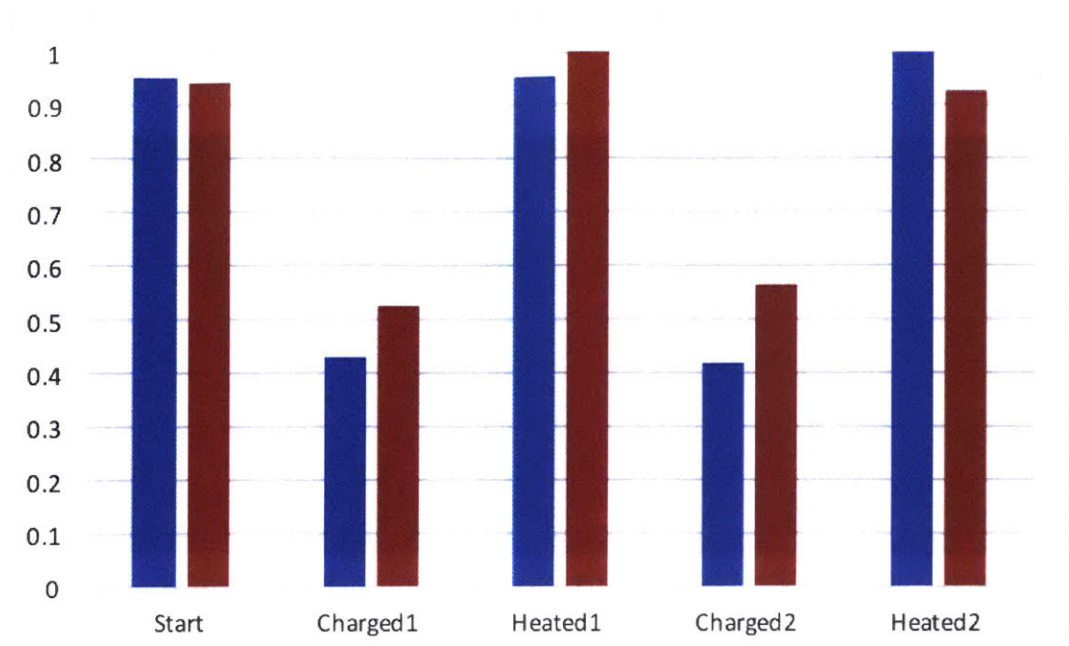
Figure 3-22: Reversible solid-state light charging and thermal discharging of 2. The blue and red indicates two different runs with different thickness thin films.
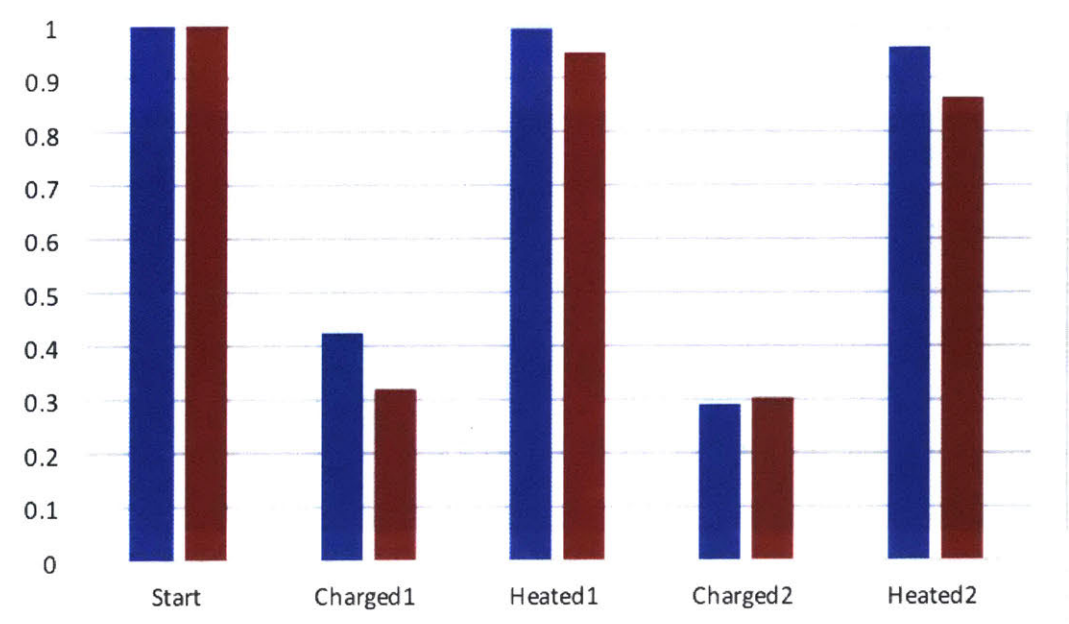
Figure 3-23: Reversible solid-state light charging and thermal discharging of 3. The blue and red indicates two different runs with different thickness thin films.

state in the solid state improved up to 33%. Of the two compounds, the additional symmetry breaking of compound 3 using the tert-butyl group was the most effective in improving thermal stability of the film increased to up to 175 °C with no signs of crystallization. This showed the effectiveness of molecular engineering for solid-state solar thermal fuel.

3.4 Conclusions

Here we demonstrated an effective molecular design to achieve solid-state STF materials with high energy density and thermal stability, without the need of polymerization or templates. Through the functionalization of azobenzene with bulky aromatic groups, a new class of STF molecules was developed that enables high-energy storage per molecule (nearly 90 kJ/mol), which translates to over 30% improvement in solid-state energy storage density compared to the previously reported azobenzene-functionalized polymer, while promoting excellent solid-state film formation. Through additional molecular design, the rate of charging increased by 60% and chargeability of the material improved by 33%. Also, the thermal stability of the solid-state film improved from 75 °C to 180 °C. Our results found that breaking the planarity of molecule plays a crucial role on solar thermal fuel properties and shed light on future directions for structural engineering of molecules to allow thermally stable and switchable STF thin film. We were able to simultaneously engineer the small molecule films to have increased energy density, while also exhibiting excellent charging and cycling properties. More broadly, the film formation design principles that enable the deposition of stable amorphous films through solution processing can be applied to other areas such as organic photovoltaics and organic light-emitting diodes. With increasing requirements for solid-state integration of small molecules for functional devices, molecular films present a tremendous avenue in terms of versatility, ease of processing, and cost reduction.

Chapter 4

Diacetylene Decorated azobenzene

4.1 Introduction

Nanotemplated solar thermal fuel work with azobenzene functionalized onto carbon nanotube showed that close packing of azobenzene is important for increasing ΔH while motivating the use of solar thermal fuels in the solid state.[9] Although outstanding progress has been made in improving and controlling properties of solar thermal fuels in the solid state, shown in the previous chapters through use of polymer template and molecular engineering, little work has been geared towards controlling the specific packing to increase ΔH of azobenzene. Furthermore, since the polymer work showed decrease in stored energy density, a better understanding of close packing of azobenzene molecules may help improve the storage properties in solid-state solar thermal fuel. The photoswitching vs. packing density and alignment of azobenzene materials has been explored for some macrocyclic[89, 90, 91] and linear[92] azobenzene derivatives, particularly for liquid crystalline materials, for applications in photolithography and actuation. The collective change of intermolecular interactions in such materials can be observed as a macroscopic solid-liquid phase transition. However, packing and alignment of azobenzene materials has been yet to be adpated to solar thermal fuel as a method for enhancing solar energy storage performance.
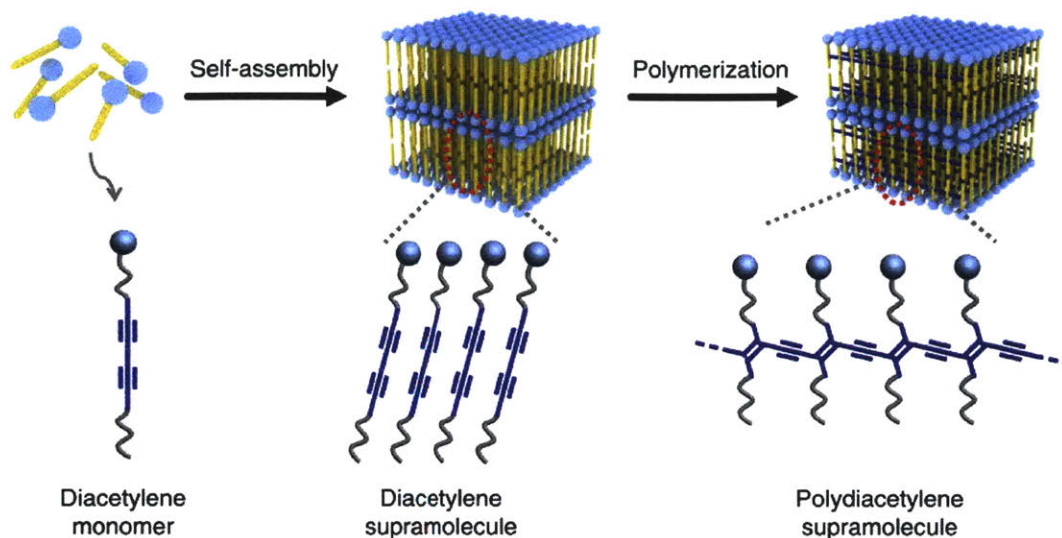
Figure 4-1: Schematic of diacetylene self-assembly and the formation of supramolecular polydiacetylene. Reproduced from [12]

In this work, we probe the opportunity for high energy storage in photon energy storage materials by using diacetylene as the template to explore the effect of degree of intermolecular interactions in the trans and cis isomer on photon energy storage. Diacetylenes are easily functionalized and prone to self-assembly, displaying crystalline-like packing due to strong intermolecular interactions. They can also be rapidly photopolymerized by UV illumination to produce polydiacetylenes bearing azobenzene-containing side chains on the rigid conjugated backbones, which resemble the structure of rigid templates decorated with closely-packed photochromic units (Figure 4-1).[12] Previous efforts on azobenzene-decorated diacetylenes and polydiacetylenes have focused on asymmetric structures where azobenzene groups functionalized on one side and long alkyl chains on the other side are designed to enable the self-assembly of molecules into vesicles and tubes[93] or bilayer films[94, 95] for applications such as photocontrolled molecular recognition and reversible optical switches.[96] Building upon the knowledge gained in these studies regarding the structural change of the azobenzene-functionalized diacetylenes, we are able to design symmetric diacetylenes that enable the high loading and ordered arrangement of the azobenzene groups. The compact systems of the azobenzene derivatives without bulky

groups are desirable to maximize the gravimetric and volumetric energy densities of photon energy storage materials. Herein, we present high energy storage materials based on the azobenzene-functionalized diacetylenes which exhibit up to 113% higher ΔH (per azobenzene unit) than that of pristine azobenzene as a result of the strong intermolecular interactions in the ordered trans state and the significant loss of these interactions in the cis conformation. In order to further understand this new type of material design space, we explore the effects of alkyl spacer lengths between the diacetylene core and terminal azobenzene groups, intermolecular H-bonding, and various groups functionalized on the azobenzene moieties. X-ray diffraction analysis was conducted to understand the packing and the intermolecular interactions of the materials, and ab initio calculations were employed to help shed light on the relative energy storage mechanisms in this series of molecules.

4.2 Experimental Methods

Materials. Dodeca-5,7-diynedioic acid and docosa-10,12-diynedioic acid were purchased from GFS chemicals. Hexadeca-7,9-diynedioic acid was synthesized following reported procedures.[97, 98] Azobenzene precursors were purchased from Sigma-aldrich and alfa aesar. All the compounds purchased from commercial sources were used as received.

Measurements. 1H and 13C NMR spectra were taken on Varian Inova-500 spectrometers. Chemical shifts were reported in ppm and referenced to residual solvent peaks (CD_2Cl_2: 5.33 ppm for ^{1}H, 53.84 ppm for ^{13}C and DMF-d_7: 8.03, 2.92, and 2.75 ppm for ^{1}H, and 163.15, 34.89, and 29.76 ppm for ^{13}C). a Bruker Daltonics aPEXIV 4.7 Tesla Fourier transform ion cyclotron resonance mass spectrometer was used for high-resolution mass determination with an electrospray (ESI) ionization source. Elemental analyses of compounds 1-4 were performed by Robertson Microlit Laboratories (Ledgewood, NJ). UV-vis absorption spectra were recorded using a Cary 5000 UV-vis spectrophotometer in a 10 mm path length quartz cuvette. Thermogravimetric

analyses were performed with a Q series TGa Q500 (TA Instruments) under nitrogen to ensure the thermal stability of compounds at high temperatures up to 250 °C. DSC analysis was conducted on a Q series DSC Q10 (Ta Instruments). Powder X-ray diffraction (PXRD) patterns were recorded on Bruker D8 Discover diffractometer using Nickel-filtered Cu-Kα radiation (λ = 1.5418 Å) with an accelerating voltage and current of 40 kV and 40 ma, respectively. Samples for PXRD were prepared by placing a thin layer of the appropriate material on a zero-background silicon crystal plate.

Solvent-assisted charging procedures and the preparation of charged samples for heat release measurements. Powder samples were dispersed in dichloromethane (ca. 0.2 mg mL^{-1}) by sonication, and were illuminated under a Blak-Ray B-100aP/R (UVP) high intensity UV lamp (365 nm, 100 W) while being stirred (placed 25 cm away from the lamp). The solution samples were kept at room temperature while being charged, and were mostly dissolved in dichloromethane when completely charged. The solutions were then dried under reduced pressure (ca. 50 mTorr) in the dark, and the resulting solid or viscous liquid was transferred to a DSC pan for heat release measurements. In order to remove any residual solvent in the uncharged (trans) powder samples, the compounds were dried in a vacuum at 100 °C overnight prior to the charging process.

X-ray diffraction studies. Low-temperature data were collected on a Siemens three-circle diffractometer coupled to a Bruker-aPEX CCD detector with graphite-monochromated Mo Kα radiation (λ = 0.71073 Å), performing ϕ- and ω-scans. The structure was solved by direct methods (SHELXS) and refined against F2 on all data by full-matrix least squares with SHELXL-2015.[99] All non-hydrogen atoms were refined anisotropically. Hydrogen atoms were included in the model at geometrically calculated positions and refined using a riding model.

ab initio simulation of the molecular structures. ab initio relaxation and calculation of the ground-state energy of the molecular structures are performed

by another member in our group, Huashan Li, at the Density Functional Theory (DFT) level with the exchange-correlation energy of the Perdew-Burke-Ernzerhof functional[100] (PBE) using VaSP.[101, 102] all the molecular structures are relaxed until the forces acting on all the atoms are less than 0.01 eV Å^{-1}. Wave function expansion cuts off at 700 eV to ensure the simulation accuracy. Lattice parameters are allowed to relax during the relaxation of crystal structures. For the simulation of freestanding molecules, we use a vacuum of at least 10 Åin all three directions to avoid self-interaction through the periodic boundary condition.

4.3 Results and Discussion

4.3.1 The structures of symmetric azobenzene-functionalized diacetylenes and polydiacetylenes

In order to understand and develop design principles for enhancing the energy density of self-assembling materials, we first designed and synthesized symmetric diacetylenes with terminal azobenzene groups to maximize the gravimetric energy density and the volume change of the molecules upon photoisomerization (Figure 4-2a). an important design principle was to control the relative strength of intermolecular interactions and the molecular packing dynamics of diacetylene derivatives before and after the photoisomerization of azobenzene units. Based on these ideas, we varied the lengths of alkyl spacers and incorporated two types of linker groups (i.e. amide and ester moieties for the presence and absence of intermolecular H-bonding) in the diacetylene structures as shown in Figure 4-2a.

Compounds 1-3 are diazobenzenes amide-linked to dodeca-5,7-diyne, hexadeca-7,9-diyne, and docosa-10,12-diyne, respectively. Depending on the length of the alkyl spacer between the diyne core and azobenzene groups, the thermal properties of the compounds change gradually, which indicates the varied strength of intermolecular
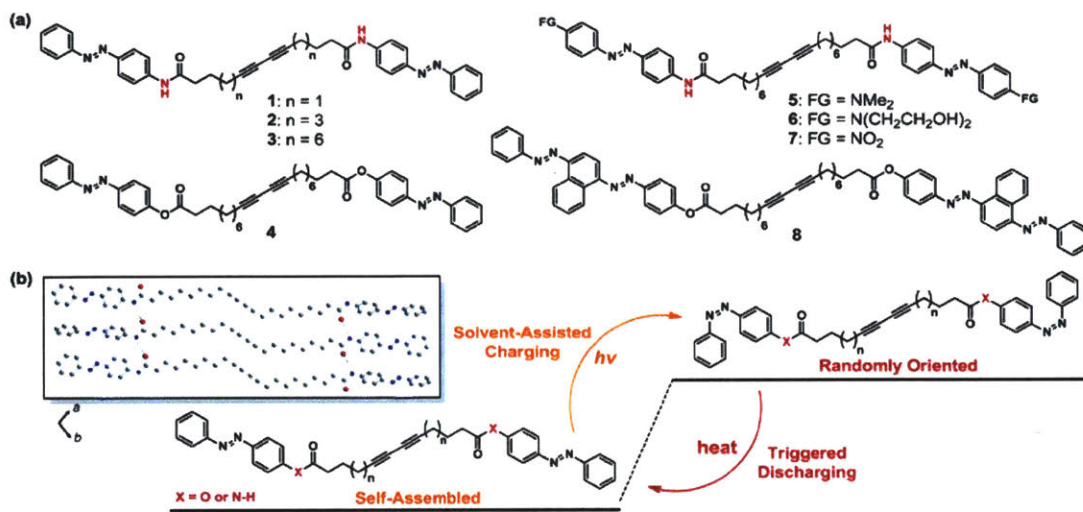
Figure 4-2: (a) azobenzene-functionalized diacetylenes with varying alkyl chain lengths, H-bonding units (marked in red), terminal functional groups, and an extended π-system. (b) a schematic image describing photoisomerization and triggered reverse isomerization of compounds 1-4. The inset shows a crystal structure of compound 3. The dotted lines indicate intermolecular H-bonding. Red, gray, blue and white spheres represent O, C, N and H atoms, respectively. H atoms without hydrogen bonding are omitted for clarity.
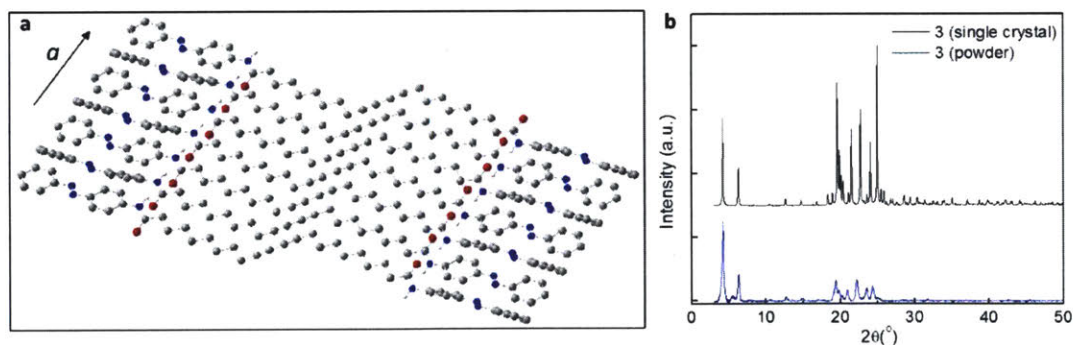
Figure 4-3: (a) Molecular packing of compound 3 shown along a axis. C=O and N-H groups are staggered, hence intermolecular H-bonding is absent along this direction. Red, gray, blue and white spheres represent O, C, N and H atoms, respectively. H atoms omitted for clarity. (b) PXRD patterns of compound 3 compared to that simulated for single crystals.

interactions; for example, compound 1 with the shortest spacer possesses the highest melting point of 266 °C, and compounds 2 and 3 bearing longer spacers exhibit lower melting points of 233 °C and 213 °C, respectively. From this observation, we can infer that the intermolecular H-bonding interaction of amide linkers in compounds 1-3 is weakened as longer alkyl spacers are present due to the steric repulsion of neighboring alkyl chains. Compound 4, docosa-10,12-diyne linked by esters to azobenzene groups, displays the lowest melting point of 136 °C, attributed to the absence of H-bonding linkers. Additionally, compounds 5-8 with various terminal functional groups (electron-donating, electron-withdrawing, and extended aromatic/conjugated groups) were synthesized to modify the optical properties of unsubstituted compounds by controlling the electron density and delocalization on azo groups.

As shown in Figure 4-2b, we hypothesize that the structural change of the azobenzene from trans to cis forms results in a different alignment of uncharged and charged diacetylene derivatives. We first obtained a crystal structure of the uncharged compound 3 using single crystal X-ray diffraction analysis as depicted in the inset of Figure 4-2b to examine the molecular arrangement. The molecules pack along their long axis, and the neighboring azobenzene groups arrange into herringbone structures. The H-bonding between adjacent amide linkers along the b axis of the lattice facilitates the packing of molecules as shown. In contrast, intermolecular H-bonding along the a axis is absent due to the staggered conformation of the adjacent C[double bond, length as m-dash]O and N-H groups (Figure 4-3a). The powder X-ray diffraction (PXRD) pattern of the as-synthesized compound 3 corresponds well with the diffraction pattern of single crystals (Figure 4-3b), which confirms the structural identity of crystalline powder and single crystals. Atomic structure optimization of the crystal structure of compound 3 monomers at the DFT level also confirms the existence of the H-bonding between the adjacent amide linkers. The cohesive enthalpy of the compound 3 crystal, calculated from the energy difference between the enthalpy of the unit cell with two monomers and the enthalpy of two free-standing monomers, is 223.0 kJ mol^{-1}, indicating considerable intermolecular interactions. Since the isomer-

ization of azobenzene requires a free-volume change of 120 $Å^3$ or more,[103, 104, 105] the ordered packing of trans isomers will be disrupted and form different molecular arrangements. Due to the non-planar conformation and the increased dipole moment of azobenzene cis isomers[106] compared to their trans counterparts, the molecules are expected to be randomly oriented, losing a significant degree of intermolecular interactions between the dyne cores, alkyl chains, and aromatic groups. From this, we want to see how the difference in molecular arrangement due to the difference between trans and cis azobenzene on diacetylene can impact the stored energy of the material.

Polymers of the diacetylene monomers are also crystalline in the ground state, and the syntheses of conjugated polydiacetylenes were easily achieved by UV irradiation (254 nm) of self-assembled azobenzene-diacetylenes in the solid state (Figure 4-4a). The yellow-to-blue transition indicates the formation of conjugated backbones (Figure 4-4b inserted photographs and Figure 4-5a), and the PXRD pattern of the polymer is mostly identical to that of the corresponding monomer, illustrating a negligible or only a small change in the packing of the molecules throughout topochemical photopolymerization.[107] ab initio simulations, however, show that no intramolecular H-bonding exists in the same b axis for the polymer chain of compound 3, due to the larger spatial separation between the N-H and the C[double bond, length as m-dash] O groups as a result of the structural constraints imposed by the rigid polymer backbone (Figure 4-6).

In this work, we have mainly focused on the high energy storage in the monomers and polymers upon azobenzene isomerization and the release of energy in the form of heat. However, if properly engineered, the azobenzene-functionalized polydiacetylene can be a multifunctional material (i.e. a photon energy storage material and a colorimetric indicator of the storage) as the photoisomerization of azobenzene groups and the consequent steric repulsion between the side chains may control the conjugation length of the polymer backbone reversibly. In fact, polydiacetylenes generally exhibit colorimetric transitions (usually from blue to red)[108] upon various stim-
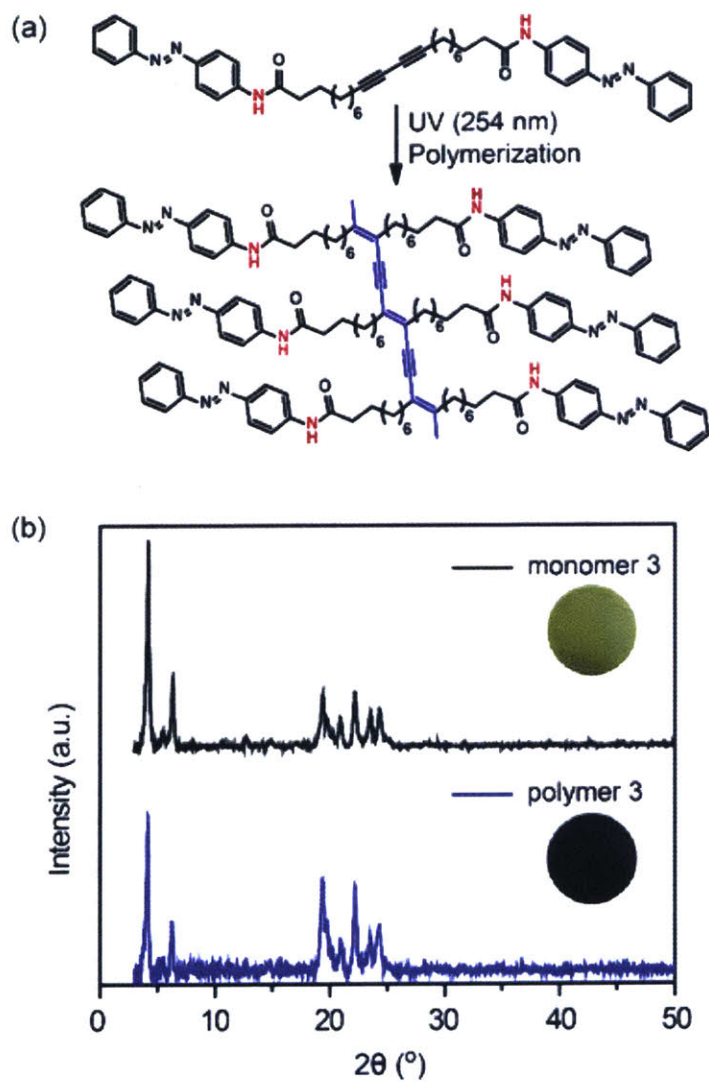
Figure 4-4: (a) a schematic photopolymerization of monomer 3 and the structure of polymer 3 with a conjugated backbone. (b) Powder X-ray diffraction patterns and photographs of monomer 3 and polymer 3 in the solid state.
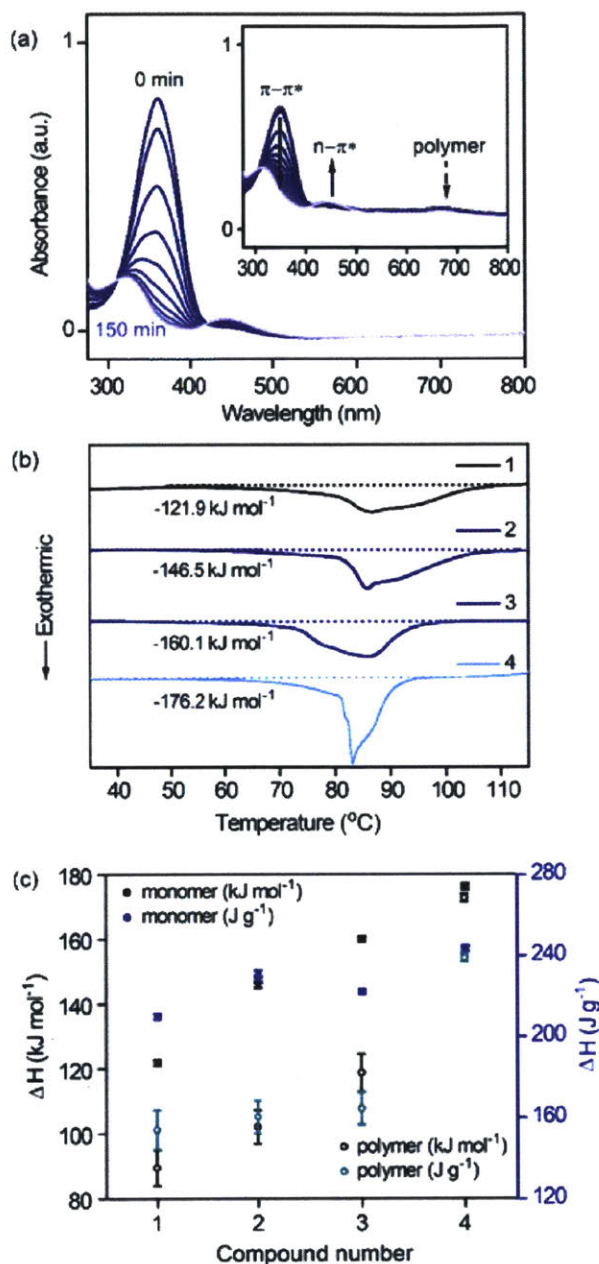
Figure 4-5: (a) UV-vis absorption spectra of monomer 3 as it is charged at 365 nm for 150 min. The dark blue line indicates the initial spectrum, and the spectra collected after irradiation are indicated with lighter blue lines. The inset is the absorption spectra of polymer 3. (b) The first DSC traces of monomers 1-4 while temperature increases at 5 °C min^{-1} (1-3) and at 2 °C min^{-1} (4). The curve areas below the dotted baselines were integrated to calculate the enthalpy changes in the respective compounds. (c) ΔH per mole and gravimetric ΔH measured for monomers and polymers 1-4.

100
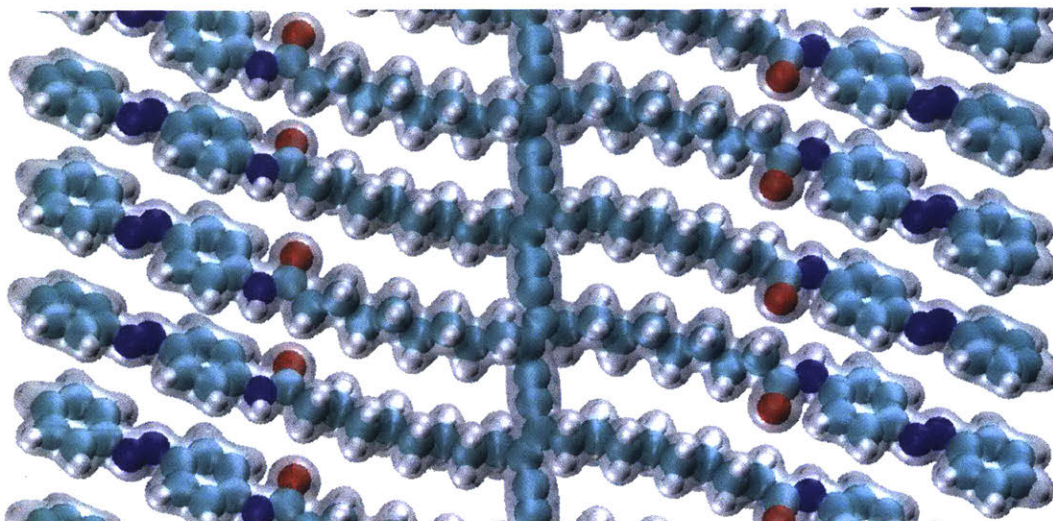
Figure 4-6: A structure of polymer 3 optimized from ab initio simulations where side chains are packed along the b axis. Blue, red, light blue, and white spheres correspond to N, O, C, and H atoms, respectively. Silver shade around the atoms represents the charge density iso-surface at the value of 0.1 e Å^{-3}. As observed from the overlapping of the charge density iso-surface, no hydrogen bonding exists between the amide groups

uli such as heat,[109] mechanical perturbation,[110] and solvents,[111] which shorten the conjugation of the polymer backbones. We also observed the reversible blue↔ red thermochromism of polymer films (Figure 4-7) which indicates their potential to respond to significant steric repulsion between side chains. The development of photochromic materials based on polydiacetylenes that exhibit clear color changes over charging and discharging is an ongoing effort.

4.3.2 Photon energy storage by photoisomerization and release by thermal reverse isomerization

As shown in Figure 4-2b, charging (trans → cis) of diacetylenes and polydiacetylenes was conducted in solution for the facile photoisomerization of azobenzene units in sufficient free volume, since solid-state charging was suppressed within the crystals due to the steric hindrance between close-packed molecules.[112] UV-vis light absorp-

101
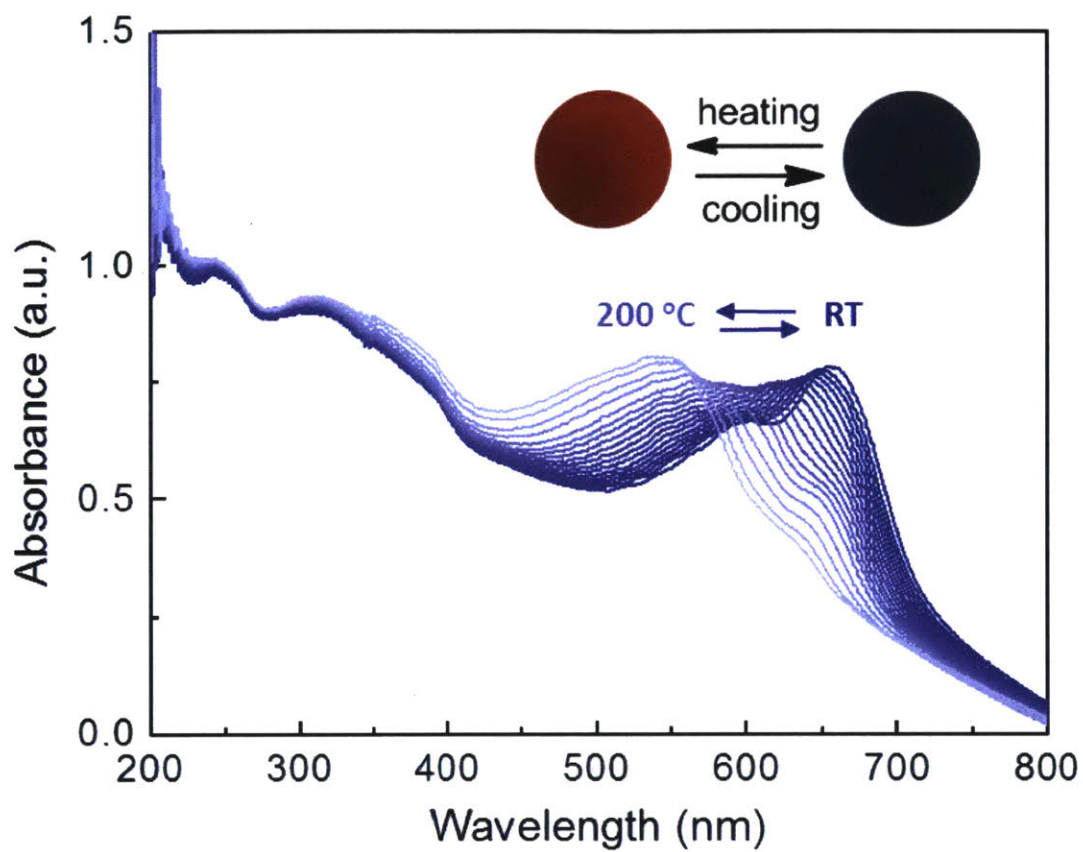
Figure 4-7: Reversible thermochromism of polymer 3 films observed by variable-temperature UV- Vis absorption spectroscopy while heating up to 200 °C and cooling down to room temperatures. Inset shows the photographs of the films that change the color reversibly.
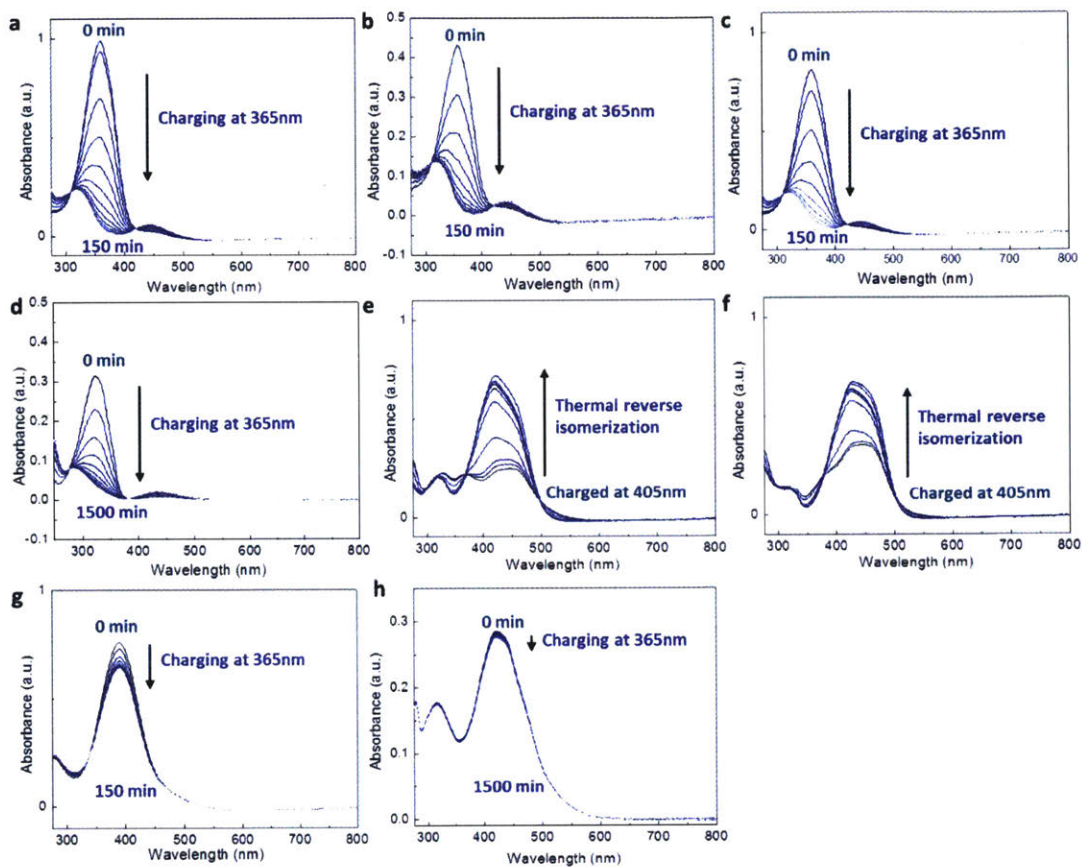
Figure 4-8: UV-Vis absorption spectra of compound 1-8 in 10 μg mL^{-1} solution of DMF (a,b,c,e,f,g) or DCM (d,h). For compound 5âĂŞ6 with terminal amino groups, light absorption feature is broadened and redshifted to a range of 350âĂŞ500 nm (eâĂŞf). Therefore, the compounds reach equilibrium of charging-discharging under ambient light, and are discharged rapidly in dark. Irradiation at 360 nm only decreases the overall intensity of the absorption peak without changing its shape. However, two distinguished peaks around 390 nm and 460 nm appear when the compounds are illuminated at 405 nm, as a result of more selectively excited π-π^* transition. Compound 7 with terminal nitro groups also exhibits single peak centered at 390 nm, and charging it at either 365 nm or 405 nm decreases its intensity only slightly due to the large overlap between π-π^* and n- π^* transitions (g). Compound 8 displays the most red-shifted absorption spectra ranging from 350 nm to 600 nm, attributed to its extended ÏĂ-system, and charging it at either 365 nm or 405 nm is the least efficient among the series of compounds (h). Heat release of monomer 5-8 was negligible, so is not discussed in this report.

tion by the solution of diacetylenes and dispersion of polydiacetylenes were monitored under illumination at 365 nm for photoisomerization (Figure 4-5a). Compounds 1-3 bearing amide linkers display an absorption peak at 360 nm assigned to the π-π^* transitions and another peak at 445 nm ascribed to the n-π^* transitions (Figure 4-5a and Figure 4-8a-c). At a photo stationary state (PSS) with enriched cis isomers, the peak at 360 nm blue-shifts toward 325 nm and the one at 445 nm increases up to the highest intensity. Compound 4 with ester linkers shows a π-π^* transition at 324 nm and n-π^* transition at 437 nm that are farther apart on the spectra compared to those of the amide derivatives (i.e. a less overlap between absorptions induced by those transitions) (Figure 4-8d). On the other hand, compounds 5-8 with terminal functional groups exhibit red-shifted light absorption and a large overlap between the π-π^* and n-π^* transitions, hence limiting the selective excitation of the π-π^* transition, undergo simultaneous conversion between trans and cis isomers even by narrow-range light absorption (Figure 4-8e-h). Therefore, compounds 5-8 were charged with very low yields, and the heat release of the charged materials was negligible. This result indicates the importance of designing photoisomer pairs that have the least overlap between the absorption spectrum of each isomer for photon energy storage applications. The absorption characteristics of polymers 1-4 synthesized from the corresponding diacetylene monomers 1-4 consist of the typical π-π^* and n-π^* transitions of monomers and additional absorbance at 650-700 nm by conjugated polymer backbones which do not limit the absorption of the photochromic units (inset of Figure 4-5a).

The charged solutions were concentrated and dried in the dark, and ΔH from reverse thermal isomerization was measured by differential scanning calorimetry (DSC). The first DSC traces of compounds 1-4 in the heating process are shown in Figure 4-5b where integration of the exothermic peak corresponds to the energy stored in the cis isomer. Complete thermal reversion of the cis state to the trans state is achieved within the temperature range of measurements, as confirmed by the following cooling scan and the subsequent DSC runs which do not exhibit any endothermic or exother-
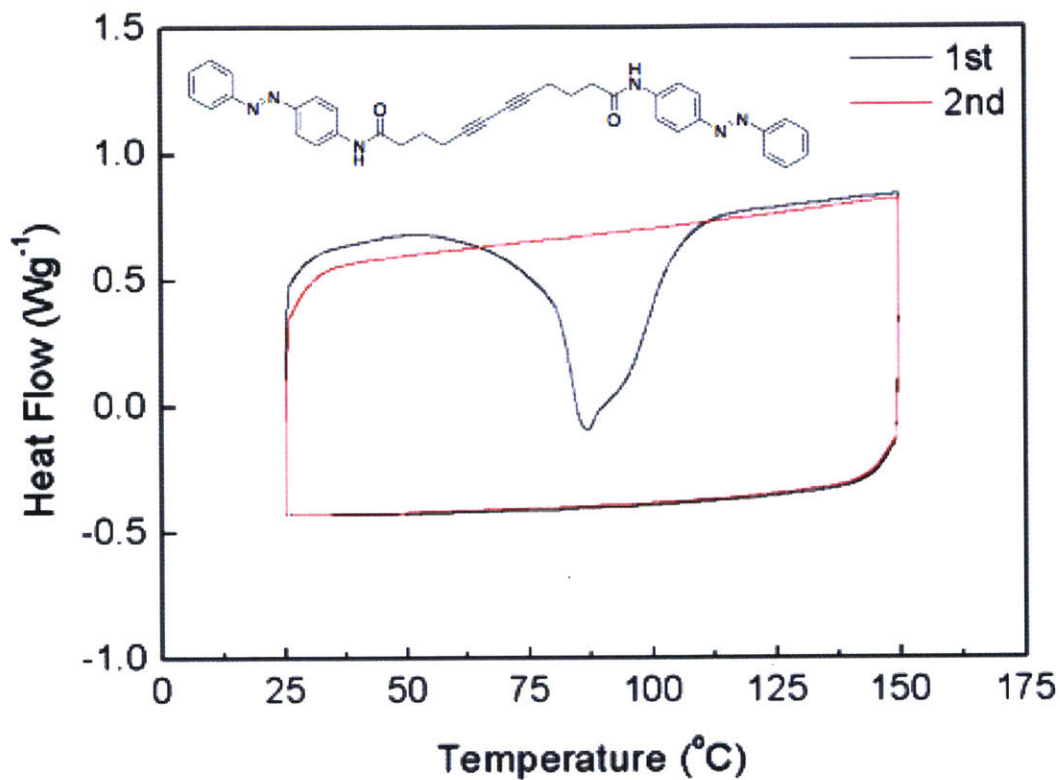
Figure 4-9: DSC analysis of charged compound 1 heated and cooled at 5 °C min^{-1} for two consecutive cycles. The heating of charged cis molecules results in the thermal reversion to trans isomers which do not exhibit endothermic or exothermic behaviors. The identical phenomenon is observed for the other compounds (2-4) within the relative temperature range.

Table 4.1: Heat release of monomers 1-4 measured by DSC

Compound	1	2	3	4
ΔH [kJ mol^{-1}]	121.9 ± 0.9	146.5 ± 1.6	160.1 ± 0.9	176.2 ± 1.0
ΔH [J g^{-1}]	209.9 ± 1.6	230.1 ± 2.5	222.1 ± 1.3	243.7 ± 1.4

mic feature (Figure 4-9). The ΔH of each compound per mole (kJ mol^{-1}), and the gravimetric energy density (J g^{-1}) are listed in Table 4.1 and illustrated in Figure 4-5c. among the amide-linked compounds 1-3, ΔH per mole (kJ mol^{-1}) increases as longer alkyl spacers are used, and it is significantly improved by 47% (1), 77% (2), and 93% (3) per azobenzene unit relative to the ΔH of pristine azobenzene (41.4 kJ mol^{-1}) even though the molecules are less than 100% charged: about 93% (1), 89% (2), and 93% (3) cis at PSS calculated from UV-vis absorbance. If completely charged, compounds 1-3 would exhibit ΔH that is 58% (1), 99% (2), and 108% (3) increased per azobenzene unit relative to that of pristine azobenzene. Compound 4 bearing the ester-linked longest alkyl spacers releases the largest energy (176.2 kJ mol^{-1}) among the series, which is improved by 113% compared to that of pristine azobenzene, even at a 88% conversion rate. The theoretical ΔH of compound 4 is 200.2 kJ mol^{-1} that is 142% increased from that of pristine azobenzene. The kinetics of thermal reverse isomerization of compounds 3 and 4 were monitored in solution at varied temperatures, and the half-life of each charged compound at 25 °C was 27.8 hours and 98.4 hours, respectively, indicating desirable thermal stability.

Figure 4-5c also shows the plots of ΔH of polymers 1-4 (Table 4.2) which are generally lower than the ΔH of the monomers (70-98% of the respective monomer ΔH). The charging and heat release of polymers were not as consistent over multiple trials, unlike the highly reproducible process of monomers (small deviations as shown in Table 4.1), which may be attributed to the polydispersity of polymer chains. Photopolymerization of self-assembled monomers in films can easily lead to the inhomogeneity of polymer/oligomer/monomer contents in the samples, even if the light exposure is carefully repeated to induce polymerization evenly throughout the entire batch. Depending on the relative monomer and polymer content in the samples,

Table 4.2: Heat release of polymers 1-4 measured by DSC

Compound	1	2	3	4
ΔH [kJ mol^{-1}]	89.5 ± 5.6	102.1 ± 5.1	118.7 ± 5.7	172.7 ± 1.3
ΔH [J g^{-1}]	154.1 ± 9.7	160.4 ± 8.0	164.6 ± 8.0	238.9 ± 1.8

the conversion and ΔH can vary. Due to these variations, the standard deviations of the measured ΔH values of polymers are larger (Table 4.2) compared to those of monomers. Lower photon energy storage in polymers compared to monomers has also been seen for azobenzene-functionalized PMMA structures back in chapter 2. We assume that the polymer aggregation in the dispersion hinders light absorption by the materials, limiting the conversion of azobenzene side chains. However, the trend of ΔH per mole (kJ mol^{-1}) with the length of alkyl chains among polymers 1-3 is similar to that among monomers 1-3, and the ΔH of polymer 4 decreases only slightly relative to that of monomer 4. also, charged polymers still release larger ΔH than pristine azobenzene, increased by 8% (1), 23% (2), 43% (3), and 109% (4). Moreover, the instant polymerization process and the colorimetric behavior of poly-diacetylene, compared to other types of polymers, make it an attractive candidate to be a colorimetric material as aforementioned.

It is surprising that all the monomers and polymers in the series exhibit larger ΔH than that of pristine azobenzene and that monomer and polymer 4 in particular store more than double the ΔH per azobenzene unit. We hypothesize that the additional energy storage would result from different intermolecular interactions in trans and cis states that enlarge the enthalpy gap between those. as seen in the crystal structures and PXRD, the strong self-assembly of molecules with trans azobenzene groups would stabilize the energy of the ground state, and the fact that solid-state charging was not realized in the set of molecules indicates a considerable energy barrier for the azobenzene conversion in the close-packed structures. The charged molecules with metastable cis azobenzenes obtained from UV irradiation in solution are likely to be randomly oriented due to the steric repulsion between non-planar azobenzene units, possessing higher enthalpy.

4.3.3 The impact of phase change of charged materials on energy storage

In order to understand the energy barrier for charging in the solid state and the relative intermolecular interactions in the charged and uncharged materials, we examined the crystallinity of compounds before/after charging and after discharging (Figure 4-12a). The as-synthesized (uncharged) compounds, both monomers and polymers, are crystalline as sharp peaks are observed by PXRD (Figure 4-10 and Figure 4-11). The charged compounds were found to lose crystallinity, as the absence of diffraction indicates, and the crystallinity is restored when they were discharged (by heat or ambient light). By observing the PXRD patterns and the phase of materials, we find that charged monomers and polymers 1-3 are amorphous solids that undergo phase transition to crystalline trans isomers when triggered at a heating rate ranging between 0.5 and 10 °C min^{-1}. Charged monomer and polymer 4 are in the viscous liquid state (shown as the inset of Fig. 4-12a) and discharged at a slower heating rate ranging between 0.5 and 2 °C min^{-1} to release the maximum energy. If triggered at a higher scan rate of 5 °C min^{-1} or 10 °C min^{-1}, compound 4 released 140 kJ mol^{-1}, 79% of the maximum capacity, indicating that crystallization of 4 upon thermal isomerization in the liquid is a slower process than that of 1-3. This implies that measured exothermicity is a combined product of azobenzene isomerization and crystallization, and that one could decouple the two phenomena by varying the rate of heating (discharging).

Comparing the relative ΔH values among the molecules, we can infer that the length of alkyl spacers and the presence of the H-bonding moiety significantly affect the enthalpy and phase of the metastable state. To estimate the enthalpy difference between the trans and cis states, originating solely from the relative degree of intermolecular interaction, we measured the crystallization energy (ΔH_c) of each compound using DSC by integrating the crystallization peak (as shown in Figure 4-12b with compound 4) for the phase transition of the liquefied trans isomer to the solid
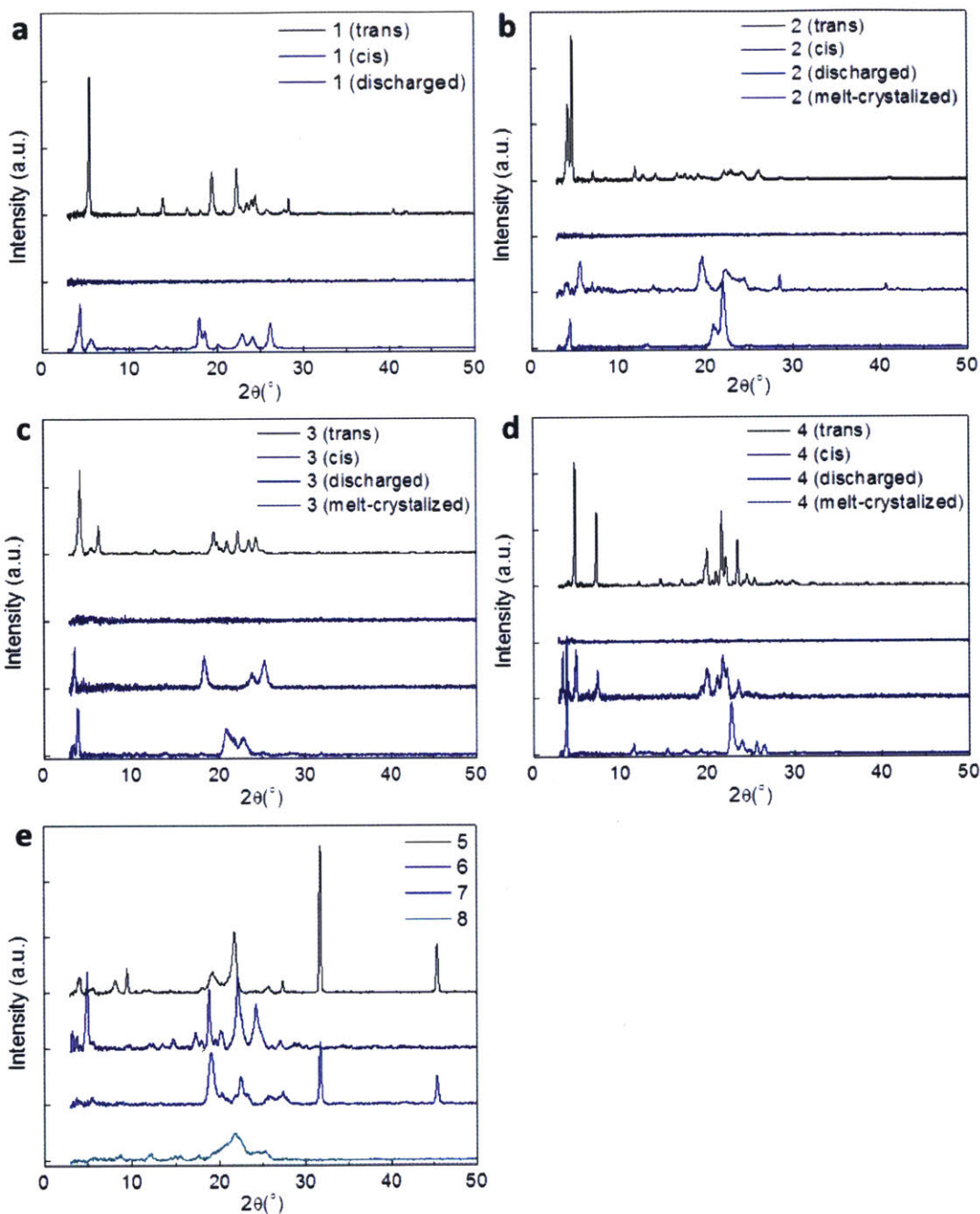
Figure 4-10: (a-d) PXRD of monomer 1-4 as synthesized (trans), charged (cis), discharged (trans), and melt-crystalized (trans). (e) PXRD of monomer 5-8 as synthesized (trans). In order to gauge how similar the isomerization-assisted phase transition from amorphous or liquid state to crystalline solid state is compared to the traditional liquid-to-solid phase transition, PXRD of compound 2-4 were also taken after melt-crystallization by DSC. The meltcrystallized solid exhibits different diffraction patterns from those of the discharged compounds often with enhanced crystallinity. Compound 1 was decomposed during melting, so meltcrystallization was not accomplished.

109
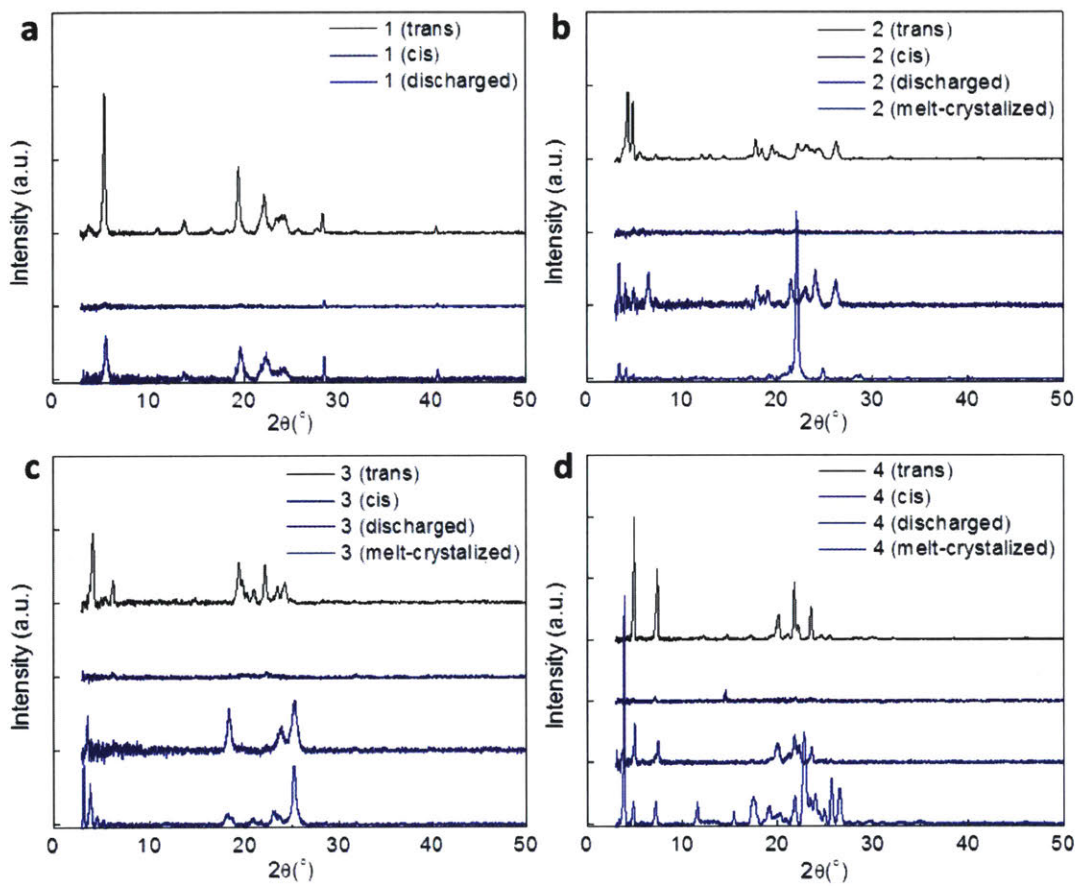
Figure 4-11: (a-d) PXRD of polymer 1-4 as synthesized (trans), charged (cis), discharged (trans), and melt-crystalized (trans).

Table 4.3: The crystallization energy (ΔHc) of compounds 2-4 measured by DSC[a]

Compound	1	2	3	4
ΔH_c [kJ mol^{-1}]	N.a.	38.6	58.9	68.0
ΔH_c [J g^{-1}]	N.a.	60.6	81.7	94.1

a. Compound 1 was decomposed at a high melting point. The temperature scan rate was 5 °C min^{-1} (compounds 2-3) or 2 °C min^{-1} (compound 4), identical to the scanning condition for $\Delta Htotal$ measurements.

state. although the phase transition occurring over the thermal reverse isomerization is not identical to that of the crystallization process from the liquid state (as shown in Figure 4-10), the transition from the randomly oriented amorphous morphology to crystalline packing is similar in both phenomena.

We find that the relative intensity of ΔH_c scales with the ΔH_{total} measured experimentally (Tables 4.1 and 4.3); ΔH_c of compounds 2-4 are 38.6 kJ mol^{-1}, 58.9 kJ mol^{-1}, and 68.0 kJ mol^{-1}, respectively. Thus, it is inferred that intermolecular H-bonding in these molecules lowers the energy gap between the ground and metastable states and that longer alkyl chains weakening the H-bonding are beneficial for large energy storage in this class of materials.

Also, we can suggest that enthalpy associated with the relative degree of intermolecular interactions or the phase of materials contributes to increasing $\Delta Htotal$ and that the high energy storage measured for azobenzene-functionalized diacetylenes and polydiacetylenes is strongly linked to the high crystallinity of the materials in the ground state and the amorphous or liquid phase of the metastable state. However, this class of materials has higher ΔH than pristine azobenzene, even without considering the phase change effect; ΔH_{total} - ΔH_c per azobenzene unit is 54.0 kJ mol^{-1} (2), 50.6 kJ mol^{-1} (3), and 54.1 kJ mol^{-1} (4), generally improved from the pristine azobenzene by 22-31%.

Figure 4-12c shows a new energy diagram of photon energy storage materials that undergo phase change by isomerization of photoswitches (azobenzene in this series of materials). ΔH_{iso} is the isomerization energy of compounds in the amorphous solid or
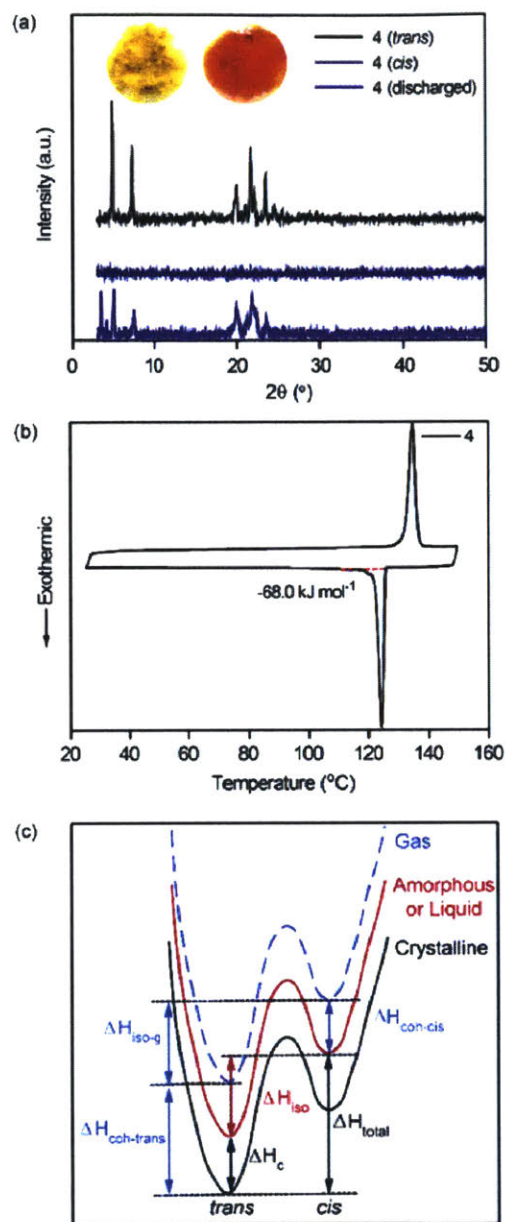
Figure 4-12: ((a) Powder X-ray diffraction of monomer 4 as synthesized (trans), charged (cis), and discharged (trans). The inset shows photographs of the as-synthesized (left) and charged (right) isomers with different phases (crystalline solid and liquid). (b) a DSC curve of uncharged monomer 4, showing melting and crystallization. The crystallization energy was obtained by integrating the crystallization peak below the dotted red baseline. (c) Energy diagram of azobenzene-derivative isomers (trans and cis) in different phases (gas, crystalline, amorphous or liquid). The meaning of ΔH_{iso}, ΔH_c, $\Delta H_{coh-trans}$, $\Delta H_{coh-cis}$, ΔH_{iso-g}, and ΔHtotal are explained in the main text.

112

liquid state, and ΔH_c is the crystallization energy of the trans isomer from either the amorphous solid or liquid state to the crystalline solid. $\Delta H_{coh-trans}$ is the cohesive enthalpy of the trans isomer from the gas state to the crystalline solid, while $\Delta H_{coh-cis}$ is the cohesive enthalpy of the cis isomer from the gas state to the amorphous solid or liquid state. ΔH_{iso-g} is the thermal isomerization enthalpy of the charged isomer in the gas phase. ΔH_{total} which is the experimentally measured heat release from the charged materials, can be expressed as the sum of ΔH_{iso} and ΔH_c.

To help fully understand this new diagram, we take compound 3 as an example and calculate all relevant thermodynamic quantities using DFT. We find that $\Delta H_{iso-g} = 119.0$ kJ mol^{-1} from our ab initio simulations, and as mentioned previously, $\Delta H_{coh-trans}$ computed as the energy difference between the enthalpy of the unit cell with two monomers and the enthalpy of two free-standing monomers, is 112.0 kJ mol^{-1}. Using the experimentally measured ΔH_{total} of 160.1 kJ mol^{-1}, we calculate $\Delta H_{coh-cis}$ according to the diagram as $\Delta H_{coh-cis} = \Delta H_{coh-trans} + \Delta H_{iso-g} - \Delta H_{total} = 70.9$ kJ mol^{-1}, which corresponds physically to the heat required to evaporate the cis monomers from their liquid state. Furthermore, if we assume that the isomerization enthalpy in the liquid state (ΔH_{iso}) is approximately the same as the isomerization enthalpy in the gas state (ΔH_{iso-g}), we can predict the crystallization enthalpy (ΔH_c) from this diagram using $\Delta H_c = \Delta H_{total}$ âĽŠ $\Delta H_{iso} = \Delta H_{total} - \Delta H_{iso-g} = 41.1$ kJ mol^{-1}. This assumption holds when the strength of intermolecular interactions in the liquid state is the same for both trans and cis isomers. Since the experimentally measured ΔH_c for compound 3 (58.9 kJ mol^{-1}) is higher than the calculated ΔH_c, this discrepancy suggests that the interaction between the trans isomers may be weaker than the cis isomers in the liquid state, as a result of the lower polarity of the trans compared to that of the cis.

Based on the understanding gained from the systematic analysis of the series of molecules in this work, we suggest the following design principle for high energy storage azobenzene-based molecules: trans isomers should be self-assembling structures to form crystalline materials, and cis isomers need to become liquid by steric distortion in

the absence of strong intermolecular interactions such as H-bonding. Molecules with high crystallization energy should be well-suited for the design of high energy density materials. The recently reported work on the azobenzene-functionalized ionic crystal and ionic liquid pair by Kimizuka and coworkers[35] also shows enhanced energy storage in the systems by photoinduced direct phase transition of materials (without the need of the solvation process). although the solid-state charging was realized for the ionic liquid, which is desirable for practical applications, the gravimetric energy density (143.3 J g^{-1} for the best molecule) is decreased significantly compared to that of the pristine azobenzene (227.3 J g^{-1}), due to bulky oligo(ethylene oxide)-based ammonium groups, necessary for lowering the melting point of ionic crystals.

In contrast, azobenzene-functionalized diacetylene and polydiacetylene derivatives reported in this work exhibit comparable or higher gravimetric ΔH (243.7 J g^{-1} for compound 4), although this high energy is only achieved by charging in solution and deposition of dried materials. although if one were to think of this as a device it would represent only a half-cycle, the goal of this work is not to explore the applications of photon energy storage materials but rather to understand key aspects of the chemistry that could allow us to further increase the energy density by combining macroscopic and molecular-level phase changes. Our results suggest a broad set of design strategies that could enable further development, optimization, and application of this new class of materials. For example, the limitation of the current system could be overcome by attaching bulky functional groups that provide sufficient free volume required for azobenzene photoisomerization in the solid state, despite the potential loss of crystallization enthalpy and the reduced gravimetric energy density. The search for photon energy storage systems that can both store high energy and change the phase in the solid state requires a systematic optimization of the molecular structures by varying the relative degree of intermolecular interactions in the ground and metastable states.

4.4 Conclusion

We present a new series of azobenzene-functionalized symmetric diacetylenes and polydiacetylenes, high energy density photon energy storage materials that can store up to 176.2 kJ mol^{-1} (or 200.2 kJ mol^{-1}, if completely charged); more than double that of pristine azobenzene, per azobenzene unit. The high energy storage is enabled by the photoisomerization of azobenzene units as well as the change in the intermolecular interactions in trans and cis states. We believe that the strong self-assembly and close-packed crystalline structure of diacetylene molecules in the ground state is essential to maximize the energy difference from the randomly oriented molecules in the metastable state. although the charging of such materials in the solid state remains a challenge, due to the suppressed photoswitching in the close-packed structure, further investigation on optimizing the balance between high crystallinity and capability to switch in films will be able to resolve this limitation.

Furthermore, we view this class of materials as a hybrid of traditional organic phase-change (PC) materials and photochromic molecules that can harvest photon energy and store latent heat as well. These hybrid materials offer the potential of new functionality to traditional organic PC materials such as paraffins and fatty acids, which possess large heats of fusion (around 150-250 J g^{-1}), and could enable long-term storage of the latent heat at room temperature due to the energy barrier for the reverse isomerization of the photoswitches. Given a broad parameter space of photoswitches and organic-based PC materials, and our newly engineering levers over controlling the trans and cis phases, this new paradigm in photon energy storage material design will enable a rapid progress in achieving higher energy density and novel functional materials. This approach stands to fully exploit the tremendous potential of these materials for renewable energy storage and heat release applications.

Chapter 5

Phototriggered Phase Change through Azobenzene Additives

5.1 Introduction

The work with diacetylene decorated azobenzene showed that the trans and cis state effects the phase of the material giving leverage on the storage energy density. The phase of a material is decided by intermolecular interactions, such as Van der Waals, dipolar interaction, and hydrogen bonding. The phase difference can arise from the unique properties which azobenzene holds compared to other photochromatic materials. The difference between the trans and cis state of azobenzene causes change in the geometry, length, planarity, and the dipole moment. The trans state has a planar geometry where the length is 9 Å while the cis state has a twisted geometry with the benzene ring tilted at 56° breaking the planarity of the structure and giving a length of 5.5 Å. [113] This structral difference causes difference in the dipole moment where the dipole moment is 0 - 1.2D for the trans state while 3.1 - 4.4D for cis. [106] Thus the property difference between the two states of azobenzene changes steric repulsion and dipolar interaction, which gave arise to phase difference between the trans and cis state for the azobenzene diacetylene. Using the difference between the trans and

the cis state, the concept of using azobenzene to influence phase change within the azobenzene based material has been also demonstrated when templated onto other materials systems. As mentioned in the previous chapter, macrocyclic[89, 90, 91] and linear[92] structured azobenzene materials demonstrated that change of the intermolecular interactions in such materials can allow macroscopic solid-liquid phase transition.

Azobenzene on template shows that the phase of the material can be determined by which state the azobenzene is in. However, what if the property difference between trans and cis azobenzene can change the phase change property of a material when azobenzene is added in as a dopant. Recently, the concept of utilizing structural difference between the trans and the cis state of azobenzene to induce change in phase change properties was applied to organic phase change material (PCM).[13] PCM stores thermal energy via latent heat from phase transition when heated above the melting point and releases the stored energy when the temperature is cooled to below the crystallization point reverting the PCM back to the original phase. Organic PCM, such as paraffin waxes, fatty acids, fatty alcohols, and polyethylene glycol, display large latent heat (heat storage based on phase change) and a wide range for melting (solid to liquid phase transition) and crystallization (liquid to solid phase transition) temperature.[114] However, conventional PCM requires a heat source and long-term storage of the thermal energy remains a challenge due to the fixed phase transition temperature, which prevents the transportation of thermally-charged PCMs away from the heat source. Since phase transition temperatures are governed by the intermolecular interactions, being able to control the key interactions within the phase of the material can control the phase transition temperature and thermal energy densities. The proof of concept of this idea was done using PCM trideconoic acid and azobenzene dopant, which is azobenzene functionalized with a tridecanoic ester group.[13] The tridecanoic ester group makes the azobenzene dopant miscible within the PCM. The difference between the trans and the cis state of the azobenzene dopant allowed for a crystallization temperature difference of up to 10 °C.

The reason for the 10 °C difference is due the difference in interaction of the PCM with the trans and cis state of azobenzene. Conventionally, n-fatty acid forms lamellar structures due to the hydrocarbon side packing (i.e. van der Waals forces), and COOH groups exhibiting polar interaction and H-bonding between the acid groups. [115, 116] The trans azobenzene dopant is expected to have little interaction with the tridecanooic acid PCM having little to no effect on the lamellar structure and on the thermal properties due to strong interaction with itself, from the aromatic cores and alkyl chain Van der Waals interaction.[117] However, the twisted conformation of the cis azobenzene disrupts the formation of lamellar structures of the PCM. The following is the photomoderated thermal energy storage and release cycle which the azo/PCM composite undergoes. As the temperature rises above the melting point (T_m) of the PCM, a composite made from azobenzene dopant and PCM melts and becomes liquid. In this state, trans azobenzene dopants can photoswitch into the twisted conformation cis azobenzene under UV irradiation. In the cis state, the liquid state of the composite can be cooled to a temperature below the original T_c, while preserving the stored thermal energy due to steric repulsion and dipolar interaction induced by the cis azobenzene disrupting the packing of the PCM. When the composite is irradiated by visible light, the dopants switch back to the trans state and triggers crystallization releasing the stored thermal energy.[13]

The previous work focused on a single PCM material, tridecanoic acid, while changing the azobenzene dopants.[13] In this chapter, a single azobenzene dopant will be used while changing the PCM material. A wide range of PCM material will be screened for a better understanding of the interaction between the PCM materials and azobenzene dopants. This will lead to criterias for design parameters of the PCM/azobenzene dopant composite. We want to ultimately achieve a ΔT_c large enough between the trans and the cis state composite, to retain the liquid state and allow storage at room temperature.
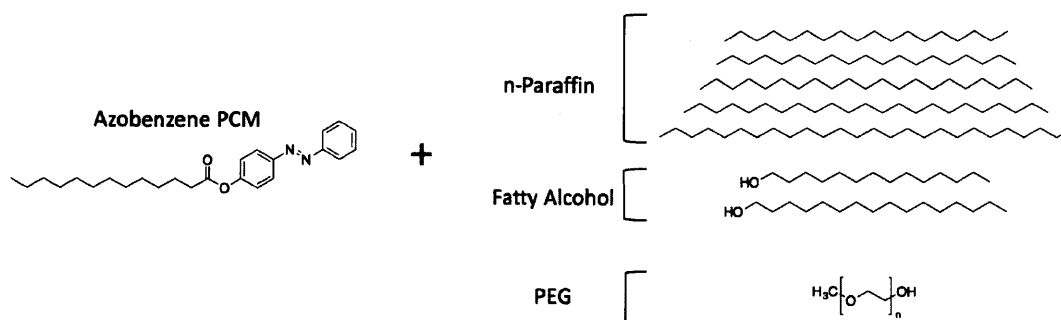
Figure 5-1: Chemical structures of the various PCM materials and azobenzene dopant. Three different types of PCM materials were selected: n-paraffin, fatty alcohol, and polyethylene glycol. Five n-paraffin, two fatty alcohol, and one polyethylene glycol(PEG) was selected for the study. The n-paraffin material was selected to understand the interactions between non-polar PCM material and the chain length of the molecule on T_c difference between the trans and the cis doped mixture. The two fatty alcohols were selected to study the presence of hydrogen bonding on ΔT_c. PEG was selected to explore the possiblity of the dopants having an affect on long polymer chain like structures.

5.2 Selection of Phase Change Materials

In this study, a wide variety of organic PCM was selected to understand the interaction between the PCM and azobenzene dopant on the T_c difference, ΔT_c, between PCM with doped the trans or cis. The azobenzene dopant used for the study was the same one as the previous study, namely azobenzene functionalized with tridecanoic ester group on the para position. Figure 5-1 shows the chemical structures of the azobenzene dopant and PCMs used. In order to understand the role the PCM plays on ΔT_c, we chose three different types of PCM. This is the n-paraffin, fatty alcohol, and polyethylene glycol. For the n-paraffin, five different molecules were selected: octadecane ($C_{18}H_{38}$), nonadecane ($C_{19}H_{40}$), heneicosane ($C_{21}H_{44}$), tricosane ($C_{23}H_{48}$), hexacosane ($C_{26}H_{54}$). For the fatty alcohol, 1-tetradecanol($C_{14}H_{29}OH$) and cetyl alcohol ($C_{16}H_{34}$)OH) was selected and lastly polyethylene glycol with molecular weight of 2000 was selected. All composites were made with 36 mol % azobenzene dopant with the corresponding PCM except for PEG, due to the large molecular weight, which was made with 50 weight %.
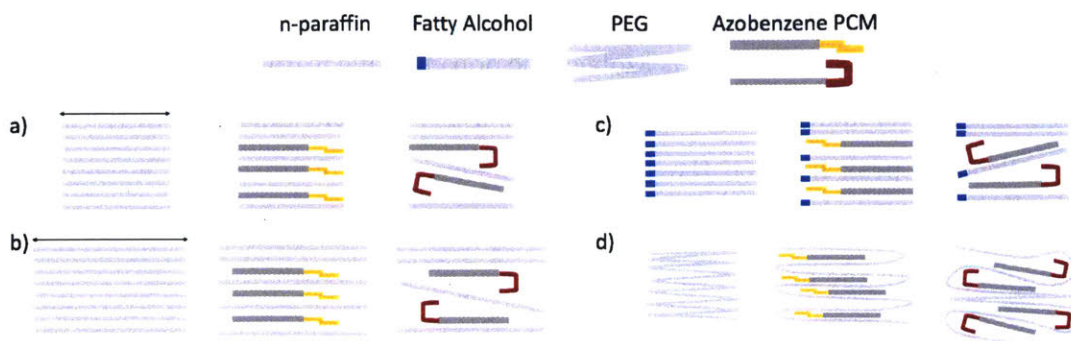
Figure 5-2: Cartoon of azobenzene based dopant in phase change material. a) and b) depicts different n-paraffin carbon chain length interacting with the azobenzene dopant molecule. c) shows the presence of hydrogen bons, in blue at the left end, and the interaction with the azobenzene dopant molecule. d) shows how the lengthy polymer chain can be affected by the azobenzene dopant.

The n-paraffin was selected to look explore the interaction of the azobenzene dopant with a non-polar PCM. Due to the relative small phase change temperature increase with increase in carbon chain length, this allows for careful testing of the composite material over a large temperature range. The dependence of chain length and ΔT_c will also be studied, as seen in Figure 5-2a,b. The fatty alcohol was selected to examine the role of hydrogen bonding on ΔT_c, Figure 5-2c. Finally the PEG was selected to explore the possibilty of the dopants having an affect on long polymer chain like structures, Figure 5-2d .

5.3   n-Paraffin and Azobenzene

The T_c of the composite was measured using differential scanning calorimetry (DSC). The cis state samples were prepared by charging with UV light at a temperature above the melting point. The DSC comparision of the trans(red line) and cis (blue line) state heneicosane/azobenzene composite can be seen on Figure 5-3a. The cis state composite crystallizes at 34.1 °C while the trans state composite crystallizes at 37.1 °C demonstrating a ΔT_c of 3 °C. The right most peak on the trans DSC curve represents the crystalllization of the trans azobenzene dopant while the left most peak

represent a minor polymorph. [118] The left most peak on the cis DSC curve represents the crystalllization of the cis azobenzene dopant while features on the slight left of the main peak indicates formation of polymorphs. [13] The difference in the main crystallization peak between the trans and the cis state confirms that the interaction between the trans and the cis azobenzene dopant forms different intermolecular interactions with the heneicosane.

From the trans DSC measurements of the heneicosane(HNC)/azobenzene(azo) dopant composite, we can see that the azo dopants crystallizes before the HNC crystallizes. Thus, the trans azo dopants are expected to form lamellar structures due to the Van der Waals interaction with the aliphatic chains and π-π stacking. [13] Then the heneicosane lamellar structure forms around the trans azo dopant lamellar structure. This is most likely to form similar lamellar stacking to that of binary n-paraffin mixtures, where each of the components of the binary mixture forms a ''lamellar block'' which is then stacked into the lattice, which needs additional XRD experiments to confirm. [119] However, in the case of the cis state, the structure prevents formation of lamellar blocks lowering the T_c of the azobenzene dopant. The low T_c allows the cis azobenzene dopant to remain dispersed throughout the composite and prevent the crystallization of the heneicosane thus lowering the T_c.

Another important factor in this work is to show the temperature limit and the percent of cis needed for obtaining reasonable ΔT_c. The temperature dependent charging percent was measured by ^{1}H NMR analysis of the cis fraction. The charging was done in the molten state heneicosane/azobenzene composite at 45°C, 60 °C, and 70 °C overnight to ensure that the charging has reached a photostationary state (Figure 5-3d). As expected at the temperature increased, the maximum charging percent decreased. However, ΔT_c did not follow the same trend. Although the charging percent at 45°C to 60 °C decreased from about 90% to 60%, ΔT_c showed little difference. However when the temperature was increased to 70 °C, a significant drop in ΔT_c occurred.

Figure 5-3: a) Differential scanning calorimetry (DSC) scans of trans state and cis state heneicosane/azobenzene composites (36 mol% doped) obtained while cooling from 70 °C at a rate of 10 °C/min, illustrating different crystallization points (T_1 and T_2) and the gap (ΔT_c). b) Temperature dependent charging percent (cis state percent) of azobenzene charged at molten state of heneicosane/azobenzene composite(blue line) and T_c difference depending on temperature charged and charging percent (red line). c) T_c vs. number of carbon. T_{PCM}, $T_{PCM+Trans}$, $T_{PCM+Cis}$ indicates the T_c of PCM, PCM/trans azobenzene dopant composite, and PCM/cis azobenzene dopant composite respectively. d) ΔT vs. number of carbon. $\Delta T_{Trans-Cis}$, $\Delta T_{PCM-Trans}$, $\Delta T_{PCM-Cis}$ indicates the T_c difference between the PCM/trans composite and the PCM/Cis composite, PCM and PCM/trans composite, and the PCM and PCM/cis composite, respectively.

123
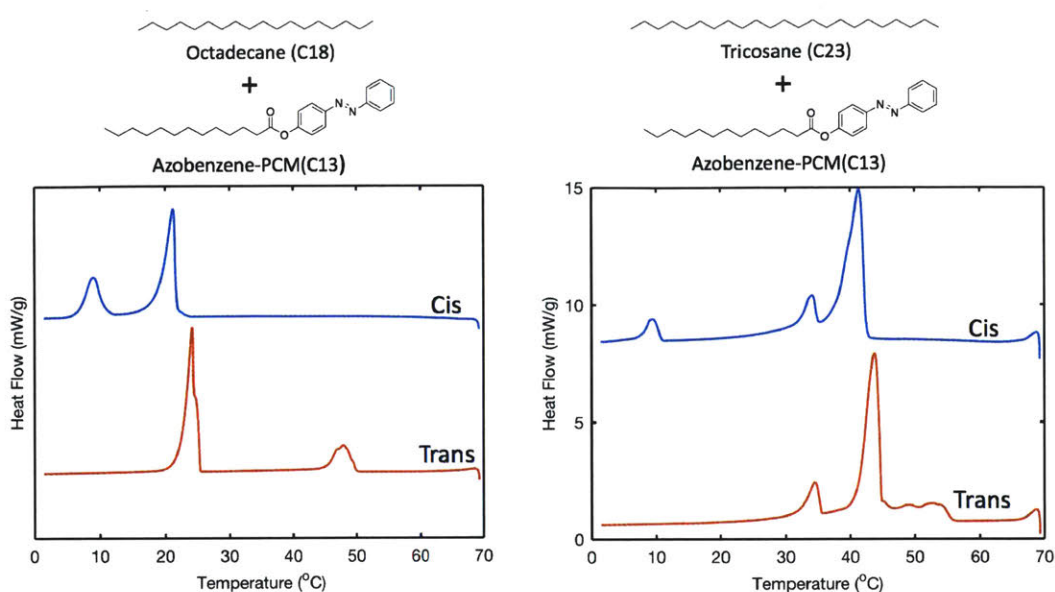
Figure 5-4: DSC scans of the trans and cis state of octadecane/azobenzene composite (left) and tricosane/azobenzene composite (right).

In the binary mixture of n-paraffin, the variation of the concentration affects the phase change temperature of the composite. [120] Furthermore adding a lower phase change temperature component lowered the overall phase change temperature of the binary mixture, where the larger the phase change temperature difference between two components, the larger this effect was observed. However, this was not the case for the n-paraffin/azobenzene dopant composite. Figure 5-3c shows the T_c of PCM only (T_{PCM}), PCM/ trans azobenzene dopant composite ($T_{PCM+Trans}$), and PCM/cis azobenzene dopant composite ($T_{PCM+Cis}$) vs. the number of carbon. Figure 5-3d shows the temperature difference between the each of the crystallization temperature shown in Figure 5-3c vs number of carbon. With increasing carbon length, the trans and cis azo dopant seemed to have different effect on the T_c. As expected for the cis azo/pcm composite, with increasing number of carbon, $\Delta T_{PCM-Cis}(T_{PCM}-T_{PCM+Cis})$ is also increasing, because the T_c difference of each of PCM and cis azo is also increasing. However, for the trans azo/PCM composite, with increasing number of carbon, $\Delta T_{PCM-Trans}$ ($T_{PCM}-T_{PCM+Trans}$) increases although the T_c difference of the PCM and trans azo is also decreasing with increasing carbon length of the PCM.

124

$\Delta T_{Trans-Cis}$ ($T_{PCM+Trans}$-$T_{PCM+Cis}$) decreases due to this.

One explanation for the increase in $\Delta T_{PCM-Trans}$ is the change of the interactions between the azobenzene dopant and chain length of the n-paraffin. To better understand this, the DSC scans for the 18 carbon long octadecane(OTC)) and the 23 carbon long tricosane (TCS) was compared(Figure 5-4). For the trans DSC scans in both cases, the trans Azo dopant and PCM DSC peak showed a significant difference. However, in both cases, the cis Azo crystallization peak is independent of the PCM crystallization peak. This shows that the trans azobenzene dopant is interacting with the two different PCM differently. In the case of the OTC, the trans azobenzene crystallization peak seemed independent of the OTC crystallization peak. However, for the TCS, the trans azobenzene peak shows formation of several polymorphs, which merges with the PCM peak. TCS and trans Azo interact strongly during crystallization, affecting the crystallization dynamics of the TCS lowering the T_c of the composite. This may be due to TCS having a higher and much closer T_c to trans azobenzene or the TCS having a stronger interaction with the Azo dopants, although further investigation is needed to verify this.

5.4   Fatty Alcohol, PEG, and Azobenzene

The DSC measurements for fatty alcohol, cetyl alcohol (CA) and 1-tetradecanol (1-TDC), and PEG were prepared using the same procedure as the n-paraffin case. The DSC comparision of the trans(red line) and cis (blue line) state for 1-tetradecanol/azobenzene composite can be seen on Figure 5-5a. The right most peak on the trans DSC curve represents the crystalllization of the trans azobenzene dopant while the main peak shows crystallization of two phases.[121]The right most peak on the cis DSC curve represents the crystalllization of a single phase while the left most peak represents crystallization of the cis azobenzene dopant.[13] The cis state composite crystallizes at 27.5 °C while the trans state composite crystallizes at 34.2 °C demonstrating an increase ΔT_c of 6.7 °C compared to the n-paraffin.
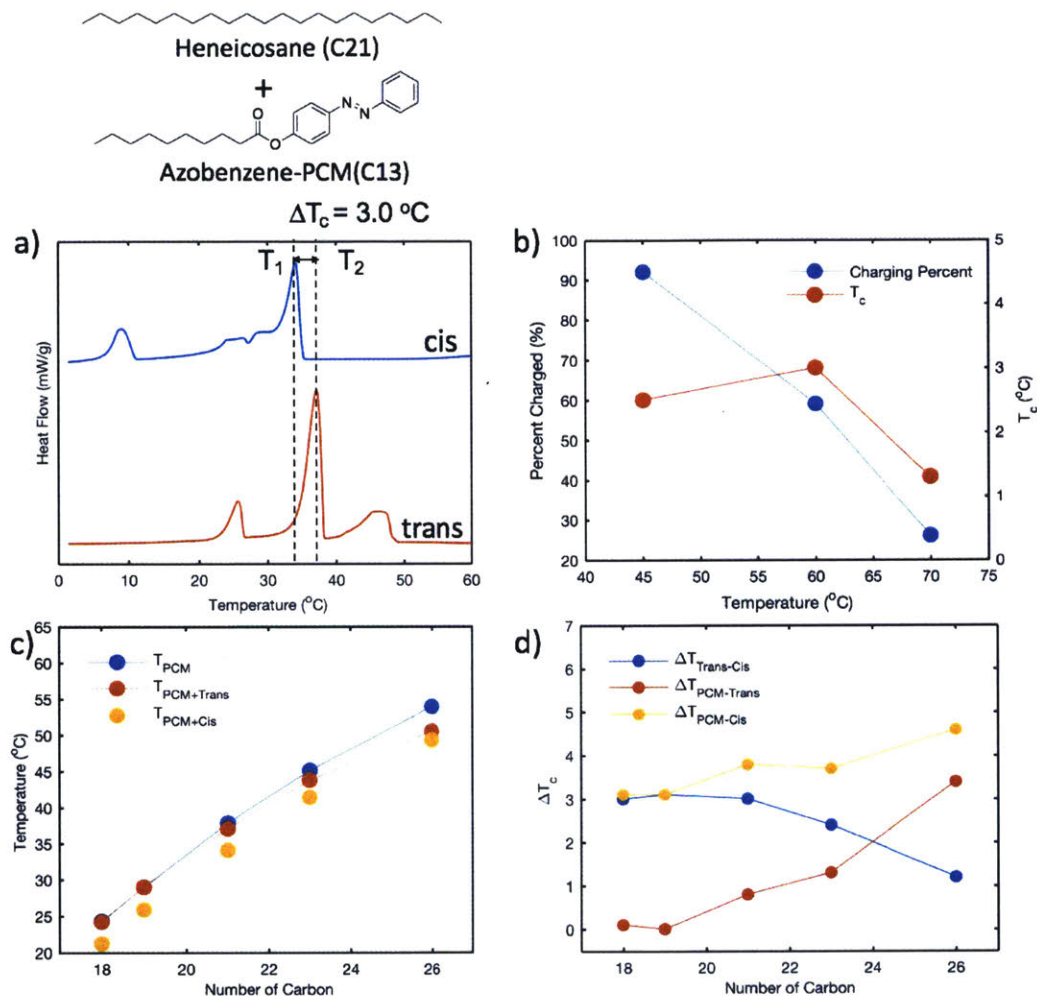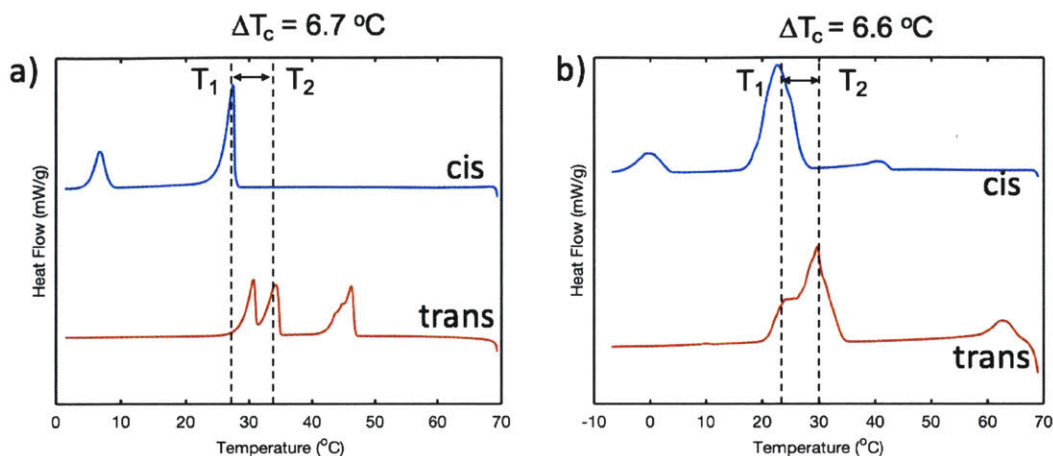
Figure 5-5: a) Differential scanning calorimetry (DSC) scans of trans state and cis state 1-tetradecanol/azobenzene composites (36 mol% doped) obtained while cooling from 70 °C at a rate of 10 °C/min, illustrating different crystallization points (T_1 and T_2) and the gap (ΔT_c). b) Differential scanning calorimetry (DSC) scans of trans state and cis state PEG/azobenzene composites.

The increase in the ΔT_c for 1-TDC is due to the presence of the OH group at the end of the fatty alcohol. The stronger the intermolecular interaction the higher the phase change temperature. Although 1-TDC had a shorter carbon chain length leading to less Van dar Waals interaction, the -OH introduces hydrogen bonding, a strong intermolecular electrostatic interaction, giving a similar melting temperature to that of the heneicosane. However, the stronger electrostatic interaction means that breaking this bond will lead to a much lower T_c. From the DSC scan (Figure 5-5a), we see that the trans azobenzene dopant and 1-TDC crystallize independently from one another. However when looking at the 1-TDC/Cis azobenzene composite, the two distinct crystallization peaks of 1-TDC become one showing that the presence of the cis azobenzene is strongly affecting the 1-TDC crystallization dynamics. This is most likely due to interaction between the 1-TDC OH group and the azobenzene nitrogen double bonds, essentially screening the OH of the PCM, causing hydrogen bonding between the molecules to weaken, although further investigation is needed. The close interaction between the cis azobenzene dopant and 1-TDC is ultimately breaking the hydrogen bonds of the PCM itself lowering the overall phase change

126

temperature.

The DSC comparision, shown in Figure 5-5b, of the trans(red line) and cis (blue line) state PEG/azobenzene composite can be seen. The T_c between the trans and the cis decreased by 6.6 °C. Depending on the material added to PEG, the interaction of PEG with itself can be weakened lowering the phase change temperatures. In a study done by Wang et al, the phase change temperature was lowered when graphene oxide was added to PEG. [122] Based on the temperature difference achieved, the cis azobenzene dopant weakens the interaction of the PEG effectively while the trans azobenzene dopant does not. Further investigation is needed to understand the interaction between PEG and azobenzene dopants and the correlation with phase change temperature. Addition of a polar component to the PCM proved to be an effective way to maximize $\Delta T_{Trans-Cis}$. Disruption of the much stronger intermolecular interaction more than doubled $\Delta T_{Trans-Cis}$ compared to non-polar PCM, which only has Van dar Waals interactions. Figure 5-6 shows the T_c vs. polar PCM and T_c difference ΔT vs. the polar PCM. Although Figure 5-6a shows that T_c is lowered in the trans state compared to the original PCM, the cis state has a larger effect in lowering the T_c allowing $\Delta T_{Trans-Cis}$ to have similar values. With no interaction between the trans azobenzene and the PCM, these results imply that a maximum of 8 °C can be achieved.

5.5 Design Principles, Future Work, and Conclusion

Through thermal analysis of azobenzene dopants and the three types of PCM, we have gained a better understanding for obtaining a larger ΔT. Since the study was focused on varying the PCM, selection of PCM to ensure higher ΔT can be made. The key is to maximize the disruption of PCM molecular interaction with the cis state Azo dopant while minimizing it for the trans state Azo dopant. An organic PCM should be selected which has a large number of polar components governing the molecular interaction. Thus PCMs with a short carbon chain but a high phase change
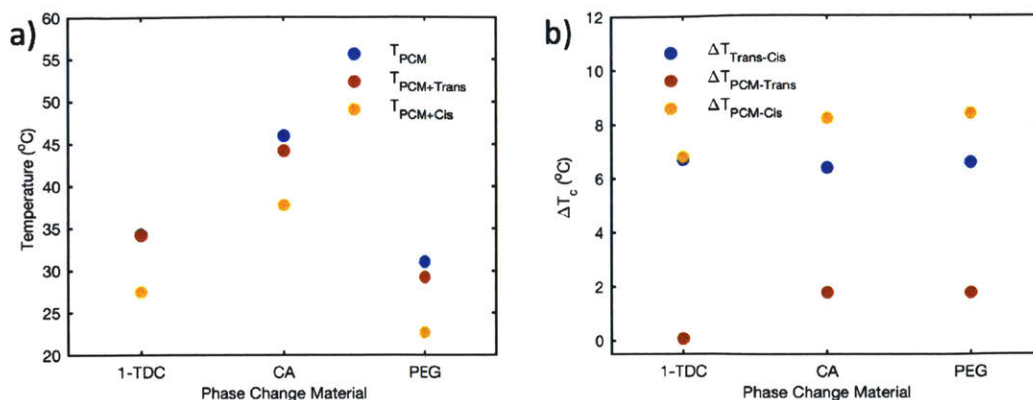
Figure 5-6: a) The T_c vs. polar PCM and b) T_c difference ΔT vs. the polar PCM. The lines are present to assist with looking at the graph. no correlation is present between the three.

temperature should be selected. As for the azobenzene dopant design, the carbon chain should be similar length to that of the PCM. However, further experiments are needed to fully understand this. Another approach may be to add polar groups, such as carboxylic acid or OH groups. This should also be investigated to see the role polar groups play in influencing ΔT. Strengthening the interaction between the dopant molecule and PCM material and driving the PCM/azobenzene composite to higher T_c for the trans may also help in increasing ΔT.

In order to further understand the exact mechanism more indepth fundamental research is needed. First off, azobenzene dopant with a longer and shorter carbon chain length should be tested to see the correlation between the length of the carbon chain on the azobenzene and $\Delta T_{Trans-Cis}$. Second, a temperature dependent X-ray diffraction measurement should be done on the trans and cis state for octadecane and tricosane based composite to understand the difference in crystallization of the PCM and azobenzene dopant for the two cases. For 1-TDC the disappearance of one of the crystallization peaks should be investigated further to understand the effect of cis azobenzene dopant on crystallization dynamics of the PCM. In addition a raman or FTIR study on the PCM/azobenzene composite should be done to see the bonds affected by the interaction between PCM and dopant. Simulation of binding energy

128

between the dopant, PCM, and dopant/PCM should also be looked at the ensure full understanding of the interaction taking place.

In conclusion, controlling the intermolecular interactions between PCMs and photochromic dopants for thermal energy storage proved to be effective in a wide variety of organic PCM. 3 types of organic PCM with 8 different PCM were selected to show the possiblility of this concept. This simple approach in a variety of PCM materials showed that controlling the molecular interaction between the PCM and photochromatic dopant is key in maximizing ΔT. Furthermore, the strength of the molecular interaction of the PCM which governs the phase change temperature plays a crucial role. The larger the strength of the molecular interaction the more dramatic effect it will have on the crystallization temperature when this molecular interaction is broken. This understanding will provide insights to thermal energy management for a wide range of potential applications such as waste heat recycling, solar thermal collection, and smart temperature systems for buildings.

Chapter 6

Conclusion

This thesis focused on the understanding and engineering a molecule with unique properties for thermal storage applications. The molecule azobenzene was selected and new approaches were undertaken to modify and engineer the material to be used as a thermal battery as well as to mediate thermal energy storage in other materials. The first approach was the concept of solar thermal fuel, which is storing the solar energy in rearraged bonds of the azobenzene and later releasing that energy in the form of heat. The second approach was to use the structural property difference of the two states of azobenzene in order to control phase change. I have synthesized, characterized, and analyzed variations of this azobenzene molecule for each of the suited purposes.

Motivated by the azo/CNT hybrid showing improvement in STF properties in the solid state, the STF research was steered towards development of solid-state STF. The chapter 2 showed the development of a solar thermal fuel capacitor platform using polymer films, first demonstrating the possibillity of using solar thermal fuel in the solid state. The polymer platform allowed fabrication of a thin film, which enabled charging, discharging, and heat release using optically chargeable molecules all within the solid-state. The polymer solar thermal fuel material allowed uniform morphologies that can span thicknesses of 100 nm to several tens of micrometers

with added tunability by employing UV-activated cross-links. Studying of the charging and discharging properties, and the heat energy stored, a macroscopic device was constructed resulting in temperature differences as high as 10 °C between the charged and uncharged, demonstrating the feasibility of these devices for solid-state applications.

As a continuation of this approach, chaper 3 showed molecularly engineered azobenzene with the aim of developing tunable and optimized STFs for solid-state applications. Three azobenzene derivatives functionalized with bulky aromatic groups (phenyl, biphenyl, and tert-butyl phenyl groups) were designed and synthesized. In contrast to pristine azobenzene, which crystallizes and makes non-uniform films, the bulky azobenzene derivatives formed uniform amorphous films that can be charged and discharged with light and heat for many cycles. Aside from increasing energy storage and promoting solid state STFs, molecular engineering proved to be a powerful and effective method in improving other solar thermal fuel properties, such as chargeability and the thermal stability of the thin film.

The second portion of the thesis utilized the difference in trans and cis azobenzene to look at phase change as a thermal energy storage mechanism. In chapter 4, a photocontrolled self-assembly and disassembly of photon energy storage materials based on new diacetylene derivatives with azobenzene moieties and with varied alkyl spacers and linkers was demonstrated. Increase in the energy stored per molecule was seen. The extra energy storage in the materials in addition to the isomerization enthalpy of azobenzene units was enabled by the different phase of materials in the ground state (crystalline solid) and in the metastable state (amorphous solid/liquid).The synthesized material not only showed solar energy storage but also revealed that phase change characteristic of organic materials can be a parameter to consider in terms of designing high energy density photon energy storage materials.

Motivated from work in chapter 4, chapter 5 looked at azobenzene dopants in organic PCM to change phase change properties. Azobenzene-based dopants were

added to organic phase change materials to photomoderate the phase change temperature. A wide variety of phase change materials were used to test the possibilty of this concept in a wide range of phase change materials. A large phase change temperature difference was seen of up to 7 °C by using the structual difference between the trans and the cis state of azobenzene. Ultimately, the phase change materials need to have strong intermolecular interaction with one another to maximize the effect brought on by the azobenzene dopant since breaking this interaction will prevent crystallization and allow cooling to lower temperatures. The azobenzene dopant proved to be an effective method for controlling phase change in a wide variety of organic phase change materials.

This thesis makes many contributions to the field of thermal energy storage using STF molecule azobenzene. The first part develops a new concept in the field of solar thermal fuel to make use of the STF in the solid state. Chapter 2 utilizes a polymer template to demostrate solid-state solar thermal fuel and shows macroscopic heat release. Chapter 3 uses molecular engineering of the azobenzene molecule to tune and improve solid-state solar thermal fuel properties. The second part explores the use of phase change for thermal energy storage was developed. Chapter 4 shows through azobenzene decorated diacetylene that phase change can be a parameter to consider for thermal energy storage and from this motivation was given to chapter 5 to look at photomoderating phase change properties of PCM using azobenzene in a wide variety of organic PCM. Each research shown in this thesis lead to the next resulting in promising directions for future work on converting solar energy to renewable energy in the form of heat. Further understanding and engineering of the azobenzene molecule can improve these concepts and open new paths, one day making big contributions to novel thermal energy storage devices.

Bibliography

[1] R. Perez and M. Perez. A fundamental look at energy reserves for the planet. *The International Energy Agency SHCP Solar Update*, 50:2–3, April 2009.

[2] Diana Ürge-Vorsatz, Luisa F. Cabeza, Susana Serrano, Camila Barreneche, and Ksenia Petrichenko. Heating and cooling energy trends and drivers in buildings. *Renewable and Sustainable Energy Reviews*, 41:85–98, January 2015.

[3] Henri Bouas-Laurent and Heinz Dürr. Organic photochromism (IUPAC Technical Report). *Pure and Applied Chemistry*, 73(4):639–665, 2001.

[4] Constantine Philippopoulos, Dimitrios Economou, Constantine Economou, and John Marangozis. Norbornadiene-quadricyclane system in the photochemical conversion and storage of solar energy. *Industrial & Engineering Chemistry Product Research and Development*, 22(4):627–633, December 1983.

[5] Roland Boese, J. Kevin Cammack, Adam J. Matzger, Kai Pflug, William B. Tolman, K. Peter C. Vollhardt, and Timothy W. Weidman. Photochemistry of (Fulvalene)tetracarbonyldiruthenium and Its Derivatives: Efficient Light Energy Storage Devices. *Journal of the American Chemical Society*, 119(29):6757–6773, July 1997.

[6] John Olmsted III, Jerry Lawrence, and Geary G. Yee. Photochemical storage potential of azobenzenes. *Solar Energy*, 30(3):271–274, 1983.

[7] Alexie M. Kolpak and Jeffrey C. Grossman. Azobenzene-Functionalized Carbon Nanotubes As High-Energy Density Solar Thermal Fuels. *Nano Letters*, 11(8):3156–3162, August 2011.

[8] Alexie M. Kolpak and Jeffrey C. Grossman. Hybrid chromophore/template nanostructures: A customizable platform material for solar energy storage and conversion. *The Journal of Chemical Physics*, 138(3):034303, January 2013.

[9] Timothy J. Kucharski, Nicola Ferralis, Alexie M. Kolpak, Jennie O. Zheng, Daniel G. Nocera, and Jeffrey C. Grossman. Templated assembly of photoswitches significantly increases the energy-storage capacity of solar thermal fuels. *Nature Chemistry*, 6(5):441–447, May 2014.

[10] Yun Liu and Jeffrey C. Grossman. Accelerating the Design of Solar Thermal Fuel Materials through High Throughput Simulations. *Nano Letters*, 14(12):7046–7050, December 2014.

[11] Tatsushi Imahori, Ryo Yamaguchi, and Seiji Kurihara. Azobenzene-Tethered Bis(Trityl Alcohol) as a Photoswitchable Cooperative Acid Catalyst for Morita–Baylis–Hillman Reactions. *Chemistry – A European Journal*, 18(35):10802–10807, August 2012.

[12] Joosub Lee, Minkyeong Pyo, Sang-hwa Lee, Jaeyong Kim, Moonsoo Ra, Whoi-Yul Kim, Bum Jun Park, Chan Woo Lee, and Jong-Man Kim. Hydrochromic conjugated polymers for human sweat pore mapping. *Nature Communications*, 5:3736, April 2014.

[13] Grace G. D. Han, Huashan Li, and Jeffrey C. Grossman. Optically-controlled long-term storage and release of thermal energy in phase-change materials. *Nature Energy(submitted)*, 2017.

[14] Susan E. Habas, Heather A. S. Platt, Maikel F. A. M. van Hest, and David S. Ginley. Low-Cost Inorganic Solar Cells: From Ink To Printed Device. *Chemical Reviews*, 110(11):6571–6594, November 2010.

[15] Serap Günes, Helmut Neugebauer, and Niyazi Serdar Sariciftci. Conjugated Polymer-Based Organic Solar Cells. *Chemical Reviews*, 107(4):1324–1338, April 2007.

[16] Martin A. Green, Anita Ho-Baillie, and Henry J. Snaith. The emergence of perovskite solar cells. *Nature Photonics*, 8(7):506–514, July 2014.

[17] Matthew Wright and Ashraf Uddin. Organic—inorganic hybrid solar cells: A comparative review. *Solar Energy Materials and Solar Cells*, 107:87–111, December 2012.

[18] Yi Ma, Xiuli Wang, Yushuai Jia, Xiaobo Chen, Hongxian Han, and Can Li. Titanium Dioxide-Based Nanomaterials for Photocatalytic Fuel Generations. *Chemical Reviews*, 114(19):9987–10043, October 2014.

[19] Prashant V. Kamat and Juan Bisquert. Solar Fuels. Photocatalytic Hydrogen Generation. *The Journal of Physical Chemistry C*, 117(29):14873–14875, July 2013.

[20] Atul Sharma, V. V. Tyagi, C. R. Chen, and D. Buddhi. Review on thermal energy storage with phase change materials and applications. *Renewable and Sustainable Energy Reviews*, 13(2):318–345, February 2009.

[21] Ilan Gur, Karma Sawyer, and Ravi Prasher. Searching for a Better Thermal Battery. *Science*, 335(6075):1454–1455, March 2012.

136

[22] Henri Bouas-Laurent and Heinz Dürr. Organic photochromism (IUPAC Technical Report). *Pure and Applied Chemistry*, 73(4):639–665, 2001.

[23] Timothy J. Kucharski, Yancong Tian, Sergey Akbulatov, and Roman Boulatov. Chemical solutions for the closed-cycle storage of solar energy. *Energy & Environmental Science*, 4(11):4449–4472, October 2011.

[24] F Weigart and Eder's Jahrbuch. Photon energy storage in organic materials-the case of linked anthracenes. *Chem. Abstr.*, 4:3170.

[25] A.V. ElÊźtïÿäsïÿąov. *Organic Photochromes*. Consultants Bureau, New York, 1990.

[26] Nicholas Turro. *Modern Moleculer Photochemistry*.

[27] Alexander D. Dubonosov, Vladimir A. Bren, and V. A. Chernoivanov. Norbornadiene–quadricyclane as an abiotic system for the storage of solar energy. *Russian Chemical Reviews*, 71(11):917, November 2002.

[28] V. A. Bren', Alexander D. Dubonosov, Vladimir I. Minkin, and V. A. Chernoivanov. Norbornadiene–quadricyclane — an effective molecular system for the storage of solar energy. *Russian Chemical Reviews*, 60(5):451, May 1991.

[29] Mikael J. Kuisma, Angelica M. Lundin, Kasper Moth-Poulsen, Per Hyldgaard, and Paul Erhart. Comparative Ab-Initio Study of Substituted Norbornadiene-Quadricyclane Compounds for Solar Thermal Storage. *The Journal of Physical Chemistry C*, 120(7):3635–3645, February 2016.

[30] Maria Quant, Anders Lennartson, Ambra Dreos, Mikael Kuisma, Paul Erhart, Karl Börjesson, and Kasper Moth-Poulsen. Low Molecular Weight Norbornadiene Derivatives for Molecular Solar-Thermal Energy Storage. *Chemistry – A European Journal*, 22(37):13265–13274, September 2016.

[31] A. A. Gorman, R.L. Leyland, M. A. J. Rodgers, and P. G. Smith. Concerning the mechanism of interaction of triplet benzophane with norbornadienes and quadracyclanes. *Tetrahedron Letters*, 14:5085–5090, 1973.

[32] Yosuke Kanai, Varadharajan Srinivasan, Steven K. Meier, K. Peter C. Vollhardt, and Jeffrey C. Grossman. Mechanism of Thermal Reversal of the (Fulvalene)tetracarbonyldiruthenium Photoisomerization: Toward Molecular Solar-Thermal Energy Storage. *Angewandte Chemie International Edition*, 49(47):8926–8929, November 2010.

[33] Hiroshi Taoda, Kiyoshi Hayakawa, Kaoru Kawase, and Hiromi Yamakita. Photochemical Conversion and Storage of Solar Energy by Azobenzene. *Journal of Chemical Engineering of Japan*, 20(3):265–270, 1987.

[34] Kouta Masutani, Masa-aki Morikawa, and Nobuo Kimizuka. A liquid azobenzene derivative as a solvent-free solar thermal fuel. *Chemical Communications*, 50(99):15803–15806, November 2014.

[35] Keita Ishiba, Masa-aki Morikawa, Chie Chikara, Teppei Yamada, Katsunori Iwase, Mika Kawakita, and Nobuo Kimizuka. Photoliquefiable Ionic Crystals: A Phase Crossover Approach for Photon Energy Storage Materials with Functional Multiplicity. *Angewandte Chemie International Edition*, 54(5):1532–1536, January 2015.

[36] Wen Luo, Yiyu Feng, Chen Cao, Man Li, Enzuo Liu, Shipei Li, Chengqun Qin, Wenping Hu, and Wei Feng. A high energy density azobenzene/graphene hybrid: a nano-templated platform for solar thermal storage. *Journal of Materials Chemistry A*, 3(22):11787–11795, May 2015.

[37] Thomas A. Singleton, Kevin S. Ramsay, Mirela M. Barsan, Ian S. Butler, and Christopher J. Barrett. Azobenzene Photoisomerization under High External Pressures: Testing the Strength of a Light-Activated Molecular Muscle. *The Journal of Physical Chemistry B*, 116(32):9860–9865, August 2012.

[38] Xiaohong Cheng, Qianqian Li, Conggang Li, Jingui Qin, and Zhen Li. Azobenzene-Based Colorimetric Chemosensors for Rapid Naked-Eye Detection of Mercury(II). *Chemistry – A European Journal*, 17(26):7276–7281, June 2011.

[39] Gayatri K. Joshi, Karl N. Blodgett, Barry B. Muhoberac, Merrell A. Johnson, Kimberly A. Smith, and Rajesh Sardar. Ultrasensitive Photoreversible Molecular Sensors of Azobenzene-Functionalized Plasmonic Nanoantennas. *Nano Letters*, 14(2):532–540, February 2014.

[40] Violetta Ferri, Mark Elbing, Giuseppina Pace, MichaelâĂĚD. Dickey, Michael Zharnikov, Paolo Samorì, Marcel Mayor, and MariaâĂĚAnita Rampi. Light-Powered Electrical Switch Based on Cargo-Lifting Azobenzene Monolayers. *Angewandte Chemie*, 120(18):3455–3457, April 2008.

[41] Gebhard Haberhauer and Christine Kallweit. A Bridged Azobenzene Derivative as a Reversible, Light-Induced Chirality Switch. *Angewandte Chemie International Edition*, 49(13):2418–2421, March 2010.

[42] Toru Ube and Tomiki Ikeda. Photomobile Polymer Materials with Crosslinked Liquid-Crystalline Structures: Molecular Design, Fabrication, and Functions. *Angewandte Chemie International Edition*, 53(39):10290–10299, September 2014.

[43] Seiya Kobatake, Shizuka Takami, Hiroaki Muto, Tomoyuki Ishikawa, and Masahiro Irie. Rapid and reversible shape changes of molecular crystals on photoirradiation. *Nature*, 446(7137):778–781, April 2007.

[44] M. Moniruzzaman, Christopher J. Sabey, and Gerard F. Fernando. Synthesis of Azobenzene-Based Polymers and the in-Situ Characterization of Their Photoviscosity Effects. *Macromolecules*, 37(7):2572–2577, April 2004.

[45] David H. Wang, Jeong Jae Wie, Kyung Min Lee, Timothy J. White, and Loon-Seng Tan. Impact of Backbone Rigidity on the Photomechanical Response of Glassy, Azobenzene-Functionalized Polyimides. *Macromolecules*, 47(2):659–667, January 2014.

[46] Christopher Weber, Tobias Liebig, Manuel Gensler, Linus Pithan, Sebastian Bommel, David Bléger, Jürgen P. Rabe, Stefan Hecht, and Stefan Kowarik. Light-Controlled "Molecular Zippers" Based on Azobenzene Main Chain Polymers. *Macromolecules*, 48(5):1531–1537, March 2015.

[47] Shangyi Fu and Yue Zhao. Orientation of Azobenzene Mesogens in Side-Chain Liquid Crystalline Polymers: Interplay between Effects of Mechanical Stretching, Photoisomerization and Thermal Annealing. *Macromolecules*, 48(15):5088–5098, August 2015.

[48] Michael Petr and Paula T. Hammond. Room Temperature Rapid Photoresponsive Azobenzene Side Chain Liquid Crystal Polymer. *Macromolecules*, 44(22):8880–8885, November 2011.

[49] Zhibin Li, Ying Zhang, Lirong Zhu, Tao Shen, and Huiqi Zhang. Efficient synthesis of photoresponsive azobenzene-containing side-chain liquid crystalline polymers with high molecular weights by click chemistry. *Polymer Chemistry*, 1(9):1501–1511, October 2010.

[50] Andrew A. Beharry, Oleg Sadovski, and G. Andrew Woolley. Azobenzene Photoswitching without Ultraviolet Light. *Journal of the American Chemical Society*, 133(49):19684–19687, December 2011.

[51] Timothy P. Osedach, Trisha L. Andrew, and Vladimir Bulović. Effect of synthetic accessibility on the commercial viability of organic photovoltaics. *Energy & Environmental Science*, 6(3):711–718, February 2013.

[52] H. Rau. *Photoisomerization of Azobenzenes*, volume 2. CRC Press, Boca Ration, FL, 1990.

[53] Jaume García-Amorós and Dolores Velasco. Recent advances towards azobenzene-based light-driven real-time information-transmitting materials. *Beilstein Journal of Organic Chemistry*, 8:1003–1017, July 2012.

[54] Jaume Garcia-Amorós, Antoni Sánchez-Ferrer, Walter A. Massad, Santi Nonell, and Dolores Velasco. Kinetic study of the fast thermal cis-to-trans isomerisation of para-, ortho- and polyhydroxyazobenzenes. *Physical Chemistry Chemical Physics*, 12(40):13238–13242, October 2010.

139

[55] H. M. Dhammika Bandara and Shawn C. Burdette. Photoisomerization in different classes of azobenzene. *Chemical Society Reviews*, 41(5):1809–1825, February 2012.

[56] Yu-Quan Shen and Hermann Rau. The environmentally controlled photoisomerization of probe molecules containing azobenzene moieties in solid poly(methyl methacrylate). *Die Makromolekulare Chemie*, 192(4):945–957, April 1991.

[57] Monika Schönhoff, Michael Mertesdorf, and Mathias Lösche. Mechanism of Photoreorientation of Azobenzene Dyes in Molecular Films. *The Journal of Physical Chemistry*, 100(18):7558–7565, January 1996.

[58] Haisheng Chen, Thang Ngoc Cong, Wei Yang, Chunqing Tan, Yongliang Li, and Yulong Ding. Progress in electrical energy storage system: A critical review. *Progress in Natural Science*, 19(3):291–312, March 2009.

[59] Morizo Tsuda and Kenji Kuratani. Isomerization of cis-Azobenzene in the Solid Phase. *Bulletin of the Chemical Society of Japan*, 37(9):1284–1288, September 1964.

[60] Guang Han, Hongtao Zhang, Jing Chen, Qian Sun, Yuying Zhang, and Huiqi Zhang. Easily crosslinkable side-chain azobenzene polymers for fast and persistent fixation of surface relief gratings. *New Journal of Chemistry*, 39(2):1410–1420, February 2015.

[61] Chengqun Qin, Yiyu Feng, Wen Luo, Chen Cao, Wenping Hu, and Wei Feng. A supramolecular assembly of cross-linked azobenzene/polymers for a high-performance light-driven actuator. *Journal of Materials Chemistry A*, 3(32):16453–16460, August 2015.

[62] David Zhitomirsky, Eugene Cho, and Jeffrey C. Grossman. Solid-State Solar Thermal Fuels for Heat Release Applications. *Advanced Energy Materials*, 6(6), March 2016.

[63] David Zhitomirsky and Jeffrey C. Grossman. Conformal Electroplating of Azobenzene-Based Solar Thermal Fuels onto Large-Area and Fiber Geometries. *ACS Applied Materials & Interfaces*, 8(39):26319–26325, October 2016.

[64] Oleksandr S. Bushuyev, Anna Tomberg, Tomislav Friščić, and Christopher J. Barrett. Shaping Crystals with Light: Crystal-to-Crystal Isomerization and Photomechanical Effect in Fluorinated Azobenzenes. *Journal of the American Chemical Society*, 135(34):12556–12559, August 2013.

[65] Sebastian Hagen, Felix Leyssner, Dhananjay Nandi, Martin Wolf, and Petra Tegeder. Reversible switching of tetra-tert-butyl-azobenzene on a Au(1 1 1) surface induced by light and thermal activation. *Chemical Physics Letters*, 444(1–3):85–90, August 2007.

[66] S. D. Evans, S. R. Johnson, H. Ringsdorf, L. M. Williams, and H. Wolf. Photoswitching of Azobenzene Derivatives Formed on Planar and Colloidal Gold Surfaces. *Langmuir*, 14(22):6436–6440, October 1998.

[67] Shaoping Bian, John M. Williams, Dong Yu Kim, Lian Li, Srinivasan Balasubramanian, Jayant Kumar, and Sukant Tripathy. Photoinduced surface deformations on azobenzene polymer films. *Journal of Applied Physics*, 86(8):4498–4508, October 1999.

[68] Mi-Jeong Kim, Bu-Gon Shin, Jang-Joo Kim, and Dong-Yu Kim. Photoinduced Supramolecular Chirality in Amorphous Azobenzene Polymer Films. *Journal of the American Chemical Society*, 124(14):3504–3505, April 2002.

[69] X. L. Jiang, L. Li, J. Kumar, D. Y. Kim, V. Shivshankar, and S. K. Tripathy. Polarization dependent recordings of surface relief gratings on azobenzene containing polymer films. *Applied Physics Letters*, 68(19):2618–2620, May 1996.

[70] Tadashi Enomoto, Hidesato Hagiwara, Donald A. Tryk, Zhong-Fan Liu, Kazuhito Hashimoto, and Akira Fujishima. Electrostatically Induced Isomerization of Azobenzene Derivatives in LangmuirâLŠBlodgett Films. *The Journal of Physical Chemistry B*, 101(38):7422–7427, September 1997.

[71] Masatsugu Shimomura and Toyoki Kunitake. Preparation of Langmuir-Blodgett films of azobenzene amphiphiles as polyion complexes. *Thin Solid Films*, 132(1–4):243–248, October 1985.

[72] Mutsuyoshi Matsumoto, Samuel Terrettaz, and Hiroaki Tachibana. Photoinduced structural changes of azobenzene Langmuir–Blodgett films. *Advances in Colloid and Interface Science*, 87(2–3):147–164, November 2000.

[73] Liang Cheng, Yanira Torres, Kyung Min Lee, Amber J. McClung, Jeffery Baur, Timothy J. White, and William S. Oates. Photomechanical bending mechanics of polydomain azobenzene liquid crystal polymer network films. *Journal of Applied Physics*, 112(1):013513, July 2012.

[74] T. Fujii, S. Kuwahara, K. Katayama, K. Takado, T. Ube, and T. Ikeda. Molecular dynamics in azobenzene liquid crystal polymer films measured by time-resolved techniques. *Physical Chemistry Chemical Physics*, 16(22):10485–10490, May 2014.

[75] Tomiki Ikeda. Photomodulation of liquid crystal orientations for photonic applications. *Journal of Materials Chemistry*, 13(9):2037–2057, August 2003.

[76] Xiaoming Zhao, Shirong Wang, Jing You, Yuteng Zhang, and Xianggao Li. Solution-processed thermally stable amorphous films of small molecular hole injection/transport bi-functional materials and their application in high effi-

ciency OLEDs. *Journal of Materials Chemistry C*, 3(43):11377–11384, October 2015.

[77] M. A. Baldo, Z. G. Soos, and S. R. Forrest. Local order in amorphous organic molecular thin films. *Chemical Physics Letters*, 347(4–6):297–303, October 2001.

[78] Takuya Naito, Kazuyuki Horie, and Itaru Mita. The Effect of Polymer Rigidity on Photoisomerization of 4-Dimethylamino-4âĂŠ-nitroazobenzene. *Polymer Journal*, 23(6):809–813, June 1991.

[79] Yiyu Feng, Hongpo Liu, Wen Luo, Enzuo Liu, Naiqin Zhao, Katsumi Yoshino, and Wei Feng. Covalent functionalization of graphene by azobenzene with molecular hydrogen bonds for long-term solar thermal storage. *Scientific Reports*, 3, November 2013.

[80] C. Barrett, A. Natansohn, and P. Rochon. Thermal Cis-Trans Isomerization Rates of Azobenzenes Bound in the Side Chain of Some Copolymers and Blends. *Macromolecules*, 27(17):4781–4786, August 1994.

[81] C. Barrett, A. Natansohn, and P. Rochon. Cis-Trans Thermal Isomerization Rates of Bound and Doped Azobenzenes in a Series of Polymers. *Chemistry of Materials*, 7(5):899–903, May 1995.

[82] Mina Han and Masahiko Hara. Intense Fluorescence from Light-Driven Self-Assembled Aggregates of Nonionic Azobenzene Derivative. *Journal of the American Chemical Society*, 127(31):10951–10955, August 2005.

[83] Mina Han, Daisuke Ishikawa, Emi Muto, and Masahiko Hara. Isomerization and fluorescence characteristics of sterically hindered azobenzene derivatives. *Journal of Luminescence*, 129(10):1163–1168, October 2009.

[84] Nandita Biswas and Siva Umapathy. Structures, Vibrational Frequencies, and Normal Modes of Substituted Azo Dyes:âĂL Infrared, Raman, and Density Functional Calculations. *The Journal of Physical Chemistry A*, 104(12):2734–2745, March 2000.

[85] Christina M. Stuart, Renee R. Frontiera, and Richard A. Mathies. Excited-State Structure and Dynamics of cis- and trans-Azobenzene from Resonance Raman Intensity Analysis. *The Journal of Physical Chemistry A*, 111(48):12072–12080, December 2007.

[86] Sung Ik Yang, Ki-Hyun Kim, Daeseung Kang, and Sang-Woo Joo. Cis-to-trans photoconversion of azobenzene self-assembled monolayers on gold nanoparticle surfaces investigated by Raman spectroscopy. *Photochemical & Photobiological Sciences*, 8(1):31–33, January 2009.

[87] D. R. Armstrong, J. Clarkson, and W. E. Smith. Vibrational Analysis of trans-Azobenzene. *The Journal of Physical Chemistry*, 99(51):17825–17831, December 1995.

[88] Takuya Naito, Kazuyuki Horie, and Itaru Mita. Photochemistry in polymer solids. 11. The effects of the size of reaction groups and the mode of photoisomerization on photochromic reactions in polycarbonate film. *Macromolecules*, 24(10):2907–2911, May 1991.

[89] Yasuo Norikane, Yuki Hirai, and Masaru Yoshida. Photoinduced isothermal phase transitions of liquid-crystalline macrocyclic azobenzenes. *Chemical Communications*, 47(6):1770–1772, January 2011.

[90] Manabu Hoshino, Emi Uchida, Yasuo Norikane, Reiko Azumi, Shunsuke Nozawa, Ayana Tomita, Tokushi Sato, Shin-ichi Adachi, and Shin-ya Koshihara. Crystal Melting by Light: X-ray Crystal Structure Analysis of an Azo Crystal Showing Photoinduced Crystal-Melt Transition. *Journal of the American Chemical Society*, 136(25):9158–9164, June 2014.

[91] Emi Uchida, Kouji Sakaki, Yumiko Nakamura, Reiko Azumi, Yuki Hirai, Haruhisa Akiyama, Masaru Yoshida, and Yasuo Norikane. Control of the Orientation and Photoinduced Phase Transitions of Macrocyclic Azobenzene. *Chemistry – A European Journal*, 19(51):17391–17397, 2013.

[92] Yasuo Norikane, Emi Uchida, Satoko Tanaka, Kyoko Fujiwara, Emiko Koyama, Reiko Azumi, Haruhisa Akiyama, Hideyuki Kihara, and Masaru Yoshida. Photoinduced Crystal-to-Liquid Phase Transitions of Azobenzene Derivatives and Their Application in Photolithography Processes through a Solid–Liquid Patterning. *Organic Letters*, 16(19):5012–5015, October 2014.

[93] Si Wu, Lifang Niu, Jing Shen, Qijin Zhang, and Christoph Bubeck. Aggregation-Induced Reversible Thermochromism of Novel Azo Chromophore-Functionalized Polydiacetylene Cylindrical Micelles. *Macromolecules*, 42(1):362–367, January 2009.

[94] Gang Zou, Hao Jiang, Qijin Zhang, Hideki Kohn, Takaaki Manaka, and Mitsumasa Iwamoto. Chiroptical switch based on azobenzene-substituted polydiacetylene LB films under thermal and photic stimuli. *Journal of Materials Chemistry*, 20(2):285–291, December 2009.

[95] Qiang Ye, Xian You, Gang Zou, Xiaowu Yu, and Qijin Zhang. Morphology, structure and chromatic properties of azobenzene-substituted polydiacetylene supramolelular assemblies. *Journal of Materials Chemistry*, 18(24):2775–2780, June 2008.

[96] Xin Chen, Lei Hong, Xian You, Yali Wang, Gang Zou, Wei Su, and Qijin Zhang. Photo-controlled molecular recognition of Íś-cyclodextrin with azobenzene con-

143

taining polydiacetylene vesicles. *Chemical Communications*, (11):1356–1358, March 2009.

[97] Hiroyuki Yamakoshi, Kosuke Dodo, Almar Palonpon, Jun Ando, Katsumasa Fujita, Satoshi Kawata, and Mikiko Sodeoka. Alkyne-Tag Raman Imaging for Visualization of Mobile Small Molecules in Live Cells. *Journal of the American Chemical Society*, 134(51):20681–20689, December 2012.

[98] Asish Pal, Panayiotis Voudouris, Marcel M. E. Koenigs, Pol Besenius, Hans M. Wyss, Volkan Degirmenci, and Rint P. Sijbesma. Topochemical polymerization in self-assembled rodlike micelles of bisurea bolaamphiphiles. *Soft Matter*, 10(7):952–956, January 2014.

[99] G. M. Sheldrick. Crystal structure refinement with SHELXL. *Acta Crystallographica Section C: Structural Chemistry*, 71(1):3–8, January 2015.

[100] John P. Perdew, Kieron Burke, and Matthias Ernzerhof. Generalized Gradient Approximation Made Simple. *Physical Review Letters*, 77(18):3865–3868, October 1996.

[101] G. Kresse and J. Furthmüller. Efficient iterative schemes for ab initio total-energy calculations using a plane-wave basis set. *Physical Review B*, 54(16):11169–11186, October 1996.

[102] G. Kresse and D. Joubert. From ultrasoft pseudopotentials to the projector augmented-wave method. *Physical Review B*, 59(3):1758–1775, January 1999.

[103] John Algers, Peter Sperr, Werner Egger, Laszlo Liszkay, Gottfried Kögel, Jérémie de Baerdemaeker, and Frans H. J. Maurer. Free Volume Determination of Azobenzene-PMMA Copolymer by a Pulsed Low-Energy Positron Lifetime Beam with in-Situ UV Illumination. *Macromolecules*, 37(21):8035–8042, October 2004.

[104] John G. Victor and John M. Torkelson. On measuring the distribution of local free volume in glassy polymers by photochromic and fluorescence techniques. *Macromolecules*, 20(9):2241–2250, September 1987.

[105] S. Xie, A. Natansohn, and P. Rochon. Recent developments in aromatic azo polymers research. *Chemistry of Materials*, 5(4):403–411, April 1993.

[106] Liu, Darren R. Dunphy, Plamen Atanassov, Scott D. Bunge, Zhu Chen, Gabriel P. López, Timothy J. Boyle, and C. Jeffrey Brinker. Photoregulation of Mass Transport through a Photoresponsive Azobenzene-Modified Nanoporous Membrane. *Nano Letters*, 4(4):551–554, April 2004.

[107] H. Bdssler, V. Enkelmann, and H. Sixl. *Polydiacetylenes*. Springer, Berlin, Heidelberg, Germany, 1984.

[108] Bora Yoon, Sumi Lee, and Jong-Man Kim. Recent conceptual and technological advances in polydiacetylene-based supramolecular chemosensors. *Chemical Society Reviews*, 38(7):1958–1968, June 2009.

[109] Bora Yoon, Hyora Shin, Eun-Mi Kang, Dae Won Cho, Kayeong Shin, Hoeil Chung, Chan Woo Lee, and Jong-Man Kim. Inkjet-Compatible Single-Component Polydiacetylene Precursors for Thermochromic Paper Sensors. *ACS Applied Materials & Interfaces*, 5(11):4527–4535, June 2013.

[110] R. W. Carpick, D. Y. Sasaki, and A. R. Burns. First Observation of Mechanochromism at the Nanometer Scale. *Langmuir*, 16(3):1270–1278, February 2000.

[111] Jaewon Yoon, Young-Sik Jung, and Jong-Man Kim. A Combinatorial Approach for Colorimetric Differentiation of Organic Solvents Based on Conjugated Polymer-Embedded Electrospun Fibers. *Advanced Functional Materials*, 19(2):209–214, January 2009.

[112] Masahiro Irie. Photochromism and Molecular Mechanical Devices. *Bulletin of the Chemical Society of Japan*, 81(8):917–926, August 2008.

[113] H. Y. Jiang, S. Kelch, and A. Lendlein. Polymers Move in Response to Light. *Advanced Materials*, 18(11):1471–1475, June 2006.

[114] Belén Zalba, José M. Marin, Luisa F. Cabeza, and Harald Mehling. Review on thermal energy storage with phase change: materials, heat transfer analysis and applications. *Applied Thermal Engineering*, 23(3):251–283, February 2003.

[115] Andrew D. Bond. On the crystal structures and melting point alternation of the n -alkyl carboxylic acids. *New Journal of Chemistry*, 28(1):104–114, 2004.

[116] Gabin Gbabode, Philippe Negrier, Denise Mondieig, Evelyn MorenoâĂĚCalvo, Teresa Calvet, and MiquelâĂĚÀngel Cuevas-Diarte. Structures of the High-Temperature Solid Phases of the Odd-Numbered Fatty Acids from Tridecanoic Acid to Tricosanoic Acid. *Chemistry – A European Journal*, 13(11):3150–3159, April 2007.

[117] Takeshi Ueki, Yutaro Nakamura, Ayuko Yamaguchi, Kazuyuki Niitsuma, Timothy P. Lodge, and Masayoshi Watanabe. UCST Phase Transition of Azobenzene-Containing Random Copolymer in an Ionic Liquid. *Macromolecules*, 44(17):6908–6914, September 2011.

[118] B. Jouti, E. Provost, D. Petitjean, M. Bouroukba, and M. Dirand. Phase diagram of n-heneicosane and n-tricosane molecular alloys. *Journal of Molecular Structure*, 382(1):49–56, August 1996.

[119] Douglas L. Dorset and Robert G. Snyder. Crystal Structure of Modulated n-Paraffin Binary Solids. *The Journal of Physical Chemistry*, 100(23):9848–9853, January 1996.

[120] Yan Quanying, Liang Chen, and Zhang Lin. Experimental study on the thermal storage performance and preparation of paraffin mixtures used in the phase change wall. *Solar Energy Materials and Solar Cells*, 92(11):1526–1532, November 2008.

[121] Jianguo Zuo, Weizhong Li, and Lindong Weng. Thermal properties of lauric acid/1-tetradecanol binary system for energy storage. *Applied Thermal Engineering*, 31(6–7):1352–1355, May 2011.

[122] Chongyun Wang, Lili Feng, Huazhe Yang, Gongbiao Xin, Wei Li, Jie Zheng, Wenhuai Tian, and Xingguo Li. Graphene oxide stabilized polyethylene glycol for heat storage. *Physical Chemistry Chemical Physics*, 14(38):13233–13238, 2012.